UNIVERSITY OF MESSINA

Department of Engineering

Doctorate in Engineering and Chemical
of Materials and Constructions
(XXX cycle)

“Experimental tests and Numerical analysis for an Air Cavity Yacht”

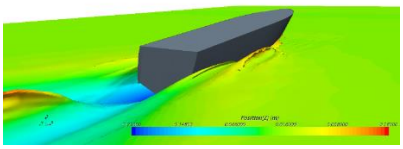

PhD Candidate: Dott. Ing. Felice Sfravara

Tutor: Prof. Ing. Vincenzo Crupi

Coordinator: Prof. Signorino Galvagno

Summary

1. Nomenclature

Definition	Symbol	Formula	Unit
Overall Length	LOA	-	m
Waterline Length	LWL	-	m
Projected Chine Length	LP	-	m
Waterline Beam	BWL	-	m
Wetted Surface	S		m^2
Longitudinal Position of Buoyancy	LCB		m
Longitudinal Position of Floating Centre	LCF		m
Vertical Position of Buoyancy	VCB		m
Wetted Surface	SW		m^2
Area to Water Line	AWL		m^2
Transversal Metacentric Height	KMt		m
Sectional Area to displacement	A		
Longitudinal Metacentric Height	KMl		m
Centimeter Trim Moment	M_u		t*m/cm
Centimeter Displacement	Δ_u		t/cm
Projected Maximum Beam	BPX	-	m
Projected Beam at generic X position	BPC	-	m
Projected Beam Transom	BPT	-	m
Projected Medium Beam	BPA	$\frac{AP}{LP}$	m
Deadrise Angle	β	-	°
Height of medium buttock line	HLM	-	m
Draft	T	-	m
Displacement Mass	Δ	-	t
Displacement Volume	∇		
Longitudinal center of gravity	x_G	-	m
Projected Area	AP	-	m^2
Velocity of Ship	V_S	-	m/s
Velocity of Model	V_M	-	m/s
Froude number	Fn		-
Length of Ship	L_S	-	m
Length of Model	L_M	-	m
Scale	λ	$\frac{L_S}{L_M}$	-
Number of Steps	N_{ST}	-	-
Position of the step relative to the transom	L_{ST}	-	m
Area Step	S_{ST}	-	m^2
Number of nozzles	N_{IN}	-	-

Dimensions - Basis x Height	B_{IN} x H_{IN}	-	m x m
Area of nozzles	S_{IN}	-	m^2
Dimensions - Basis x Height Rails	B_R x H_R	-	m x m
Transversal Distance Between Rails	TD_R	-	m
Number of rails	N_R	-	-
Volumetric Flow Rate	Q		m^3/s
Flow rate Coefficient	CQ	$\frac{Q}{S_{IN}V_M}$	-

2. Introduction

Abstract

This chapter introduce the reader in the principal motivations of this research. There are also explained the principal objectives of the thesis with the methodologies used in order to reach the results obtained. A brief outline of the thesis with a brief explanation of each chapter.

2.1 Background and motivation

Each moving object in the earth or the principal industrial processes or simply the daily activities of humans involve the use of some kind of fluids. This interaction can be advantageous or disadvantageous. The deep knowledge of the main features of fluid flow allows to manage it with great advantages in terms of efficiency and sustainability, principally when the problem is the reduction of the resistance during the movement of a body.

In the case of naval engineering, there is a strong interaction between the fluid and the ship. This interaction leads to a different effects, the most important one is the resistance during the navigation. The resistance of a ship is composed by two principal components: frictional resistance and wave resistance. Both of them must be reduced in order to keep the resistance low. The wave component is strongly dependent by the shape of the hull, so in preliminary phase, is possible to find, with different techniques, the better shape for reducing it. More complex is the reduction of the frictional component, because it depends on the contact between the surface of the ship and the water.

The most difficult problem is the reduction of this component with methodologies applicable on the ships. There are many examples of drag reduction on flat plate, for example application of particular coatings or particular geometry but these passive methods are not suitable for the application on the ship.

Another way is the injection of the air under the hull, this condition allows to separate the surface of the ship from the water. There are many examples of application of this method on flat plate

models or on displacement hulls. This method seems the most promising one. These studies show that the injection of the air with a stable layer of air allows to reduce the frictional resistance.

This work was partially supported by European Union funding. The principal aspect of this work is the application of the air cavity on a high speed ship in model scale and real scale.

2.2 Objectives and principal points of the research

Thanks to many studies in literature is possible to know that the air injection under a stepped flat plate or under scale model of ship leads to a reduction of frictional resistance. There are also new applications on real scale ship. This technology is also under study and it is not widely used yet.

Objective of the research is to improve the knowledge of air-cavity phenomena with a systematic study on different design bottom hull solution for the same type of planing hull. The approach is oriented to find the better design solution for the application of air-cavity on a yacht of 18 meters. Four different scale models have been tested to different velocities and air flow.

The second part of the thesis involves the validation of computational fluid dynamics method for this kind of problem and so to quantify the potentiality of the CFD for solving this complex phenomena under the hull. The method used is the URanse (Unsteady Reynolds Navier Stokes method). The results could be used for modifying the hull geometry in order to better accommodate the air layer.

2.3 Outline of the thesis

The literature overview chapter introduces the reader to the literature of the two principal techniques for solving the problem of resistance prediction in naval engineering, the experimental methods and the numerical approach. A review of the history of the air cavity is proposed in this chapter with particular focus on the experimental and numerical approaches.

The Nomenclature chapter helps the reader to understand the meaning of different symbols inside the thesis.

Background theory chapter introduces the reader to the principal equation to the basis of the fluid dynamic flow, with the derivation of the Navier Stokes Equations. A brief review of the principal hypothesis is reported in this chapter with the principal boundary conditions used in naval field in order to solve the problem of the flow around the hull.

Experimental tests is the chapter that concerns the description of the experimental part of this research. A brief review of the ITTC method in the towing tank tests is shown with particular interest on the Froude' Law. In the second sub-chapter the reader find a detailed description of all hull shapes used for the experimental tests, with general and specific dimensions. The third sub-chapter analyses the construction making phase with a detailed explanation of the all tests performed in the towing tank of Naple. The last sub-chapter concerns a review of all results and discussion about the use of air cavity in this kind of hulls.

Computational Fluid Dynamic is the chapter that concerns the use of the numerical approach for solving this kind of problem. A first part explains the general approach used by all commercial software. A step-by-step explanation of all settings is reported with the CFD method with all parameters about mesh and solver controls. The method is developed in order to find the better settings for air injection condition and an uncertainty analysis is proposed during the numerical simulations. In order to test the method, another case study is proposed.

The last chapter concerns a resume of principal aspects of the thesis and the main results obtained during the three years of doctorate.

3. Literature Overview

Abstract

This chapter introduce the reader in the state of art of the towing tank tests, the state of art of evolution of numerical approach and the last development of the air cavity technology.

3.1 The towing tank test

Since 1452 Leonardo da Vinci carried out tests on different models of ships for resistance prediction. In his work, three ships with the same general dimensions but with different aft-and-fore shapes have been tested (Tursini, 1953). The interest on this problem pushed other researchers to find solutions for defining new experimental methods. The first approach was to build woven models towed by falling weights inside a tank (Baker, 1937). Todd proposed a paper with a general methodology for experimental tests in the 1951 (Todd, 1951). In all these experiments the real problem was to scale the results from the model scale to full scale. The solution to this problem has been proposed by Froude, his idea was to divide the total resistance in two different independent components: frictional and wave (Froude, 1955). The literal words of Froude were “The (residuary) resistance of geometrically similar ships is in the ratio of the cube of their linear dimensions if their speeds are in the ratio of the square roots of their linear dimensions”. The residuary component cited by Froude is the total resistance minus the resistance of an equivalent flat plate with the same wetted area and length and moving with the same velocity of the hull (at model and full scale). The idea was to divide the total resistance in the part produced by the viscous effects between the hull surface and the water, the other part produced by the waves. Froude made his first experimental tests with falling weights method but he was not satisfied because of the limitations of this technique. Successively, Froude proposed a new towing tank with the use of a mechanical propelled carriage system for towing the model in a tank. The friction component was obtained with experimental tests on equivalent flat plate at model and full scale or with a formula proposed by Froude. This component was subtracted to the total component of the resistance at model scale and the result was the residuary component of resistance at model scale. Thanks to Froude law, the residuary component was scaled in full scale and added to the frictional equivalent flat plate component so obtaining the total resistance to full scale. The two mains specifications in order to apply this method were: the model scale and the full scale must be with the same shapes (geometric similitude) and the ratio between the velocities must be in ratio of the square roots of their linear dimensions. The frictional formula proposed by Froude was independent by an important number:

Reynolds number. From the 1927 until to 2006 different formula for the frictional component of resistance have been proposed (Lazauskas, 2005). The first researcher introduced a new formula in towing tank test was Schoenherr but only in 1957 the International Towing Tank Conference introduced the new procedure (ITTC, 1957). In this procedure the viscous effects were defined by a single formula without considering the effects of the 3-D shape of the hull. The ITTC introduced another extrapolation technique in order to take in account this particular effects (International Towing Tank Conference, 1978). All the towing tank use the ITTC'57 or ITT'78 method, both of these methods are based on a law very old but reliable and useful for resistance prediction. The method during the years is changed respect to the formula used for solving the friction component of the resistance in order to take in account the scale effects and the great difference between the Reynolds number at model scale and at full scale. In this research all experimental tests have been conducted in Towing tank of Naple with the ITTC'57 methodology (principally used for high speed hull).

3.2 Evolution of analytical and numerical approach

From the beginning of the use of numerical and analytical methods, the idea was to solve the problem of total resistance prediction with the separation of this quantity in two independent components: free-surface and wave component and frictional component.

Before the advent of modern computer with great power capacity, the solution of fluid flow around the ship were based on analytical methods. All these methods were based on a simplification: the inviscid flow condition, the viscous effects were neglected. The first result presented in literature with an analytical method for solving the resistance problem was proposed by Michell (Michell, 1898). In this case, the ship had a slender shape and the viscosity of the fluid was neglected. All the boundary conditions were linearized and the boundary condition relative to hull surface was defined along the centre line. Michell found a mathematical expression for the pressure distribution around the ship. The integration of this quantity along the hull allowed to know the pressure resistance. In the 1951, Havelock proposed for the first time the use of the energy concept (Havelock, 1951). The wave resistance was measured thanks to this energy, the novelty of the approach was the use of sources and sinks elements. These elements were respectively emitter and absorber of energy. The sources were positioned along the centre line and the intensity of energy was dependent by the position and the local angle of the waterline. Thanks to the sum of the sources effects the wave resistance could be determined. The first idea of optimization of hull shape was proposed by Inui (Inui, 1980), the optimization concerned the wave component of resistance, also in this case the viscous effects were neglected. In the same period the same author proposed a study in order to quantify the non linear effects of the free-surface on the wave resistance (Inui and Kajitani, 1977). Thanks to the introduction of the computers and with the increase of the computational power many different methods have been developed during the last years based on numerical techniques. The first improvement respect the analytical methods was to define a hull surface with quadrilateral elements called panels and the possibility to apply the boundary condition of the hull on these quadrilateral elements respecting the 3D shape of the hull. The method is known as panel method and the application of this method in fluid dynamics was explained by Hess (Hess, 1990). At first,

the panel method was used in aerodynamic problems but with the idea proposed by Dawson (Dawson, 1977) also in naval problems this method became useful. Dawson solved the problem of the flow around the ship applying the panel method both for the hull surface and for the free-surface. The limitation was that Dawson applied linearized boundary conditions for the free-surface. A refinement of the Dawson approach with a real free surface boundary condition was successively developed by Janson (Carl-Erik Janson, 1997).

During this years, researchers exploring also methods for solving the other component of resistance, the frictional one. The problem was to solve the boundary layer near the hull surface. Also in this case, the help of the computational power is very important. In the 1968, the first solution for the boundary layer around a 2D object was presented by Kline et al. (Kline et al., 1968) . The great problem of these models was the prediction of the flow around the stern of the ship, principally in the flow separation zones. Larsson (Larsson et al., 1990) during the workshop in Gothenburg, described all methods and focused the attention on the necessity to solve this problem with new methods. These new methods should be able to solve simultaneously the boundary layer problem and the free-surface conditions.

The most promising one was the Reynolds-Averaged Navier stokes method (RANS). The RANS method (successively explained) allows to remove the fluctuations of the velocity components produced by the turbulence and reduce the problem of turbulence with an artificial modelling of the Reynolds stresses components (six unknown components). The researchers focused on three different key elements in order to solve with computational approach the RANS equations: the grid generation, the algorithm development and the turbulence modeling. The last one was the most important one because it involves the use of a mathematical model in order to approximate a physical behavior. The great effort of all researchers was to find the better model of turbulence for each industrial case. This assumption is important because a single turbulence model is not sufficient for all industrial cases. A great explanation of all turbulence models have been proposed by Wilcox (Wilcox, 2006).

The great potentiality of RANS methods have been discussed during other different workshops (Kodama et al., 1994) and the increase of the computer power allowed to increase the efficiency of this method, principally for solving the full-scale viscous flow with the free-surface problem. A grid-dependence study of the RANS method with a computational grid regenerated to follow the free surface condition has been proposed by Hino (Hino, 1994). The numerical approach concerned the use of three different grids with different elements density. The solutions have been compared with each other and with experimental data and the grid dependence of these solution has been discussed. The hull under investigation was a Series 60. Another study proposed by the same author concerned the influence of the turbulence models on the final results (Hino, 1995). The author used two different one-equation turbulence models for the prediction of the resistance of two tankers (HSVA Tanker and the Dyne Tanker). The results were in great accordance with the experimental results. The author used the one-equation turbulence model approach, but with the increase of the computer power other different turbulence methods have been developed.

A great international workshop has been organized in Gothenburg in 2000 (Larsson et al., 2003). The principal theme of the workshop was the application of computational fluid dynamics in solving the ship flow. The principal objectives of the workshop were understanding the better solution for the turbulence modeling and the capacity of wave prediction also away from the hull with this new numerical method. The results were very important because with this new approach the flow around the stern was appropriately computed, the full-scale viscous flow may be computed without problem and the wave prediction near and away from the hull was predicted accurately. In the end of the workshop, an important concept has been recommended: the necessity of an uncertainty analysis during the process of verification and validation of the numerical approach.

In the last years, the application of numerical methods for the resistance prediction is widely used in ship design, principally for problems of optimization shape in order to reduce the total drag. Techniques that use the URANSe (the Unsteady application of the RANS methods) are applied to avoid the towing tank tests and speed up the optimization process. A typical study is the hydrodynamic hull shape optimization as reported by Wilson et al. (Wilson et al., 2010) for standard ship or the prediction of drag of new type of ships such as catamarans (He et al., 2013). An important aspect is the simulation of the interaction between fluid and rigid body motion of the ship or any floating object. In the first case a typical example is the calculation of the trim and sinkage (Formaggia et al., 2008), in the second case typical examples are the study of offshore wind turbine (Quallen and Xing, 2016) or system such as wave energy converter (Brusca et al., 2015). In case of large deformation caused by fluid-dynamics pressure or forces the use of rigid body motion is not adequate, so new methodologies with the use of direct coupling between mechanical and fluid-dynamics solvers can be used. In this sense, analysis of shape deformation of parachute is a typical example (Takizawa et al., 2015) or the shape deformation of sails (Cella et al., 2017). The URANSe method has a great approximation: the turbulence is solved with a model. In the last years, a new techniques allows to solve the all scales of the turbulence eddies directly, without approximation. This technique is called Direct Numerical Simulation (DNS) and involves a great requests of computational power, a brief review of this technique has been reported by Moin and Mahesh (Moin and Mahesh, 1998). The direct numerical simulation is used in order to solve problem of wall turbulence in a channel flow (Myoungkyu and Moser, 2015) or usually it is used for solving problem of transport of solid particle caused by an incompressible flow (Kidanemariam and Uhlmann, 2014). In the field of naval ship, this technique is still avoided because the domain is too big and the time solution could be too much expansive. In new computational fluid dynamic software there is a new approach: Large Eddy Simulation (LES). It is a good compromise between the URANSe method and the DNS one. In this case part of the scale of the turbulence eddies is solved in a direct way (naturally with specific conditions in the sizing of the mesh) and part of these eddies are solved with the classic turbulence models. This technique is under investigation and the principal challenges have been described by Fureby (Fureby, 2016). An interesting application of the LES method is the cavitation. In this phenomena is interesting to understand the cavitation structures and the influence of the turbulence on these structures. An application of the LES for cavitation problems of a hydrofoil is proposed by Ji et al (Ji et al., 2015). The same technique is applied by Balaras et al. (Balaras et al., 2015) for solving the problem of cavitation around a submarine propeller, the technique allows to solve the tip vortices of the propeller in open water condition. Also in this case, the time of

simulation is increased respect to the URANSe solution but it could be a good compromise in cases where the study of turbulence eddies is very important.

3.3 Air Cavity technology

The initial theoretical modeling for air cavities under plate have been developed by Butuzov (Butuzov, 1968). This idea was transferred to ships with a full-scale trials of a boat with an air cavity (Butuzov et al., 1988). An alternative to the air-cavity is the microbubbles method. The pioneer in this field were McCormick and Bhattacharyya (McCormick and Bhattacharyya, 1973). Successively Kodama proposed an experimental test with circulating water tunnel (Kodama et al., 2002). An interesting device in combination with the use of micro-bubbles application is proposed by Kumagai et al. (Kumagai et al., 2015). A low pressure zone is produced rear a hydrofoil and the injection of the micro-bubbles is conducted in this zone taking in advantage the optimal environmental condition produced by the device. Merkle and Deutsch highlighted that the microbubbles method is ineffective for low velocity range (Merkle and Deutsch, 1989) and Ferrante and Elghobashi showed that, with the increase of Reynolds number, the reduction of frictional resistance decreased (Ferrante and Elghobashi, 2004). The disadvantages of the technology with microbubble, showed by authors, pushed the studies in the direction of air-cavity. A brief review of all technologies for friction drag reduction is proposed by Ahmadzadehtalatapeh and Mousavi (Ahmadzadehtalatapeh and Mousavi, 2016). Ceccio (Ceccio, 2010) proposed different applications and a detailed explanation of the distribution of the air under the hull during the injection. The economic saving is another aspect to take in account, a brief examination is reported by Mäkiharju et al. (Mäkiharju et al., 2012). Many authors studied the principal characteristics of the cavity in various conditions, experimental and numerical tests have been conducted in various forms and a brief review is proposed here. Matveev shown the principal parameters that influence the cavity of air (Matveev, 2003) with a numerical study for the simplified configuration of a rear-ward-facing step on the lower surface of horizontal wall for choosing the correct position of propulsion and lifting devices. Another important study was about the interaction between waves and cavity, it was solved with a numerical simplified approach by Matveev (Matveev, 2007). A study of air-ventilated cavities under a simplified hull has been undertaken by Matveev (Matveev, 2012), experiment with a 56-cm-long stepped-hull model were carried in an open-surface water channel at flow velocities of 28-86 cm/s. Following the report on flat plate case with air cavity proposed in the Emerson Cavitation Tunnel of Newcastle University by Slyozkin (Slyozkin et al., 2014), Butterworth et al. proposed an experimental test on an existing container ship model with a middle section of 2.2 m (Butterworth et al., 2015) and a 0.43 x 0.09 m^2 area for air cavity. The model experiments produced results ranging from 4% to 16% drag reduction. Always on the flat plate, application of submerged superhydrophobic (SHPo) surface is proposed by Lee et al. (Lee et al., 2016) with an entrapped gas called plastron, the application is suitable for laminar flow. Jang et al. (Jang et al., 2014) conducted experimental tests on the flat plate and successively on the model with also a self-propulsion test equipped with air lubrication system. Amromin (Amromin, 2016) reported an analysis of the interaction between the air cavity and the boundary layer. The scale factor of the air layer drag reduction has to be take in account. Indeed this effect could change significantly the results when they are transferred directly to full scale model. In this terms, an investigation of the scaling factor is reported by Elbing et al.

(Elbing et al., 2013). There is a great interest also in the shipyard industries for this technology, Mitsubishi Heavy Industries developed an air lubrication system and carried out tests in order to verify the efficiency in terms of frictional resistance reduction (Mizokami et al., 2013). There are less experiment tests for planing hulls; an important example is proposed by Matveev (Matveev, 2015) where there is a numerical method for prediction of drag reduction validated with experimental data. The same author developed a platform, with the necessary instruments, for testing different typologies of Air Cavity Ships (ACS) in order to improve and optimize this kind of technology (Matveev et al., 2015). An experimental work with analysis of the total resistance, trim, sinkage and wave pattern for high speed craft with artificial air cavity is proposed by Gokcay et al. (Gokcay et al., 2004). The experimental data are not only important for better understanding the artificial air cavity phenomena but also in order to validate, in this kind of problem, the URANSe (Unsteady Reynolds-Averaged Navier Stokes equation) methods. In the case of ACS, the problem is the multiphase flow with different scales interaction, the big one that concerns the waves' free surface and the small one that concerns the free surface of cavity (Cucinotta et al., 2017a, 2017b).

In the case of ACS, the problem is the multiphase flow with different scales interaction, the big one that concerns the waves' free surface and the small one that concerns the free surface of cavity (Cucinotta et al., 2017a, 2017b). An initial approach with commercial software is reported by Maimun et al. (Maimun et al., 2016).

4. Background Theory

Abstract

This chapter is about the theory of fluid-dynamic around a ship. The first part concerns the principal physical conditions in order to obtain the Navier Stokes equations. There is a complete description of the boundary conditions and the main assumptions for solving this complex phenomena.

The first objective of a naval architect engineer is to know, in preliminary phase, the resistance of the ship during the navigation to a specified velocity condition. In order to obtain this quantity, the engineer must know the physic principle of the fluid dynamics around the ship.

The start point of each consideration are two simple physical concepts applied to an infinitesimal incompressible fluid element: the conservation of mass and the Newton's second law. Inside an infinitesimal element the total net transport of mass out of element have to be zero in absence of sources inside the element (Eq. 4.1 – Continuity Equation).

$$\frac{\partial u}{\partial x}+\frac{\partial v}{\partial y}+\frac{\partial w}{\partial z}=0 \qquad (4.1)$$

The Newton's second law starts with a simple equation:

$$\overrightarrow{dF}=dm\,\vec{a} \qquad (4.2)$$

A physical consideration is that in a fluid mechanic problem three different types of forces must be considered: body forces $\overrightarrow{dF_b}$, viscous forces $\overrightarrow{dF_v}$ and pressure forces $\overrightarrow{dF_p}$.

Considering a coordinate system with the z-axis along the direction of the gravity, the only body force needs to be considered is the gravity force (Eq.4.3).

$$\frac{dF_{bz}}{dm} = -g \tag{4.3}$$

The pressure forces depend by the gradient of the pressure along all directions inside the infinitesimal element (Eq. 4.4-4.5-4.6).

$$\frac{dF_{px}}{dm} = -\frac{1}{\rho}\frac{\partial p}{\partial x} \tag{4.4}$$

$$\frac{dF_{py}}{dm} = -\frac{1}{\rho}\frac{\partial p}{\partial y} \tag{4.5}$$

$$\frac{dF_{pz}}{dm} = -\frac{1}{\rho}\frac{\partial p}{\partial z} \tag{4.6}$$

The viscous forces depend by the stresses inside the infinitesimal element, there are tangential viscous stresses and normal viscous stresses. The sum of each component of stress along respectively x-y-z direction defines the total viscous force along that direction (Eq. 4.7-4.8-4.9).

$$\frac{dF_{vx}}{dm} = \frac{1}{\rho}\left[\frac{\partial \sigma_{xx}}{\partial x} + \frac{\partial \sigma_{yx}}{\partial y} + \frac{\partial \sigma_{zx}}{\partial z}\right] \tag{4.7}$$

$$\frac{dF_{vy}}{dm} = \frac{1}{\rho}\left[\frac{\partial \sigma_{xy}}{\partial x} + \frac{\partial \sigma_{yy}}{\partial y} + \frac{\partial \sigma_{zy}}{\partial z}\right] \tag{4.8}$$

$$\frac{dF_{vz}}{dm} = \frac{1}{\rho}\left[\frac{\partial \sigma_{xz}}{\partial x} + \frac{\partial \sigma_{yz}}{\partial y} + \frac{\partial \sigma_{zz}}{\partial z}\right] \tag{4.9}$$

The great hypothesis to the base of the Navier Stokes equation is the one defined by Newton. The stress components σ_{ij} are proportional to the rate of strain tensor (Eq. 4.10) with constant of proportionality the dynamic viscosity μ (Eq. 4.11). This correlation allows to define the stress components in function of the velocities.

$$S_{ij} = \frac{\partial u_i}{\partial x_j} + \frac{\partial u_j}{\partial x_i} \tag{4.10}$$

$$\sigma_{ij} = \mu\, S_{ij} \tag{4.11}$$

All these considerations lead to the Navier Stokes equations, a second order nonlinear system of differential equations (Eq. 4.12-4.13-4.14) and the continuity equation (Eq. 4.15). The entire system is a set of four equations that together constitute a closed system for the four unknown variables: Pressure (*p*), vector velocity (*u,v,w*).

$$\frac{\partial u}{\partial t} + u\frac{\partial u}{\partial x} + v\frac{\partial u}{\partial y} + w\frac{\partial u}{\partial z} = -\frac{1}{\rho}\frac{\partial p}{\partial x} + \nu\left(\frac{\partial^2 u}{\partial x^2} + \frac{\partial^2 u}{\partial y^2} + \frac{\partial^2 u}{\partial z^2}\right) \quad (4.12)$$

$$\frac{\partial v}{\partial t} + u\frac{\partial v}{\partial x} + v\frac{\partial v}{\partial y} + w\frac{\partial v}{\partial z} = -\frac{1}{\rho}\frac{\partial p}{\partial y} + \nu\left(\frac{\partial^2 v}{\partial x^2} + \frac{\partial^2 v}{\partial y^2} + \frac{\partial^2 v}{\partial z^2}\right) \quad (4.13)$$

$$\frac{\partial w}{\partial t} + u\frac{\partial w}{\partial x} + v\frac{\partial w}{\partial y} + w\frac{\partial w}{\partial z} = -\frac{1}{\rho}\frac{\partial p}{\partial z} - g + \nu\left(\frac{\partial^2 w}{\partial x^2} + \frac{\partial^2 w}{\partial y^2} + \frac{\partial^2 w}{\partial z^2}\right) \quad (4.14)$$

$$\frac{\partial u}{\partial x} + \frac{\partial v}{\partial y} + \frac{\partial w}{\partial z} = 0 \quad (4.15)$$

The system of Navier Stokes equation is elliptical with partial differential equations, this means that each boundary in the domain must have an initial condition. The domain around the ship has different boundaries: the hull surface, the free surface and the domain far from the hull. For each of these boundaries a condition must be imposed.

On the hull surface, the so called no-slip condition have to be imposed. This condition is relative to the components of velocity:

$$u = v = w = 0$$

On the free surface, where there are two phases in contact, liquid and gas, two different boundary conditions have to be defined.

The first one is a dynamic condition that expressing that the two phases on this surface must have the same velocities. This condition is imposed with the equality of the forces of the two phases. The equations 4.16-4.17 define the equality between the tangential components (*s,t*) for the water (*w*) and for the air (*a*).

$$\sigma_{(ns)_w} = \sigma_{(ns)_a} \quad (4.16)$$

$$\sigma_{(nt)_w} = \sigma_{(nt)_a} \quad (4.17)$$

In the case of the normal component (Eq. 4.18) of the force respect to the free surface, must be taken in account the effect of the surface tension (Δp_γ).

$$(\sigma_{(nn)} - p)_w = (\sigma_{(nn)} - p)_a + \Delta p_\gamma \quad (4.18)$$

The second one is a kinematic boundary that expressing the no flow through the surface. In this case the condition is that the vertical component of the velocity *w* must be equal to the derivative of the wave height respect the time (Eq. 4.19)

$$w = \frac{d\zeta}{dt} \quad (4.19)$$

Another important condition is the one to infinity. The extension of the domain is not limited. All disturbances have to go zero far from the hull surface.

There are three principal ways to solve the problem of resistance prediction of ship: empirical methods, experimental methods and numerical methods. The work proposed in this research uses the experimental techniques in order to obtain the resistance of all models proposed. Thanks to results from these techniques a numerical approach has been investigated and validated for a model and successively used for other one.

5. Experimental tests

Abstract

A first part of this chapter describes the method used for solving the problem of resistance prediction with the use of the towing tank. The second chapter explains the hull shapes tested and all the tests conducted in the towing tank. Third chapter puts the attention in the building part of the models and in the final chapter all results and discussion are presented.

5.1 Method for towing tank tests

If the variables inside the system of differential equations and in the boundary conditions are made dimensionless, the result is a system of differential equations governed by four dimensionless parameters: the Reynolds number (*Rn*), the Froude Number (*Fn*), the Weber (*Wn*) number and the Euler number (*En*). This transformation of the Navier-Stokes equations is explained by White (White, 2014).

The Reynolds number (Eq.5.1) is a parameter that allows to take in account the effects of the viscosity of the fluid. It is directly inside the equations of Navier Stokes. The Froude number (Eq.5.2) is a parameter that allows to take in account the effects of the gravity on the free surface, it appears inside the dynamic boundary condition on the free surface. The Weber number (Eq. 5.3) is a parameter that allows to take in account the surface tension effects, with particular interest on the spray and breaking waves. The Euler number (Eq.5.4) is a parameter that allows to take in account the effects of cavitation, this number is important only for cases where there is cavitation conditions.

$$Rn = \frac{VL}{\nu} \qquad Eq.(5.1)$$

$$Fn = \frac{V}{\sqrt{gL}} \qquad Eq.(5.2)$$

$$Wn = \frac{\rho U^2 L}{\gamma} \qquad Eq.(5.3)$$

$$En = \frac{p_a}{\rho U^2} \qquad eq.(5.4)$$

The sufficient and necessary condition for flow similarity between geosim bodies (two bodies with the same shape) at different scales is the condition of constancy of these four parameters (Larsson and Raven, 2010). If the above parameters are unchanged between two geosim bodies, the solution in no dimensional form is unchanged.

Inside the towing tank, by definition, the model has a length smaller than that of the ship, in order to keep all parameters equal to real scale the model speed should be adjusted and it is not possible to keep the four parameters at the same time equal. For example, in order to keep the same Froude number the velocity of the model has to be smaller than of that of the full scale, contrarily for the consistence of the Reynolds number or Weber number the velocity has to be higher. Only one parameter at a time can be maintained equal to real scale and the other three have to be sacrificed.

The Euler number concerns cavitation problems, usually in the flow around the hull no cavitation problem are found and it is possible to sacrifice this parameter. The Weber number governs the spray and the surface tension effects, they have a little effect on the total of resistance and this number can be sacrificed (Larsson and Raven, 2010). The choice is reduced between two parameters, the Reynold number and the Froude number.

Thanks to the studies of Froude (Froude, 1955), the approach for calculating the resistance of the ship in experimental way is based on an important concept: the possibility to split the resistance or the total coefficient of resistance (Eq. 5.5) in two independent parts governed by the Froude number (residuary part - C_R) and the Reynolds number (frictional part C_F).

$$C_T = \frac{R_T}{1/2\rho S V^2} \qquad Eq.(5.5)$$

$$C_T = C_F(Rn) + C_R(Fn) \qquad Eq.(5.6)$$

In the towing tank is conducted the test with a a geosim model to the same Froude number of the hull at full scale. In order to have the same Froude number, the velocities to model scale and full scale must be defined by the equation:

$$V_M = V_S \sqrt{\frac{L_M}{L_S}} \qquad Eq.(5.7)$$

The test in the towing tank allows to obtain the total resistance of the model and so the total coefficient of resistance C_{TM}. The second step is to use the ITTC'57 formula in order to find the frictional component of the model (Eq.5.8). In this equation the number of Reynolds is the one in model scale.

$$C_{FM} = \frac{0.075}{(\log Rn_M - 2)^2} \qquad Eq.(5.8)$$

Considering that the residuary component of the model is equal to the one at full scale (Eq.5.9) and adding the frictional component, this time with the Reynolds number at full scale, the total coefficient at full scale is obtained (Eq.5.10).

$$C_{RM} = C_{TM} - C_{FM} = C_{RS} \qquad Eq.(5.9)$$

$$C_{TS} = C_{RS} + \frac{0.075}{(\log Rn_S - 2)^2} \qquad Eq.(5.10)$$

5.2 Design and shape of all models tested

The starting point was the original hull form (Model A) without cavity. This hull form was relative to an Abacus Marine yacht which main dimensions and constructive characteristics are shown in Table 1. This model is used as a basis for the successively comparison with the models with different bottom shape. The hull design is shown in Figure 1 and all the hydrostatic characteristics are reported in Figure 2. The original hull is a typical planning hull with V shape.

Symbol	Ship	Model	Unit
LOA	17.53	2.92	m
LWL	14.88	2.48	m
LP	16.20	2.70	m
BWL	4.35	0.72	m
BPX	3.72	0.62	m
BPA	3.20	0.54	m
BPT	3.66	0.61	m
T	1.00	0.17	m
Δ	34	0.15	t
S	69	1.92	m^2
AP	52.2	1.45	m^2
x_G (% of LOA)	35.18 %	35.18 %	-

Table 1 - Main dimensions of original hull model (Model A)

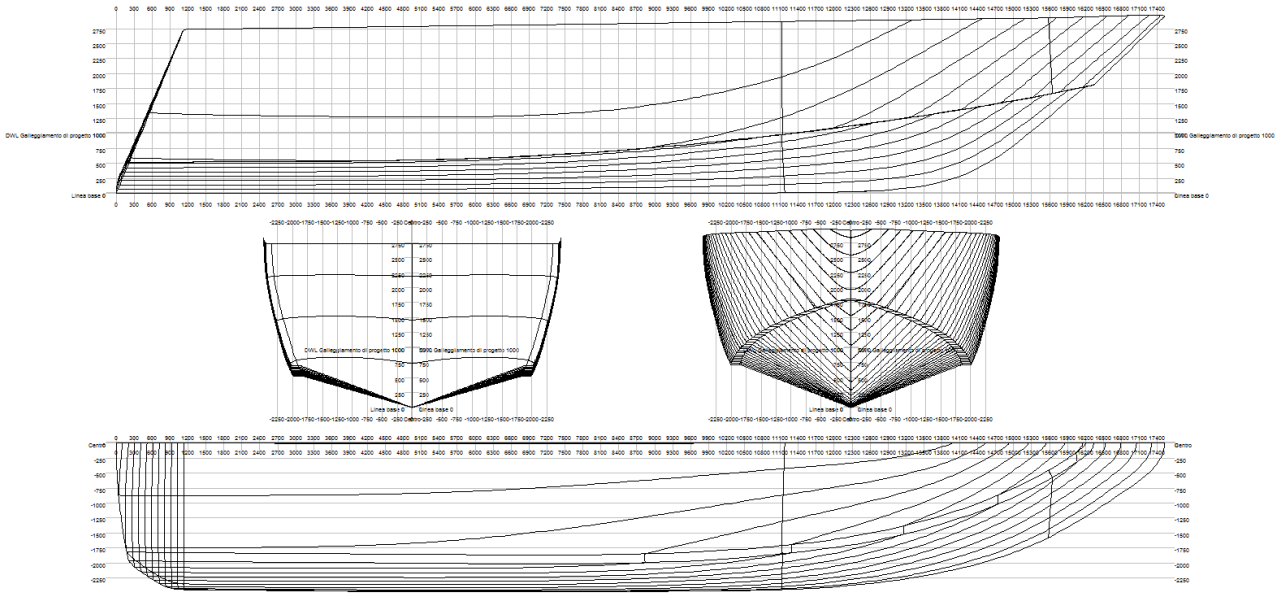

Figure 1 - Lines plan at full scale of Model A

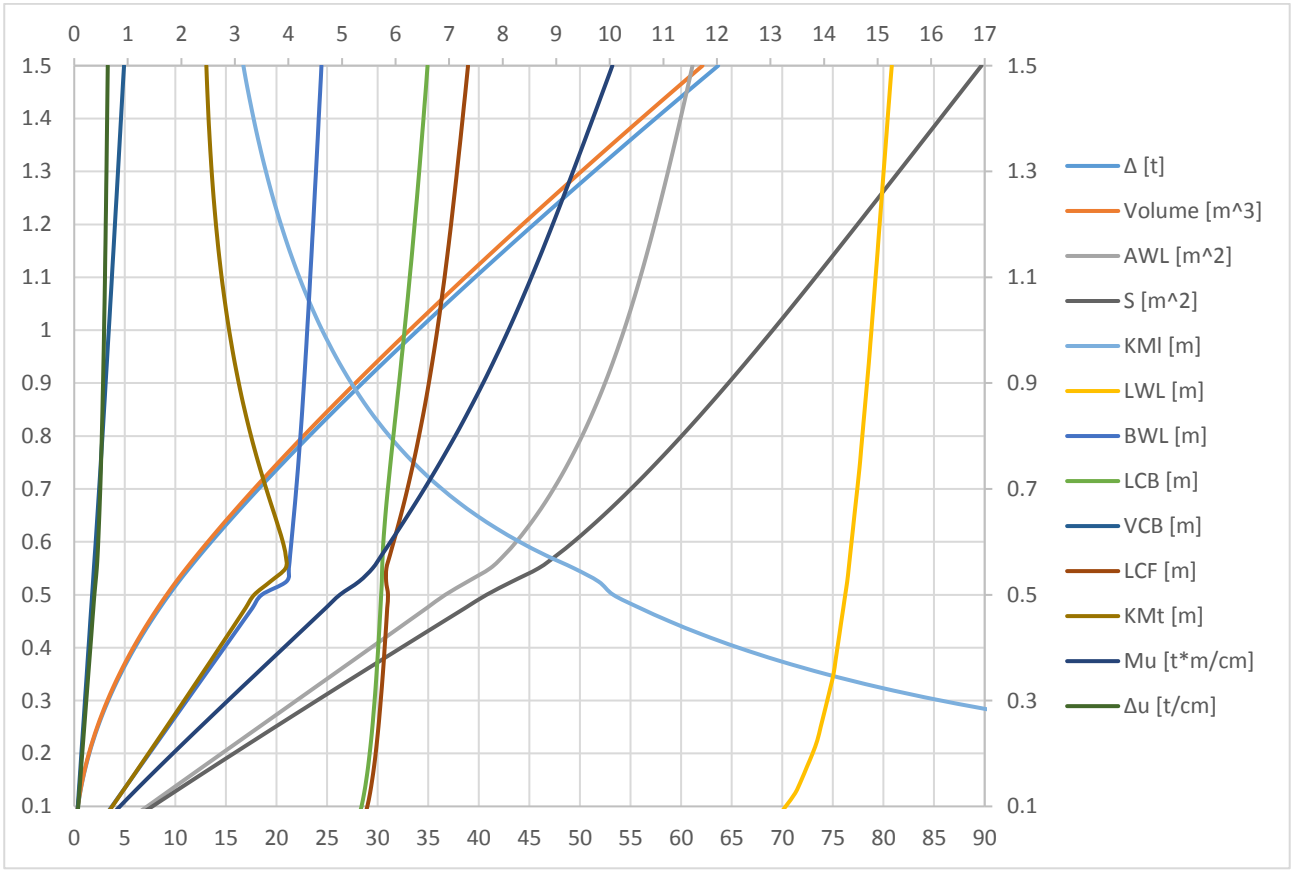

Figure 2 - Hydrostatic quantities of Model A at full scale

The sectional are to the project draught is shown in Figure 3 for the mother hull. There is not discontinuity along the longitudinal position of the sectional area.

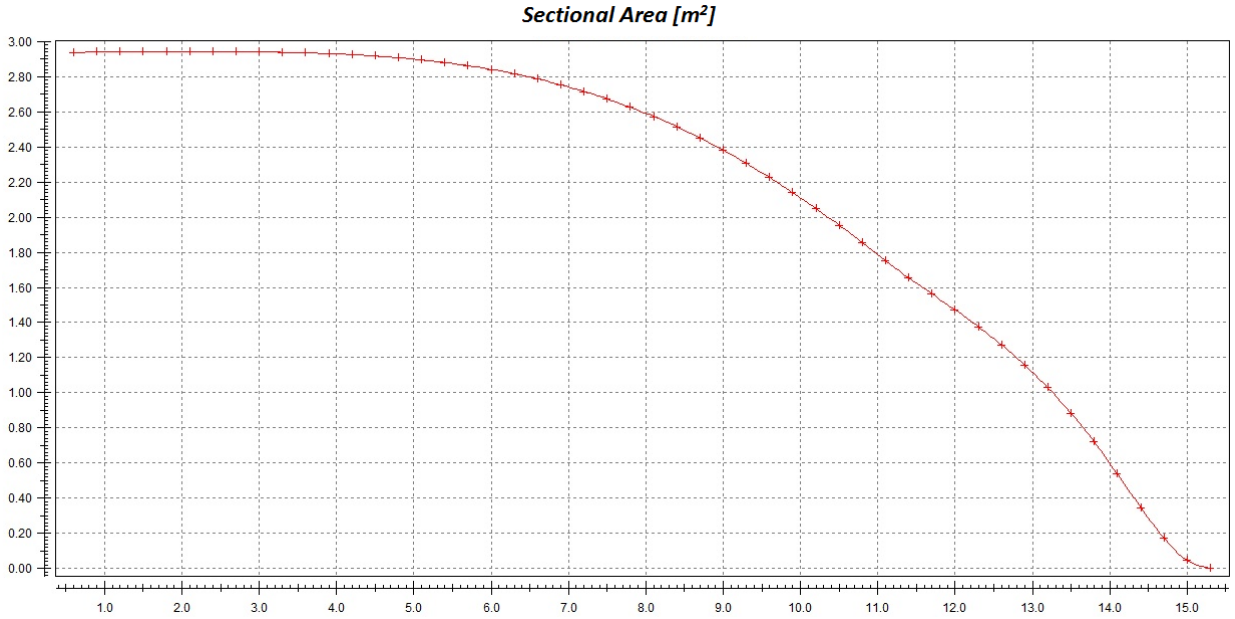

Figure 3 - Sectional Area along the longitudinal position to the Displacement of Project - Model A at full scale

In order to describe appropriately the geometry of the hull, besides the traditional characteristics, other geometric dimensions are also described, according to Larsson and Eliasson (Larsson and Eliasson, 2000). Three principal curves and several parameters based on the projected area AP are reported for every model. AP is the projection of the bottom part of the hull (part between the keel and the chine) on a horizontal plane (OXY in this case). Respect this area four dimensions could be defined: BPT (transom projected Beam), BPX (maximum projected beam), BPC (beam at a generic X position in longitudinal direction) and the Projected Length LP (Figure 4). In the Figure 5 is reported the definition of the deadrise angle β. The last parameter is the Height of the buttock line (HLM) at 0.25 BPA from the symmetry plane (Figure 6). This height is measured respect to a line tangent to the bottom of the hull at stern.

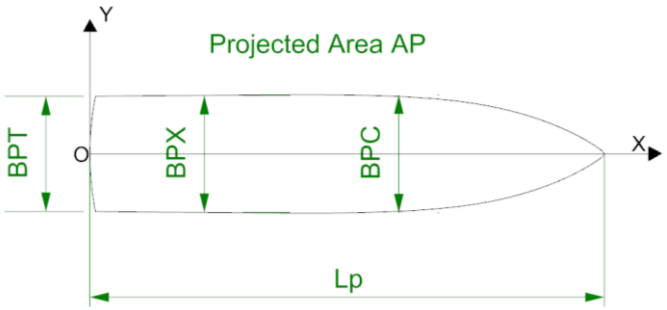

Figure 4 - The projected area with the main characteristics,

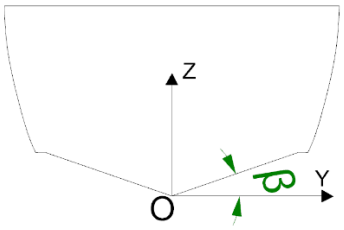

Figure 5 - Deadrise Angle

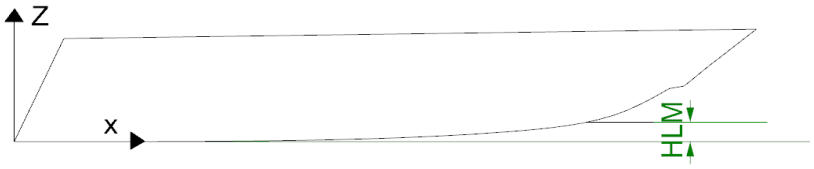

Figure 6 - Buttock at 0,25 BPA from the symmetry plane and definition of the HLM

The Figure 7 shows a CAD representation of the original hull form and in Figure 8 is reported the deadrise angle in function of the longitudinal position. The first part of the hull has a constant deadrise angle, it starts to increase to a 30% of the Lp. As shown in Figure 9, the beam along the longitudinal position is constant for the most part of Lp. In the same Figure, the height of longitudinal profile is zero for the first 40% of Lp.

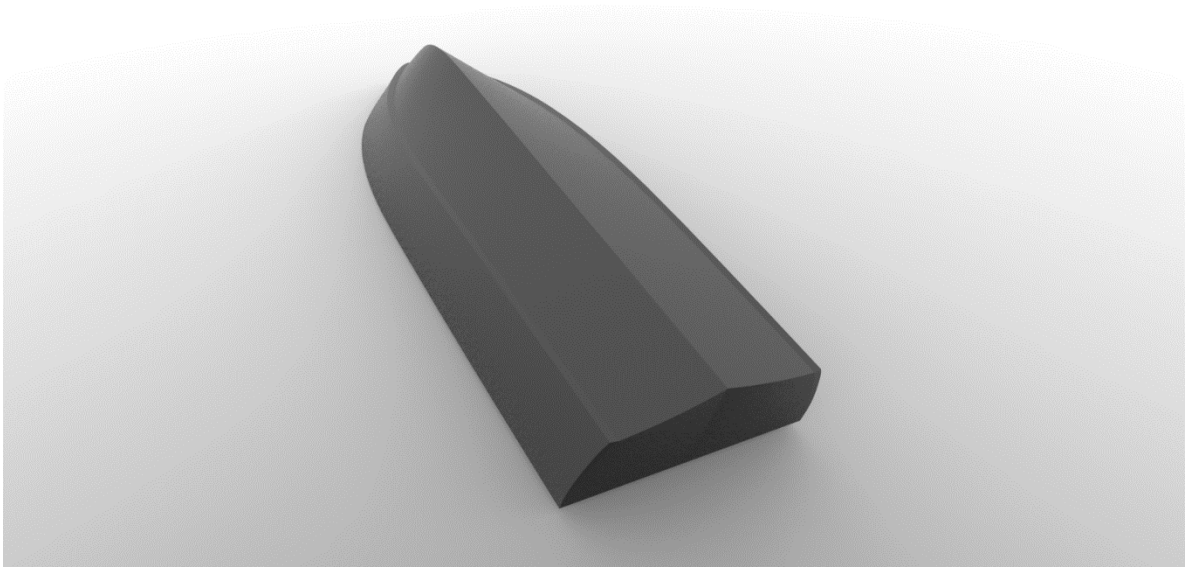

Figure 7 - Hull form (Model A) without cavity

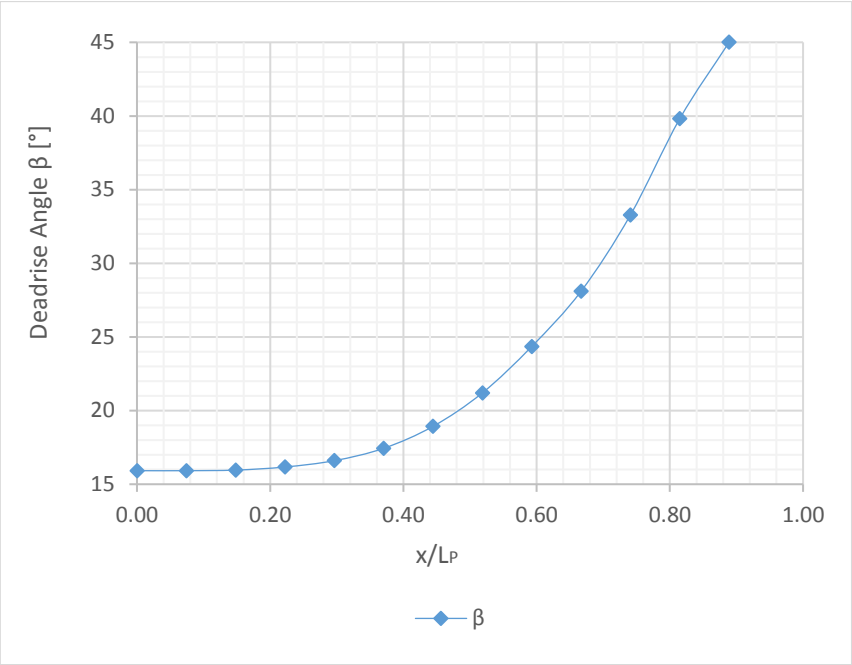

Figure 8 - The deadrise along x/LP - Model A

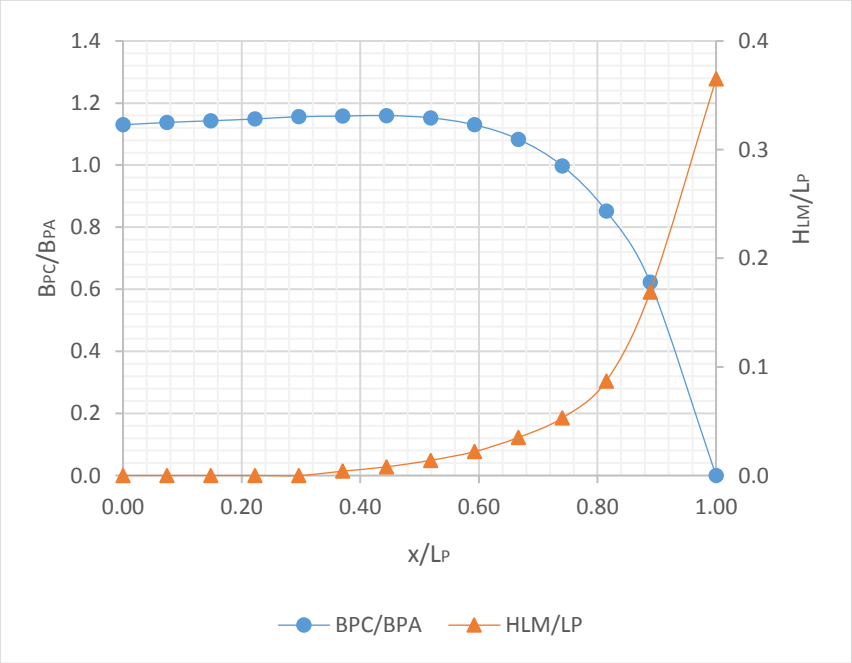

Figure 9 - The distribution of the projected beam and the distribution of HLM along x/LP - Model A

The design philosophy, for this kind of ACS, was to imagine a cavity that could take advantage to the bottom low pressure, typical of planing hulls. This low pressure develops naturally aft the pressure peak in correspondence of the stagnation line (Morabito, 2014). In this region, the total pressure can be near to the local hydrostatic pressure, and, in presence of steps, can reach negative values (in relative terms).

Unlike the traditional displacement ACS, in order to take advantage of this phenomenon, the cavity proposed by the author, is much less deep and the ventilation plant is very small with a great advantage in terms of power saving. In this way, rather than an air-cushion, the idea was to create an air-layer. This approach allows obtaining a bottom cavity that does not alter very much the original hull geometries and that is less invasive, in particular for the seakeeping and the increment of the wetted surface.

The first design of the bottom cavity has been a single large hollow, called “stepped hull” (Model B). The body plan of the hull is reported in Figure 10 and the hydrostatic characteristics are reported in Figure 12. The chine of the hull is the same of the original one and, as shown in the body plan the step has been added to 8 m (model scale) away from the stern.

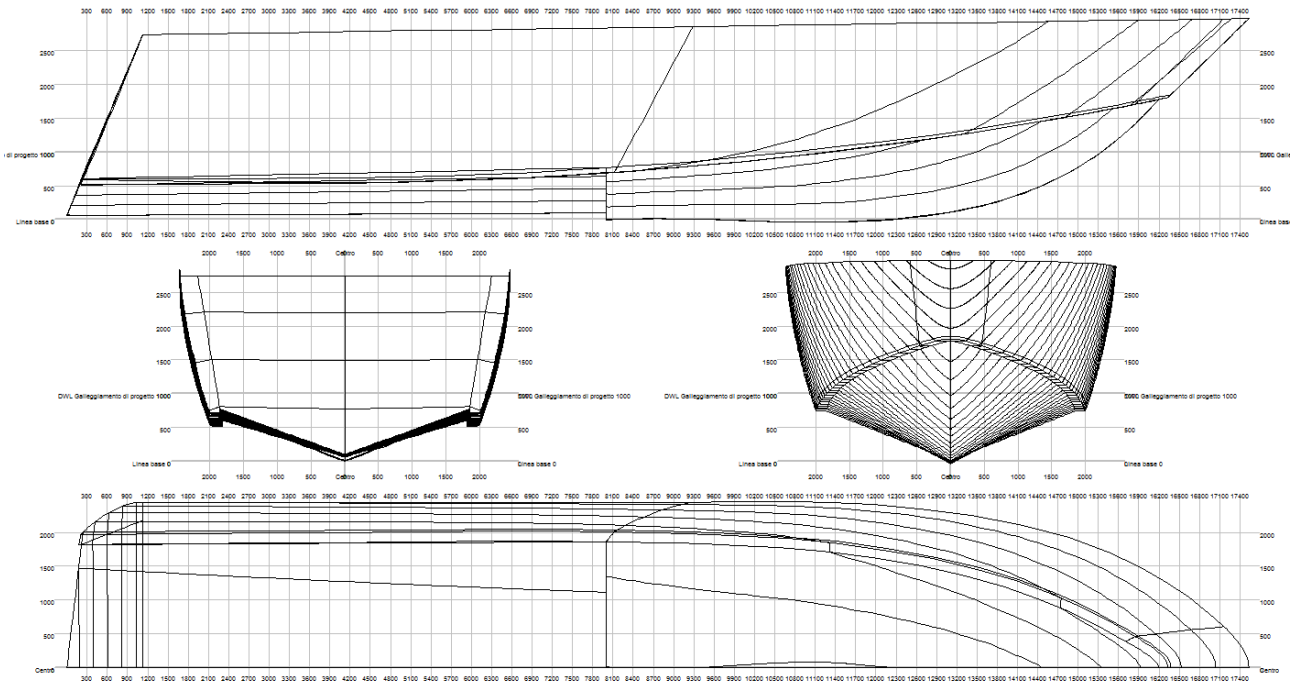

Figure 10 - Lines plan of Model B at full scale

In Figure 11 is shown the sectional area at full scale with the presence of the discontinuity in the position of the step to a position reported in L_{ST} Table 2.

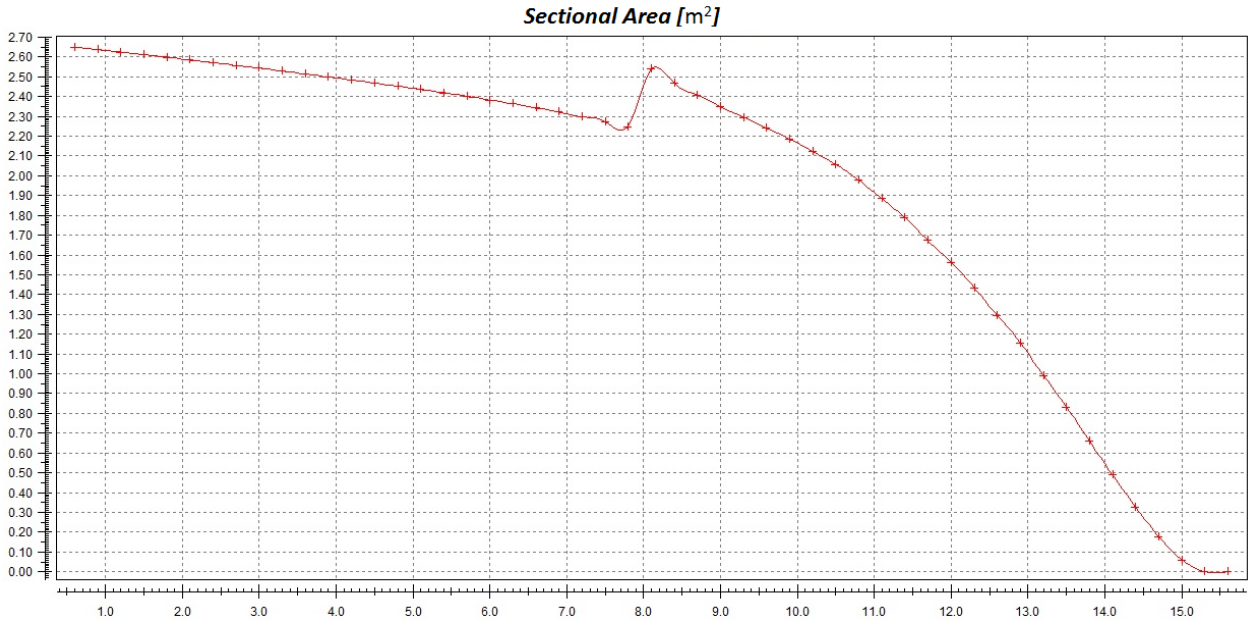

Figure 11 - Sectional Area along the longitudinal position to the Displacement of Project - Model B at full scale

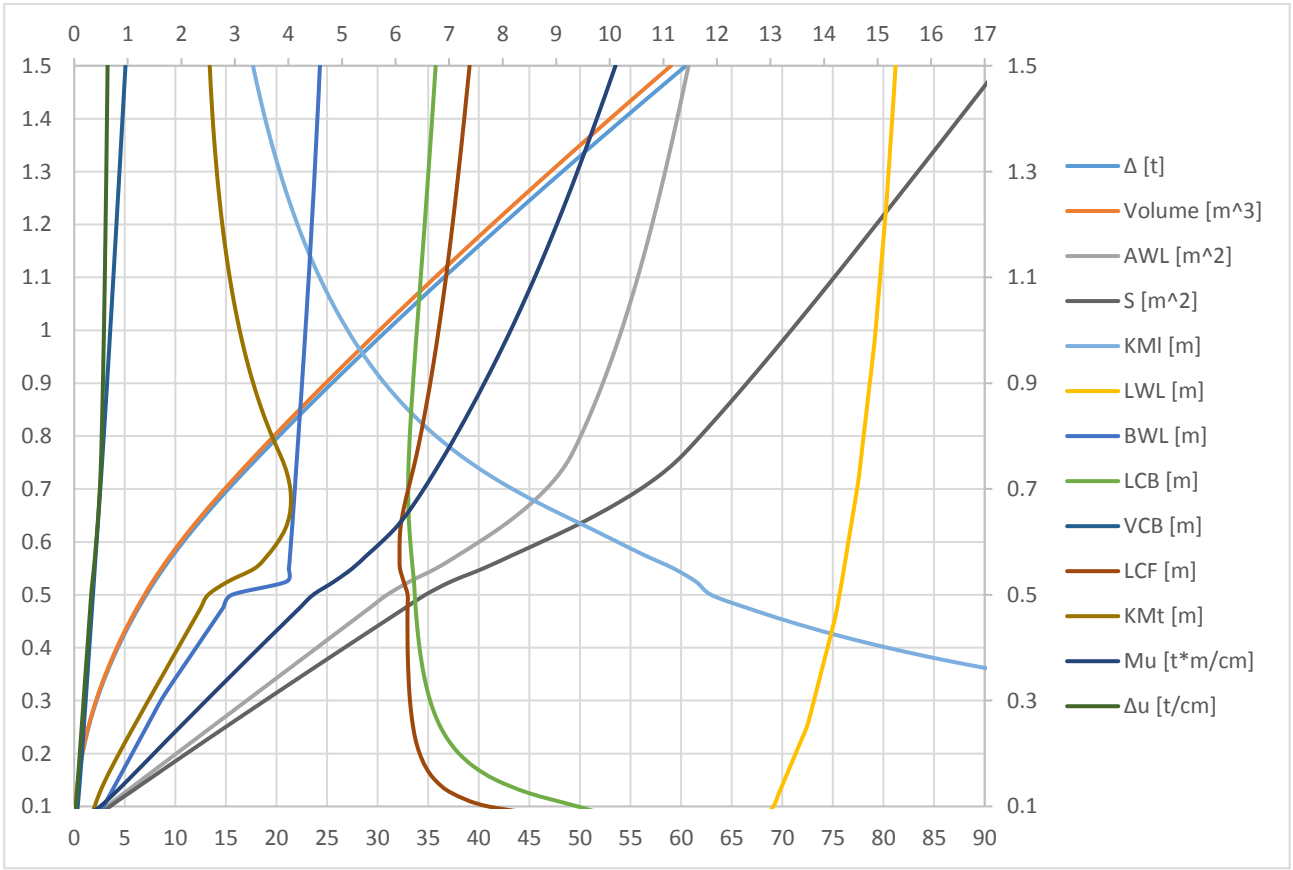

Figure 12 - Hydrostatic quantities of Model B at full scale

In Matveev (Matveev, 2015) a study that concerns the influence of the height of the step and the position in the bottom has been investigated, in the conclusions of this paper it highlights the lack of experimental data in cavity ship with stepped solution. The principal idea of this solution is related to ventilation behind a wedge attached to a horizontal wall. Figure 13 shows hull form of the stepped hull with a focus on the surface zone interested by air cavity. The Table 2 shows the main dimensions of this model, with position of the step, surface of the step and surface of the nozzles. In this case the percentage between the surface of the step and surface of the nozzles (fill rate) is 92.5%. The number of nozzles is 40.

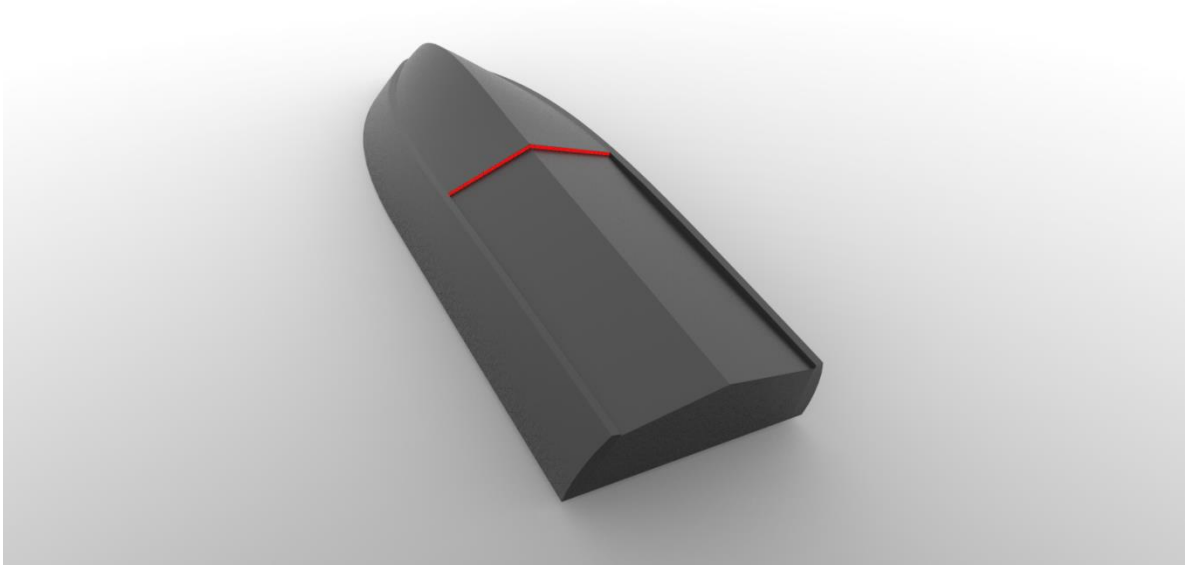

Figure 13 - Monostep solution (Model B)

Dimensions	Ship	Model	Unit
LWL	14.96	2.49	m
LP	16.2	2.7	m
BWL	4.32	0.72	m
BPX	3.72	0.62	m
BPA	3.2	0.53	m
BPT	3.66	0.61	m
T	1.00	0.17	m
Δ	34	0.15	t
S	70.9	1.97	m^2
x_G (% of LOA)	36.49 %	36.49 %	-
AP	51.84	1.44	m^2
N_{ST}	1	1	-
L_{ST}	8.00	1.33	m

S_{ST}	0.332	0.009	m^2
N_{IN}	40	40	-
B_{IN} x H_{IN}	0.085 x 0.09	0.0142 x 0.015	m x m
S_{IN}	0.307	0.0085	m^2

Table 2 - Main dimensions Model B

In Figure 14 are reported the graphs with the geometric parameters. The trend of the deadrise angle is the same of the original hull. There is a discontinuity of the parameter HLM for the presence of the step (Figure 15). The idea for this model was to keep the same principal parameters of the original hull.

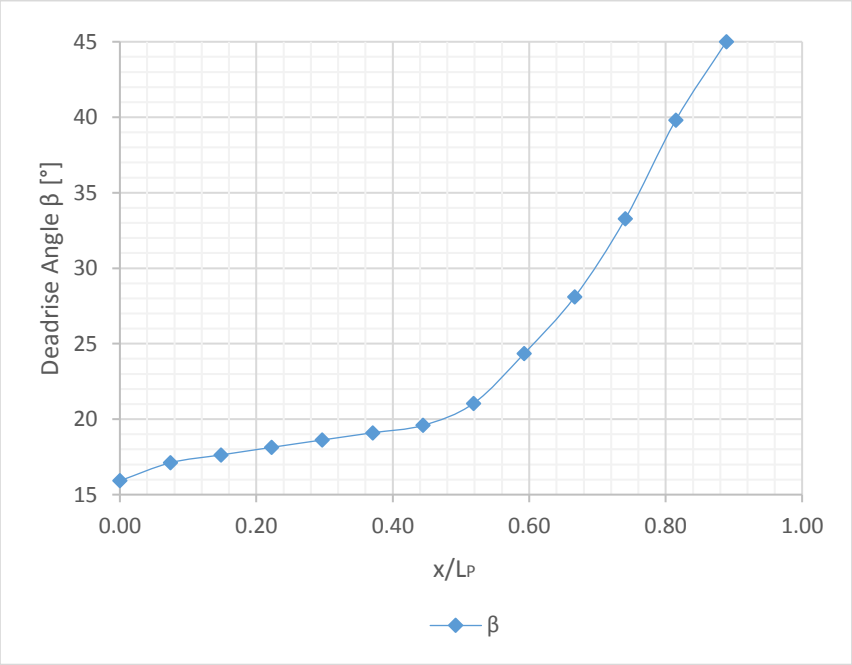

Figure 14 - The deadrise and on right along x/LP - Model B

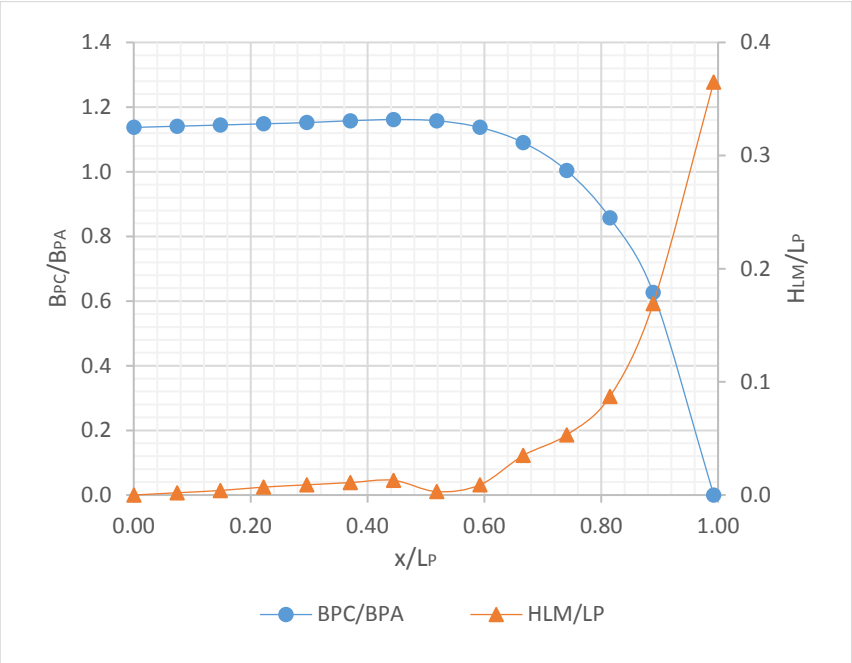

Figure 15 - the distribution of the projected beam and the distribution of HLM along x/LP - Model B

A second configuration (Model C) is a multi-steps solution. The body plan of the model is showed in Figure 16 and the hydrostatic quantities in Figure 17. The position of the steps is 5 m and 9 m away from the stern.

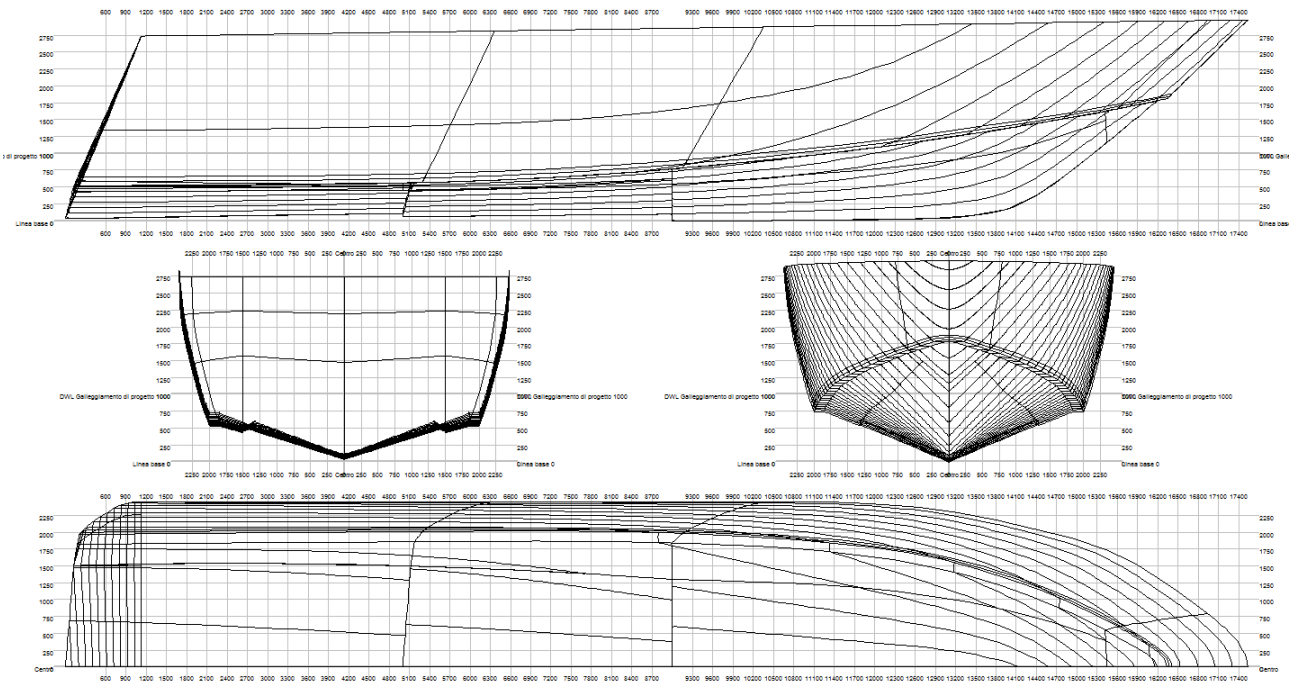

Figure 16 - Lines plan reported in real scale of Model C

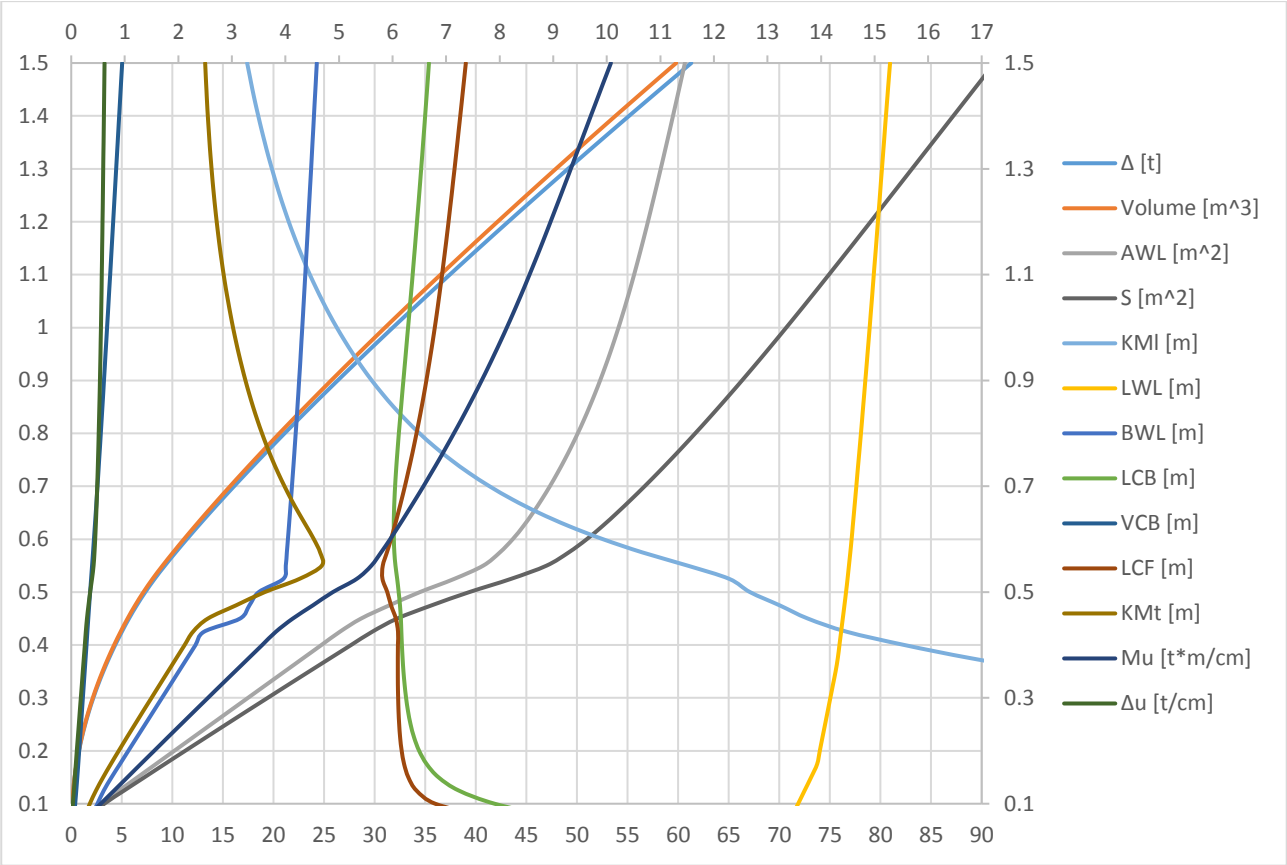

Figure 17 - Hydrostatic quantities of model C in real scale

In the case of Model C the sectional area curve is different respect to each other. In this case there are two discontinuities, in the position of the first step and in the position of the second step as shown in Figure 18.

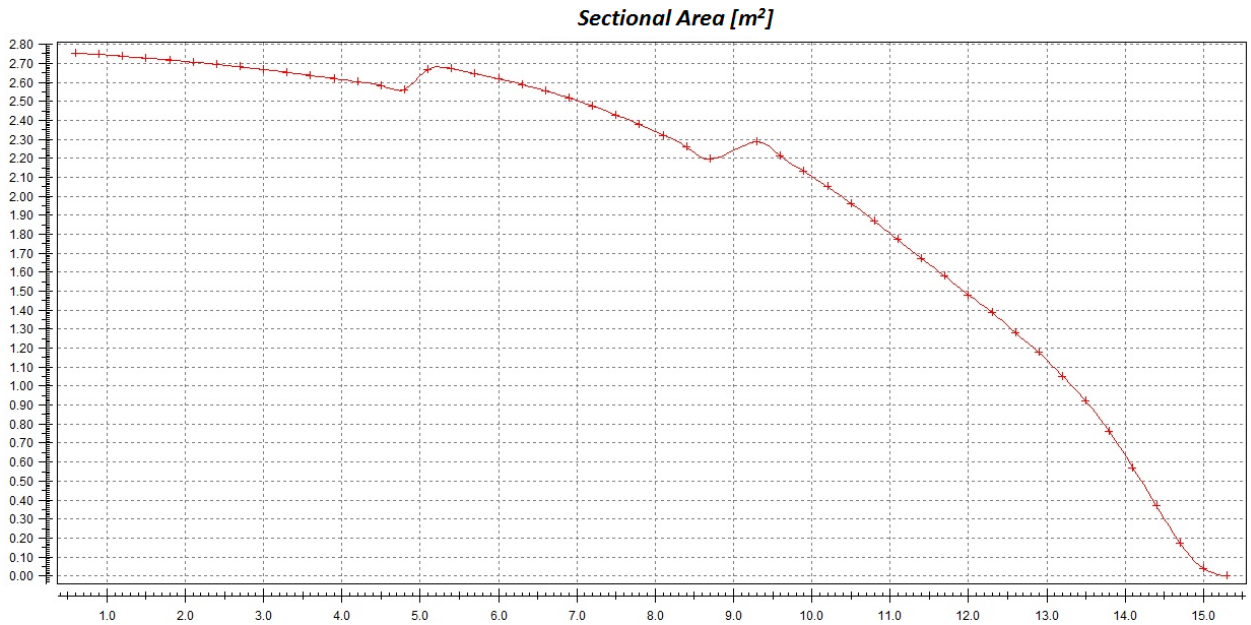

Figure 18 - Sectional Area along the longitudinal position to the Displacement of Project - Model C at full scale

This kind of solution is suggested if the air-cavity length could not be extended to the whole hull length, principally to low speed conditions. A series of steps are used in the bottom of the hull (Figure 19), with different injections of air along the vessel length. The multi-step solution requires more modifications in the bottom of the original hull, respect to mono-step solution but the air cavity should be more stable. The Table 3 shows the main dimensions of this model, with position of the two steps, relative area of the steps and total area of the nozzles. The number of the nozzles is 8 for the first step and 8 for the second step, in the first case the fill rate is 93 % and in the second step is 92 %. In Figure 20, the three parameters above described are represented respect to x/LP. A parametric CAD has been developed for a faster reconstruction of the geometry model and for eventual changes in the future (Figure 19).

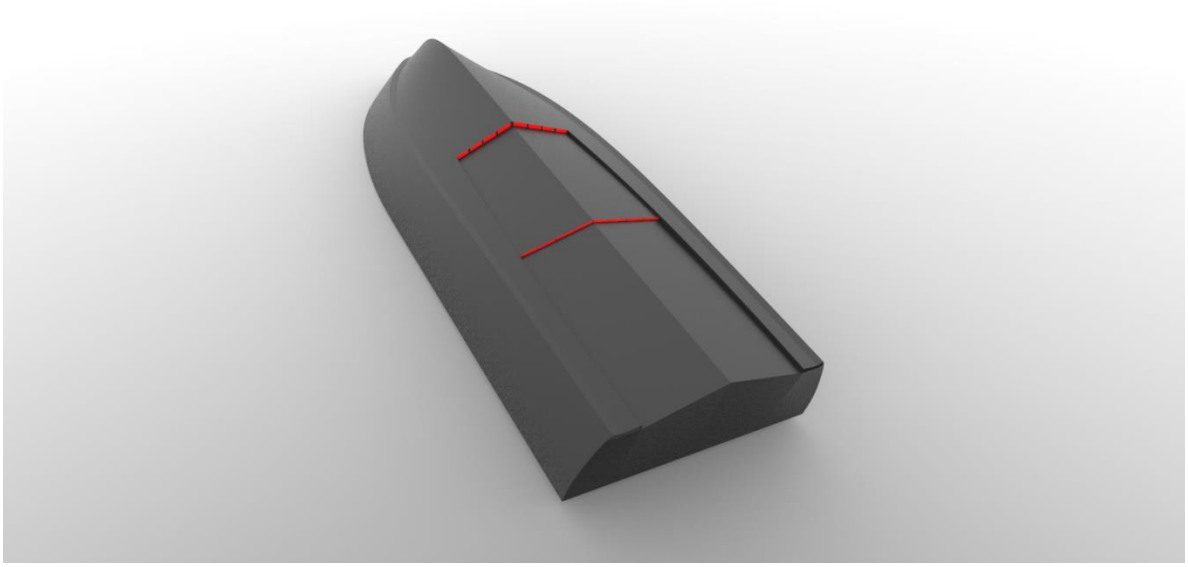

Figure 19 - Multi-steps hull (Model C)

Dimensions	Ship	Model	Unit
LWL	14.908	2.485	m
LP	16.2	2.7	m
BWL	4.314	0.719	m
BPX	3.72	0.62	m
BPA	3.2	0.54	m
BPT	3.66	0.61	m
T	1.000	0.167	m
Δ	34	0.153	t
S	70.7	1.963	m^2
x_G (% of LOA)	35.88 %	35.88 %	-
AP	52.2	1.45	m^2
N_{ST}	2	2	-

Main Dimensions STEP 1			
L_{ST1}	5.00	0.833	m
S_{ST1}	0.150	0.004	m^2
N_{IN1}	8	8	-
B_{IN} x H_{IN}	0.38 x 0.046	0.063 x 0.0076	m x m
S_{IN1}	0.14	0.0038	m^2
Main Dimensions STEP 2			
L_{ST2}	9.00	1.5	m
S_{ST2}	0.234	0.0065	m^2
N_{IN2}	8	8	-
B_{IN} x H_{IN}	0.3 x 0.09	0.05 x 0.015	m x m
S_{IN2}	0.216	0.006	m^2
Total Contribution of Steps			
S_{IN}	0.356	0.0098	m^2

Table 3 - Main Dimensions of Model C

In the case of Model C, the deadrise is slightly different with respect to the original hull because of the presence of two steps (Figure 20). The beam of the chine have been maintained constant with respect to the original hull. The value of HLM is different respect to the original hull. There are two discontinuities and the longitudinal profile is modified in order to accommodate these two steps (Figure 21).

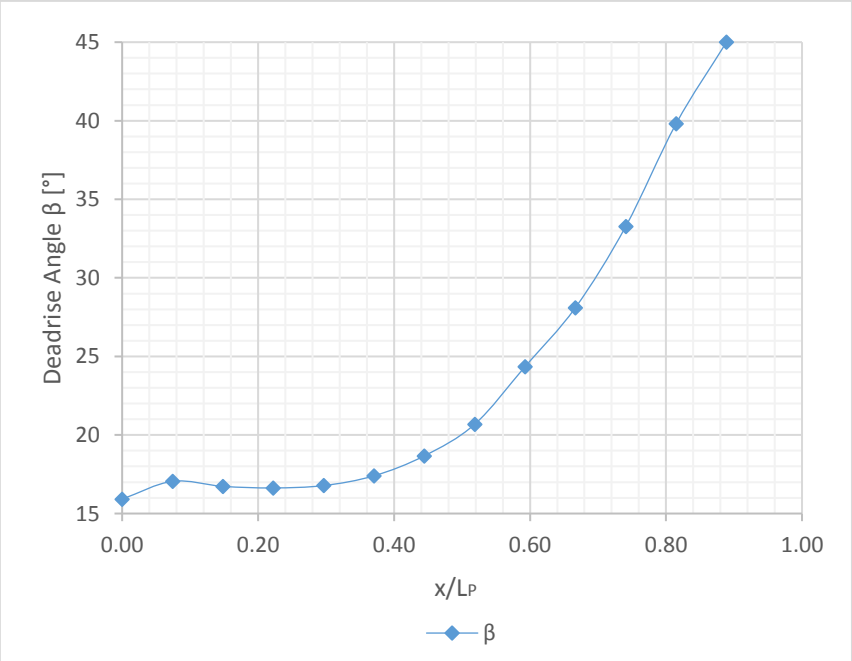

Figure 20 - The deadrise along x/LP - Model C

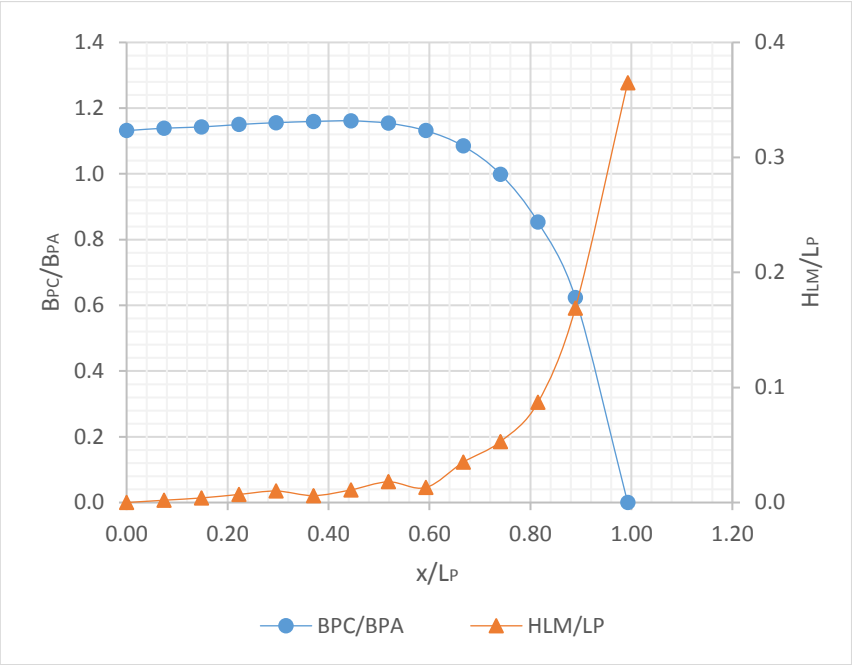

Figure 21 - The distribution of the projected beam and the distribution of HLM along x/LP - Modelc C

The last configuration (Model D) is obtained with a cavity identical to that of Model B, but with the insertion of longitudinal rails (Figure 25). The body plan is reported in Figure 22 and the hydrostatic quantities are reported in Figure 23.

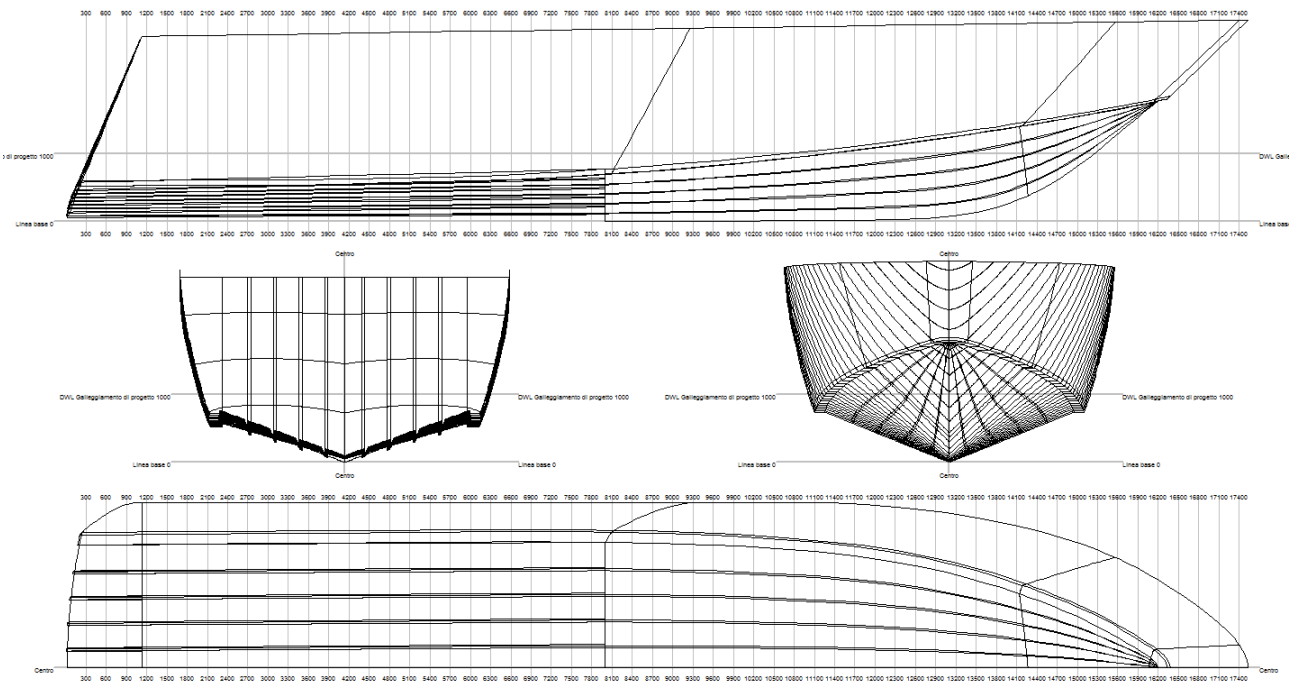

Figure 22 - Lines plan in real scale of Model D

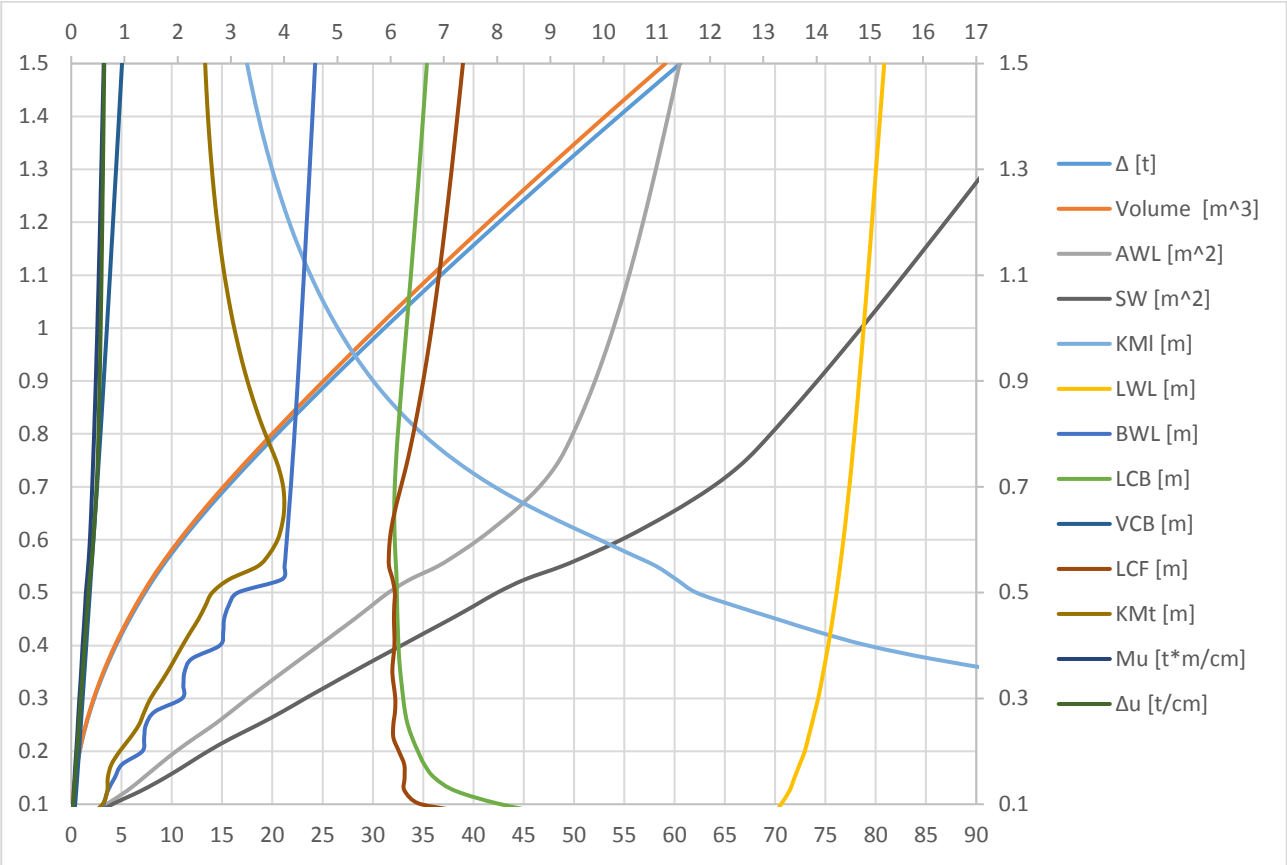

Figure 23 - Hydrostatic quantities of Model D in real scale

The sectional area to the displacement of project is reported in Figure 24. The position of the step is shown in this graph with the discontinuity to the correspondent position.

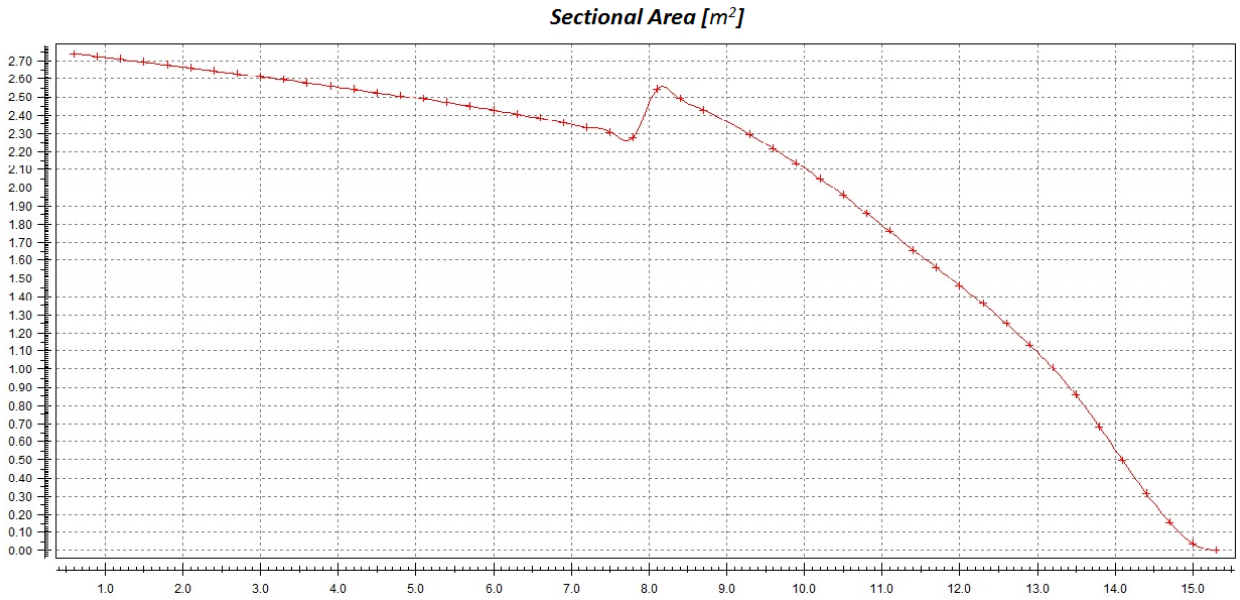

Figure 24 - Sectional Area along the longitudinal position to the Displacement of Project – Model D

A great problem for the stability of the air-cavity is the escape of the air in transversal direction, due to the V-shape of the hull. The presence of longitudinal rails allows channeling the flow reducing the possibility to escape from transversal direction. The numbers and dimensions of these channels depend to the dimension of longitudinal rails. The Table 4 shows the main dimensions of this model. In this case the area of the step where is possible to obtain air injection is reduced by the section area of the longitudinal rails, so the area is 0.304 m^2. The fill rate respect to this area is 92 %. In the table are reported the dimensions of rectangular section of the rail and the distance between each other and in Figure 26 the three parameters above described are represented respect to x/LP.

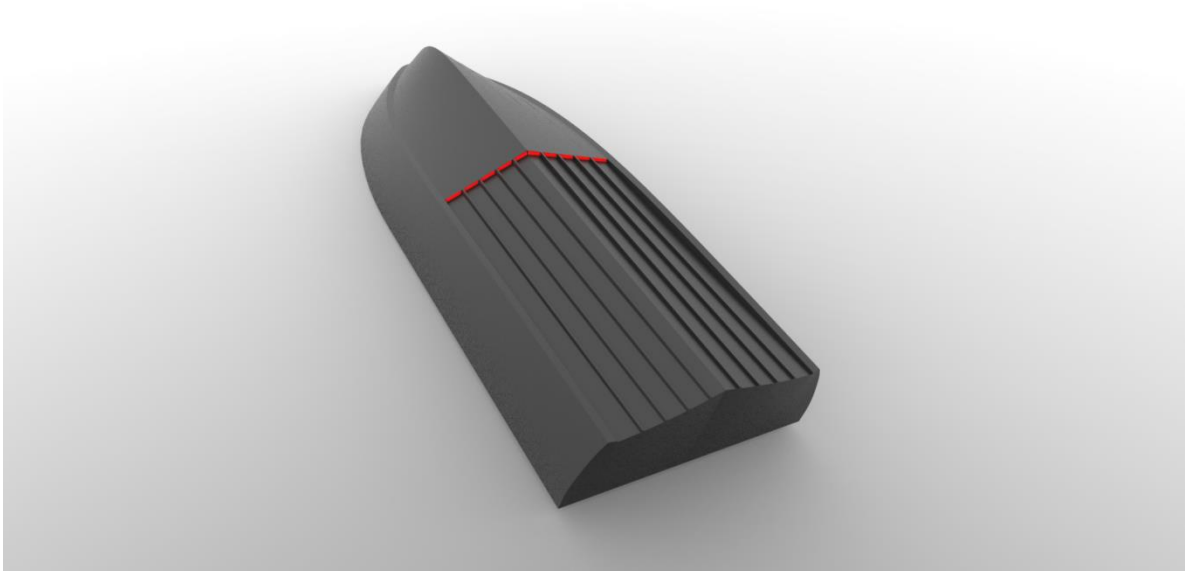

Figure 25 - Longitudinal rails hull (Model D)

Dimensions	Ship	Model	Unit
LWL	14.884	2.481	m
LP	16.2	2.7	m
BWL	4.314	0.719	m
BPX	3.72	0.62	m
BPA	3.2	0.54	m
BPT	3.66	0.61	m
T	1.000	0.167	m
Δ	34	0.153	t
S	78.6	2.182	m^2
x_G (% of LOA)	35.92 %	35.92 %	-
AP	52.2	1.45	m^2
N_{ST}	1	1	-
L_{ST}	8.00	1.333	m

S_{ST}	0.304	0.0084	m^2
N_{IN}	10	10	-
B x H	0.31 x 0.09	0.051 x 0.015	m x m
S_{IN}	0.279	0.0077	m^2
Longitudinal Rails Dimensions			
N	8	8	-
B_R x H_R	0.041 x 0.059	0.007 x 0.01	m x m
TD_R	0.340	0.056	m

Table 4- Main Dimensions of Model D

The deadrise trend shown in Figure 26 is the one without considering the deadrise of the rails.The rails have a bottom surface parallel to the one of the hull. They have not been designed for to decrease the average value of the deadrise. This choice has been done in order to keep the average deadrise equal to original one. These rails have been designed only for better directing the air flow during the injection.

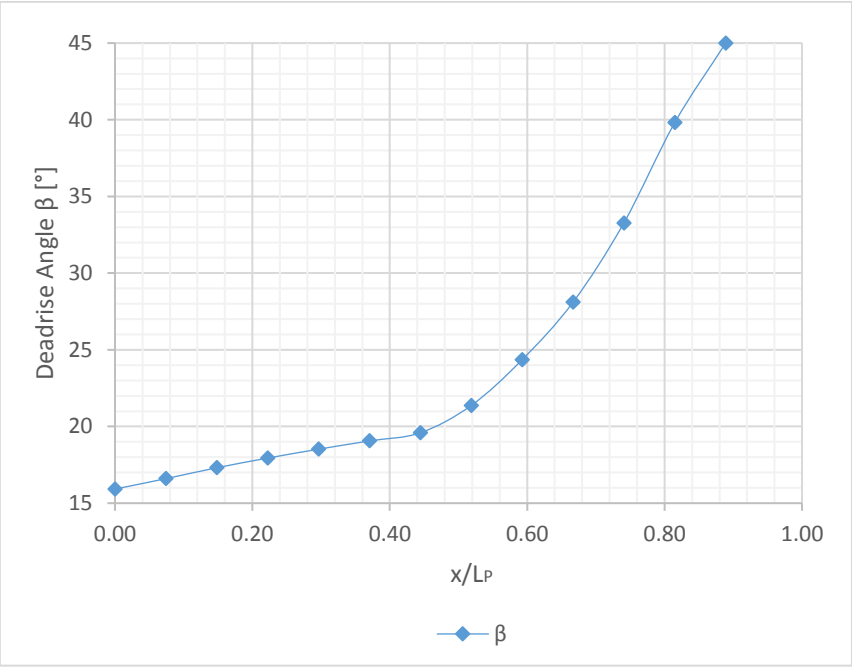

Figure 26 - The deadrise and along x/LP - Model D

Figure 26 shows the trend for the beam of the chine and the HLM and these two parameters are the same of the original hull.

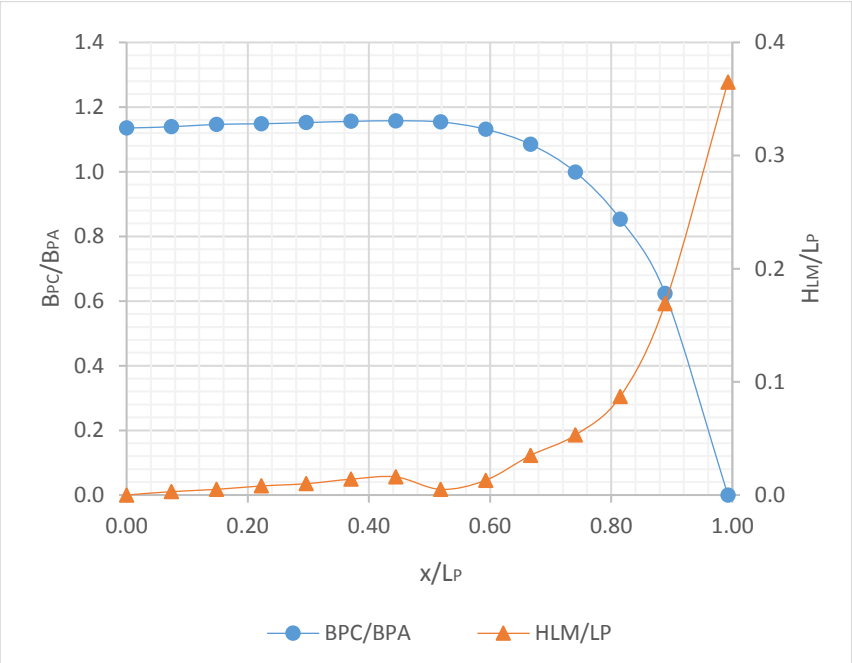

Figure 27 - The distribution of the projected beam and the distribution of HLM along x/LP - Model D

In all the proposed solutions, the percentage of area for air flow injection is between 90 % and 93 % of the total area of the correspondent step. In general, the addition of element as steps or rails increases the wetted surface (Figure 28), this at expense of friction drag, because this resistance is heavily dependent by that area. The major increase of the wetted surface is in Model D, due to the presence of the longitudinal rails. The other dimensions are the same for every model.

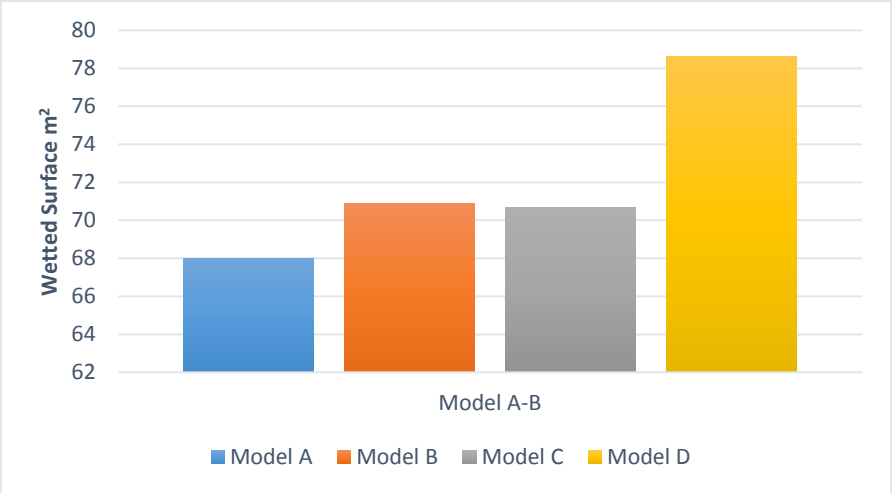

Figure 28- Wetted Surface Area

The general idea during the phase of design was to keep all the principal dimensions of modified hulls (angle of deadrise, BPC and HLM) equal to the original one in order to evaluate the difference of the performances caused by only the different of the bottom shapes. It clears that this condition was difficult for the hull with two steps where the geometry is slightly different with respect to the other three.

5.3 Model manufacturing

The number of models for the towing tank test is four, but in order to reduce the costs, a single chassis model has been defined, and the four different bottom hulls have been fixed to the chassis with fasteners (Figure 29). The design of the different bottoms has been normalized to an only length in order to simplify the setup of the chassis. The principal dimensions are shown in Figure 29 while picture of the chassis model is shown in Figure 30.

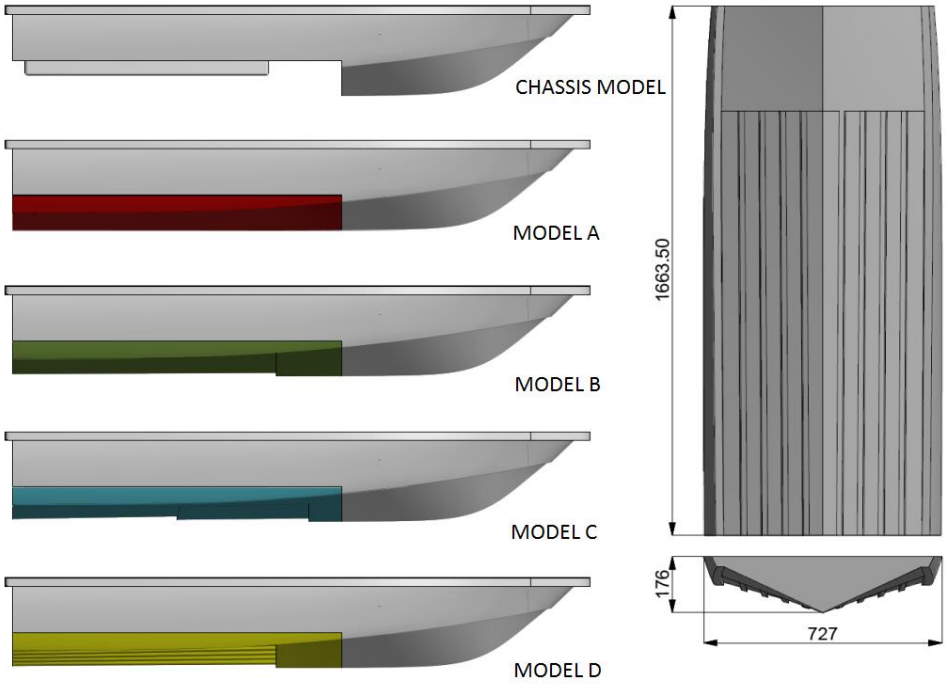

Figure 29 - Chassis model and different bottom on left - Dimensions in mm of unified bottom on right

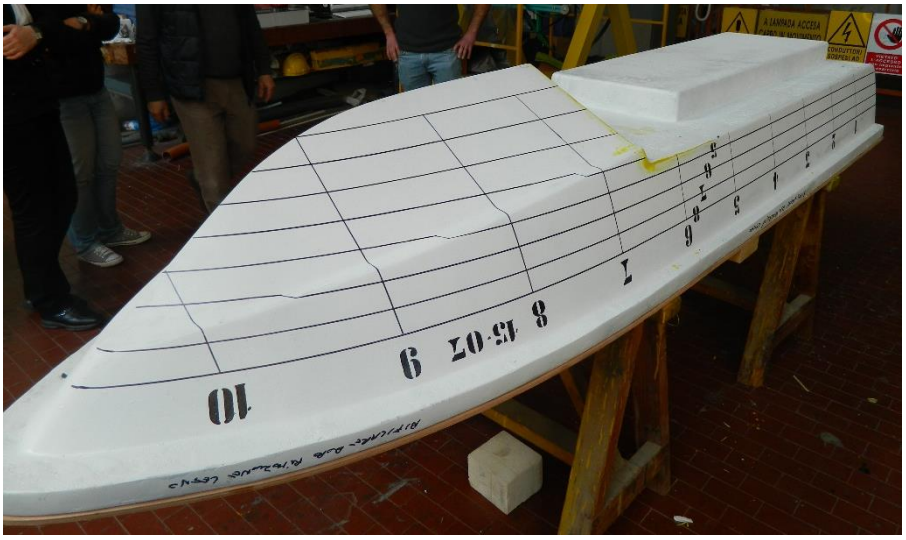

Figure 30 - Particular of the chassis of the model without the bottom

The four bottom models are shown in Figure 31. Respectively from left to right there are: the original hull, the Model B with a single step, the model C with two steps and the last model (Model D) with the presence of rails.

Figure 31 – Bottom models

The material of the model is Glass Reinforced Plastic and wood. The chassis and the different bottom hull are sandwich structures, with core in polystyrene and skins with different layer of fiberglass. Two parts have been obtained inside the chassis model for the connection with the dynamometric carriage, the central one for the entrainment of the model by the carriage and the anterior one for keeping aligned the model during the tests. According to the requirements of these tests, a constant and regulated air supply has been delivered to the model (Figure 32). The air was to be delivered by a centrifugal system with a maximum flow rate of 11 m^3/min. The flow of the air and the angular velocity of the rotor are controlled, with a closed loop the necessary flow is delivered to the system.

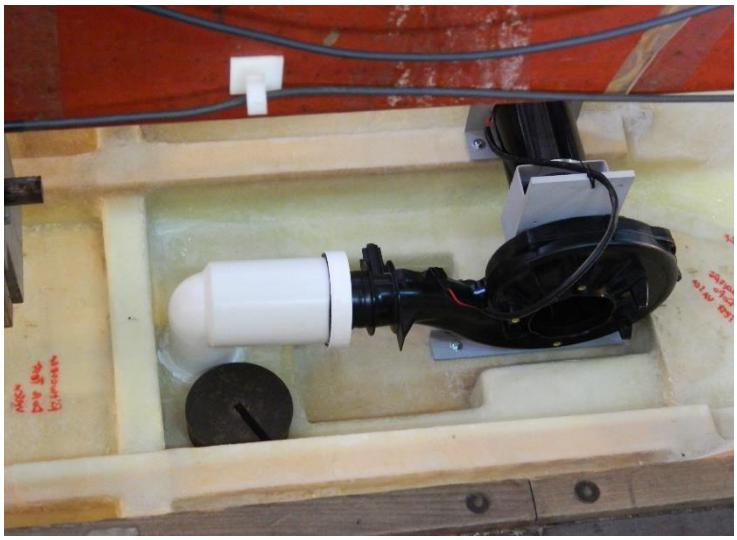

Figure 32 - Particular of the radial blower

The model has been designed in order to accommodate all necessary auxiliaries for making sea trials. In order to do this kind of trials the model can be equipped with steering and propulsion system. The steering system is defined by two rudders steered by one electrical motor with possibility to rotate between +/- 45 degrees. The propulsion system is defined by two contra-rotating propellers with five blades and 190 mm of diameter, the rotation of propellers is covered by two electrical motors with a total power of 3kW. The propulsion and steering system are shown in Figure 33.

Figure 33 – Rudders and Propellers

The power for the all elements on board is supplied by a system of 20 lithium batteries (two packs are shown in Figure 34) with a total power of 10.24 kWh in three different tension (12/24/48 V). The entire system is governed by an in-house software developed by ATEC robotics thanks to a Wireless system.

Figure 34 - Lythium Batteries

In order to keep safe the equipment inside the hull during the sea trials, a cover has been designed for the hull and for the steering system. The general dimensions are shown in Figure 35.

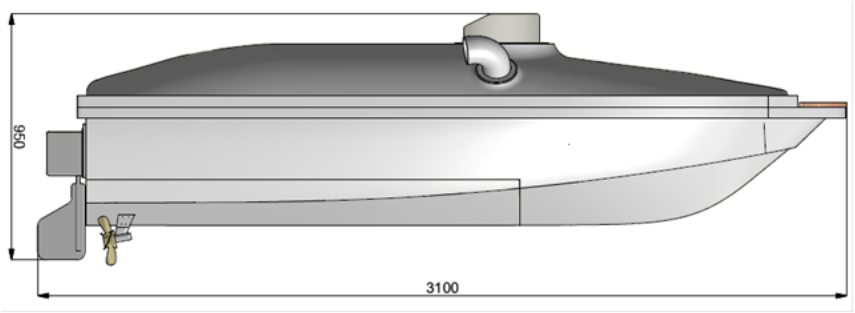

Figure 35 - General dimensions of the model

The Figure 36 (on left) shows a 3D representation of the model with all components (propellers, rudders, cover) and in the same picture, on right, is shown a picture with the real model. The porthole in the center of the ship has been designed in order to position the system for the wireless signal.

Figure 36 – Complete arrangements of the model

During the tests of this research, the model has been equipped only with the air injection system and the hull has been tested without appendages as shown in Figure 37. The total amount of weight of the model has to be equal to 0.155 t, in order to respect the proper immersion in geometric similarity with the real boat. The air is supplied via a piping system to the nozzles; the more difficult accommodation of air supplier has been for the Model C, for the presence of two steps with two different piping systems.

Figure 37 - The hull model in the towing tank

The principal aim of the tests is to obtain a better knowledge of the air ventilation phenomena, respect to different bottom hull shape. The tests focus on extrapolation of the resistance curves, varying the velocities and the air flow rate. The maximum velocity of the model depend, by means

the similitude of the Froude number (Eq.5.11), to the maximum velocity of the yacht, taking into account the maximum velocity possible for the carriage system.

$$Fn = \frac{V_S}{\sqrt{gL_S}} = \frac{V_M}{\sqrt{gL_M}} \qquad (Eq.5.11)$$

$$V_M = \frac{V_S}{\sqrt{\lambda}} \qquad (Eq.5.12)$$

The maximum velocity of the yacht is 32 knots (16.49 m/s) so, for the (Eq.5.12), the maximum velocity of the model is 6.72 m/s. This velocity is inside the work range of the towing tank. The complete series of velocities for every single trial is reported in Table 5. For each trial, the model hull and flow rate are fixed.

V_M (m/s)	V_S (m/s)	V_S (knots)	Fn
2.520	6.17	12.0	0.510
3.150	7.71	15.0	0.638
3.780	9.26	18.0	0.765
4.410	10.80	21.0	0.893
5.040	12.34	24.0	1.020
5.670	13.89	27.0	1.148
6.300	15.43	30.0	1.275
6.720	16.46	32.0	1.360

Table 5 - Series of velocities for single trial

The reference model was the Model A (original hull) and for this model only three trials for resistance curves have been conducted to three different displacements (Figure 38). For each model with air-cavity, were carried out one trial without air flow and six trials with different air flow rate. A total of 24 trials were carried out for a total amount of 192 tests conducted. In the Table 6 are reported the flow rate and displacement for every trial. The flow rate is in the range between 5500 l/min and 10500 l/min. The displacement is correspondent to 34 t of the yacht.

Number of Trial	Model	Flow rate [l/min]	Δ_M [t]	Δ_S [t]
Trial 1	Model A	No air	0.139	30.9
Trial 2	Model A	No air	0.153	34
Trial 3	Model A	No air	0.167	37
Trial 4	Model B	No air	0.153	34
Trial 5	Model B	5500	0.153	34
Trial 6	Model B	6500	0.153	34
Trial 7	Model B	7500	0.153	34
Trial 8	Model B	8500	0.153	34
Trial 9	Model B	9500	0.153	34
Trial 10	Model B	10500	0.153	34
Trial 11	Model C	No air	0.153	34
Trial 12	Model C	5500	0.153	34
Trial 13	Model C	6500	0.153	34
Trial 14	Model C	7500	0.153	34

Trial 15	Model C	8500	0.153	34
Trial 16	Model C	9500	0.153	34
Trial 17	Model C	10500	0.153	34
Trial 18	Model D	No air	0.153	34
Trial 19	Model D	5500	0.153	34
Trial 20	Model D	6500	0.153	34
Trial 21	Model D	7500	0.153	34
Trial 22	Model D	8500	0.153	34
Trial 23	Model D	9500	0.153	34
Trial 24	Model D	10500	0.153	34

Table 6 - Trials conducted. For each trial eight different velocities have been carried out

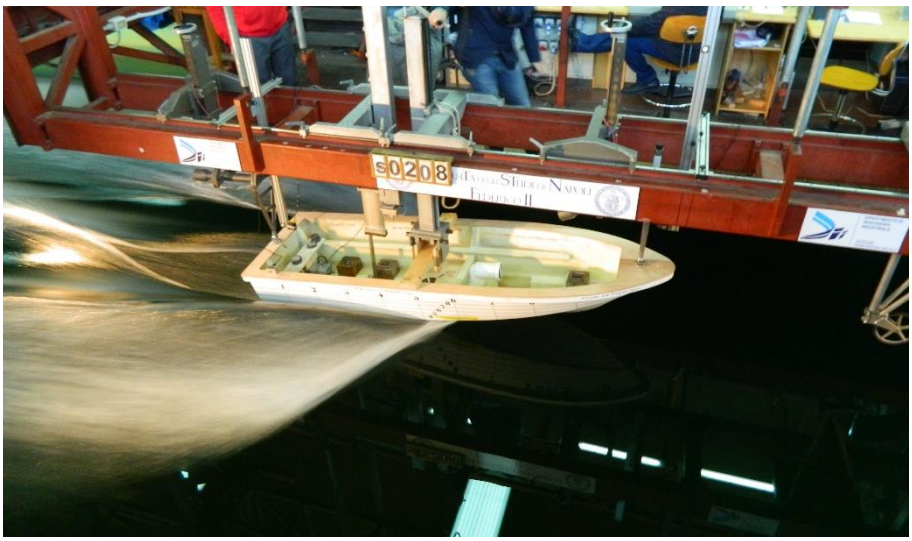

Figure 38 – A towing tank test on model A

5.4 Results and Discussion of experimental Tests

The trials produced series of resistance curves that are an important starting point for a better understanding of the behavior of the model with and without air. The first group of trials concerns the Model A i.e. the original mother-hull. These tests have been conducted with three different displacement. The values of displacement of the full-scale boat were 30.9 t, 34.0 t and 37.0 t. The curves are similar but there is a natural increase of resistance with the increase of the displacement. All the curves are reported in model scale quantities.

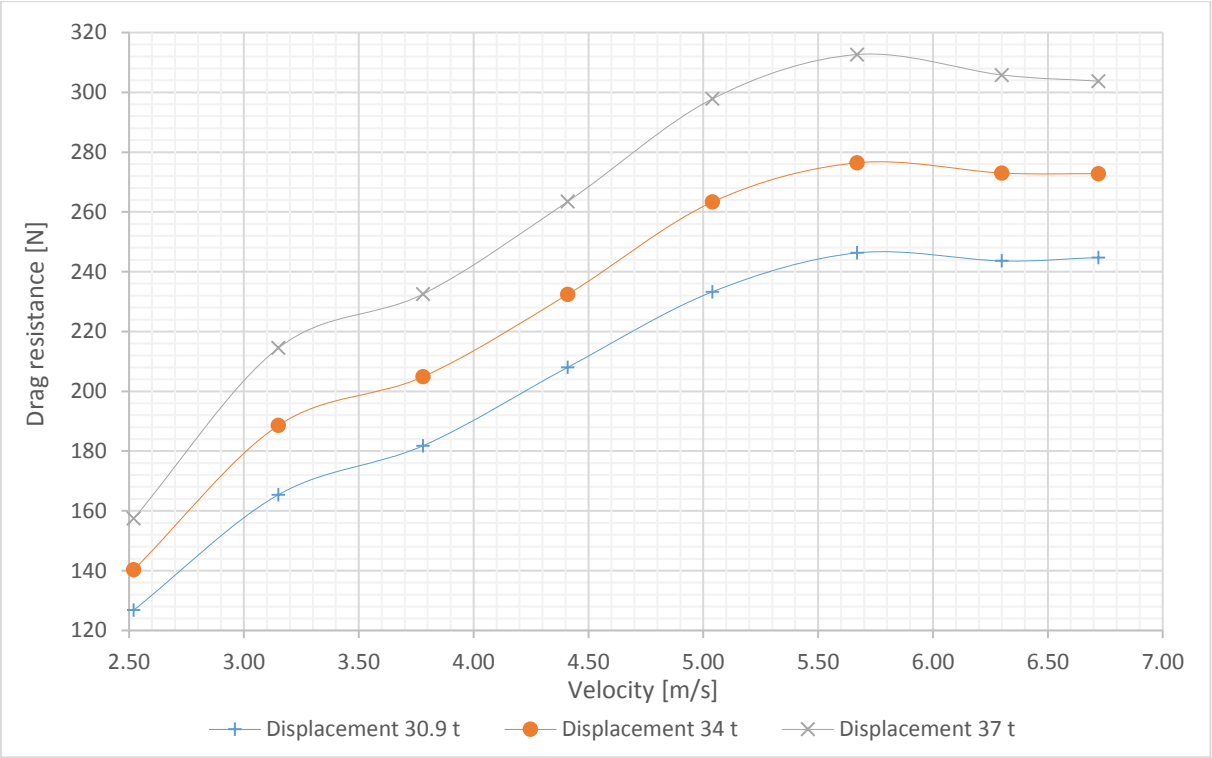

Figure 39 - Drag curves for Model A

An estimation of the Drag components has been conducted for the mother-hull (Model A), in the 34 t configuration (Figure 40). Since the model is not ventilated, the theory for the Drag components evaluation is well consolidated. This helps to understand the importance of the air injection, especially at high Froude Numbers, for which Frictional Drag can reach almost the 50 %.

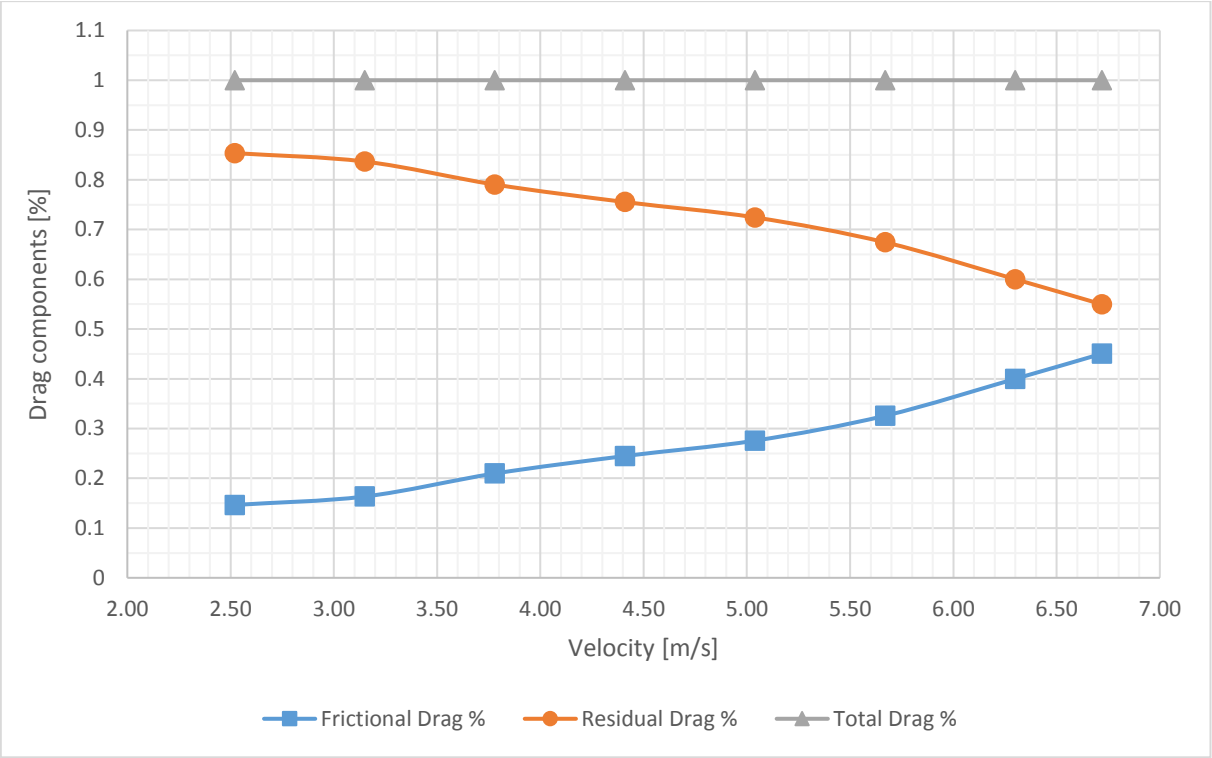

Figure 40 – Drag components for Model A (34 t)

The Model B has been tested to 34 t conditions (0.153 t in scale model) and the trend of the curves without air injection is very similar to the one of the mother hull. Figure 41 shows the general trend of all curves tested to different flow rate. There is an important drop of the curves between the no-air test and all others tests with air. The drop of the curves is little and almost constant respect to the flow rate for an interval of velocities between the first tested velocity and about 5.04 m/s, after this velocity the decrease of power requested is evident. This trend is shown for both of models in Figure 41.

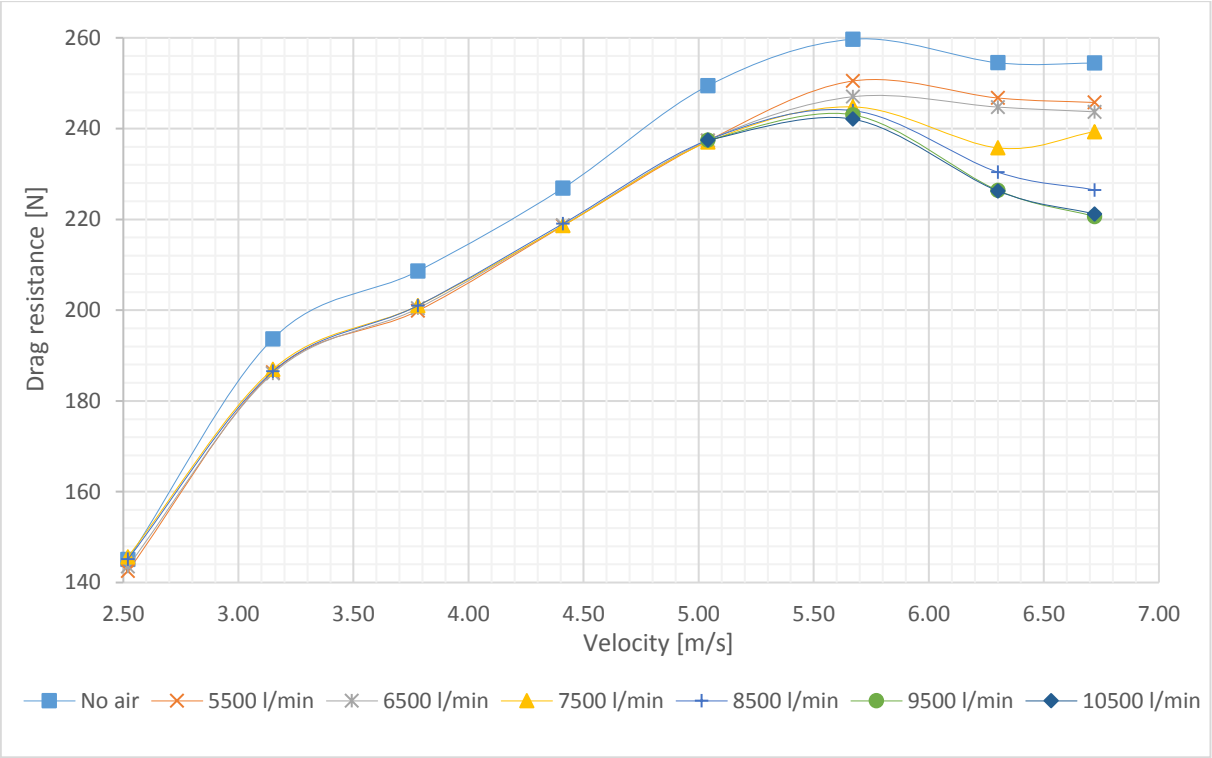

Figure 41 - Drag curves to vary flow rate- Model B

A better understanding of the influence of the flow rate on the resistance is shown in Figure 42. In this graph the curves have the same trend until to the velocity of 24 knots. The curves to a low velocity are not influenced by the flow rate, the decrease of resistance is the same. Over the 24 knots, the influence of flow rate is important and the decrease is highly influenced by the air flow rate.

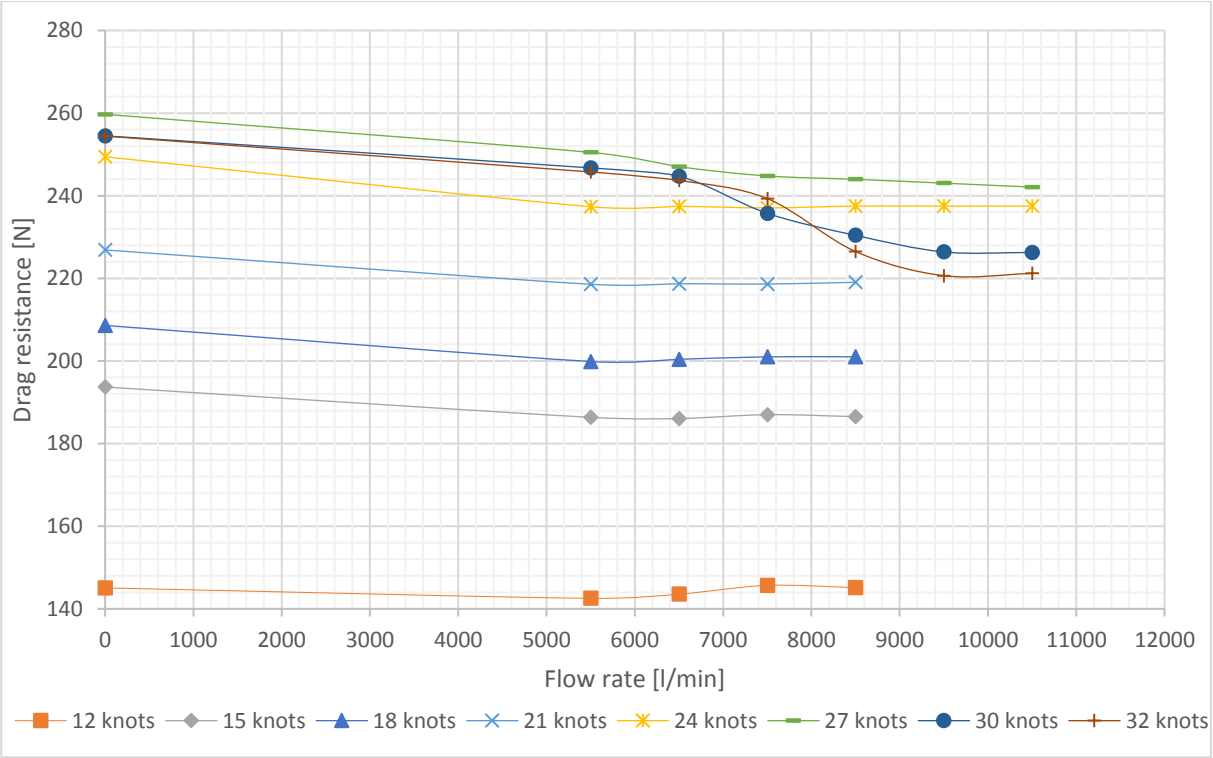

Figure 42 - Drag resistance VS flow rate to vary velocities - Model B

In Table 7 is reported the power saving with respect to the Model A. The values are the best one for that condition of velocity. It interesting to note that for the maximum velocity, the optimum flow rate is not to 10500 l/min. At lower speeds it is not necessary to keep the flow rate at maximum value because the optimum resistance condition is achieved to a low flow rate air injection.

V_M	Minimum Drag	Flow rate to minimum drag	Power Saving with respect to Model A
[m/s]	[N]	[l/min]	%
2.52	142.5	5500	-1.6%
3.15	186.1	6500	1.5%
3.78	199.9	5500	2.7%
4.41	218.6	5500	6.5%
5.04	237.1	7500	10.9%
5.67	242.1	10500	13.8%
6.30	226.3	10500	19.4%
6.72	220.6	9500	22.0%

Table 7 - Maximum power saving and correspondent flow rate - Model B

The Model C has been tested to 34 t conditions (0.153 t in scale model) and the trend of the curves without air injection is very similar to the one of the mother hull and to the Model B. Figure 43 shows the general trend of all curves tested to different flow rate. Also in this case there is an important drop of the curves between the no-air test and all others tests with air.

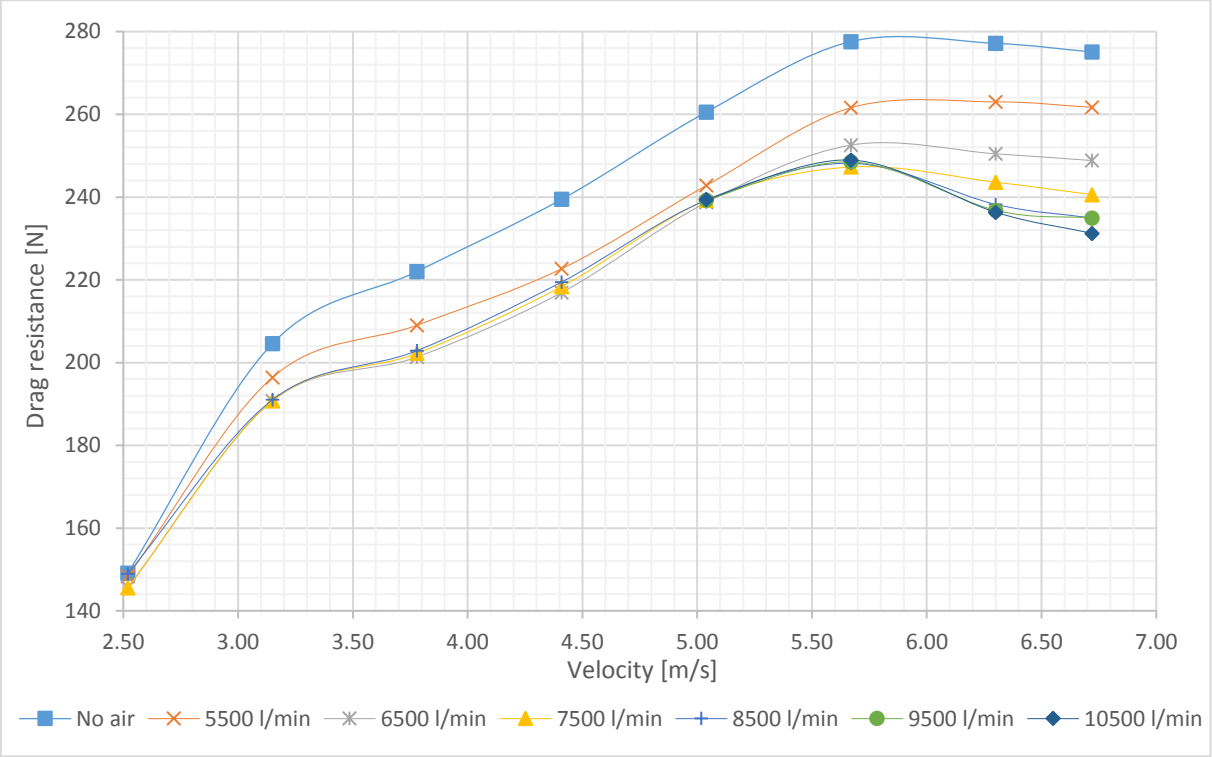

Figure 43 - Drag curves to vary flow rate- Model C

The drop of the curves is little and almost constant respect to the flow rate for an interval of velocities between the first tested velocity and about 5.04 m/s, after this velocity the decrease of power requested is evident as shown for the Model B.

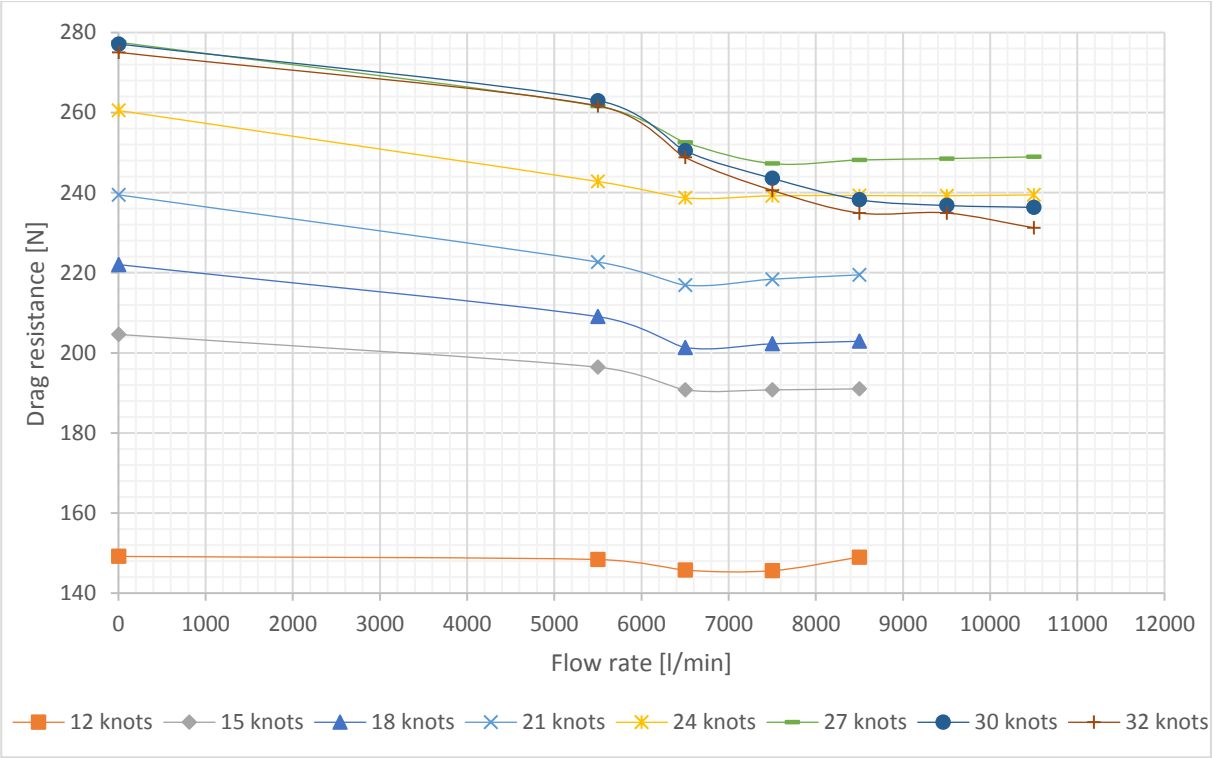

Figure 44 - Drag resistance VS flow rate to vary velocities - Model C

In Table 8 is reported the power saving with respect to the Model A. The values are the best one for that condition of velocity. In this case it is necessary to keep the flow rate to the maximum value when the velocity is 6.72 m/s and 6.30 m/s. At lower speeds also in this case it is not necessary to keep the flow rate at maximum value because the optimum resistance condition is achieved to a low flow rate air injection.

V_M	Minimum Drag	Flow rate to minimum drag	Power Saving respect to Model A
[m/s]	[N]	[l/min]	%
2.52	145.6	6500	-4.1%
3.15	190.8	6500	-1.4%
3.78	201.4	6500	1.6%
4.41	216.9	6500	6.9%
5.04	238.7	6500	9.8%
5.67	247.3	7500	11.2%
6.30	236.3	10500	14.6%
6.72	231.2	10500	16.8%

Table 8 - Maximum power saving and correspondent flow rate - Model C

The last trial of tests concerns the Model D; the trend of the curves for this model is little different respect the Model B and C. In this case, there is not a great drop respect to no-air test, until to the flow rate equal to 7500 l/min the curves are very similar in quality and quantity terms. Therefore for this model a higher flow rate is necessary for having a drop of the requested power.

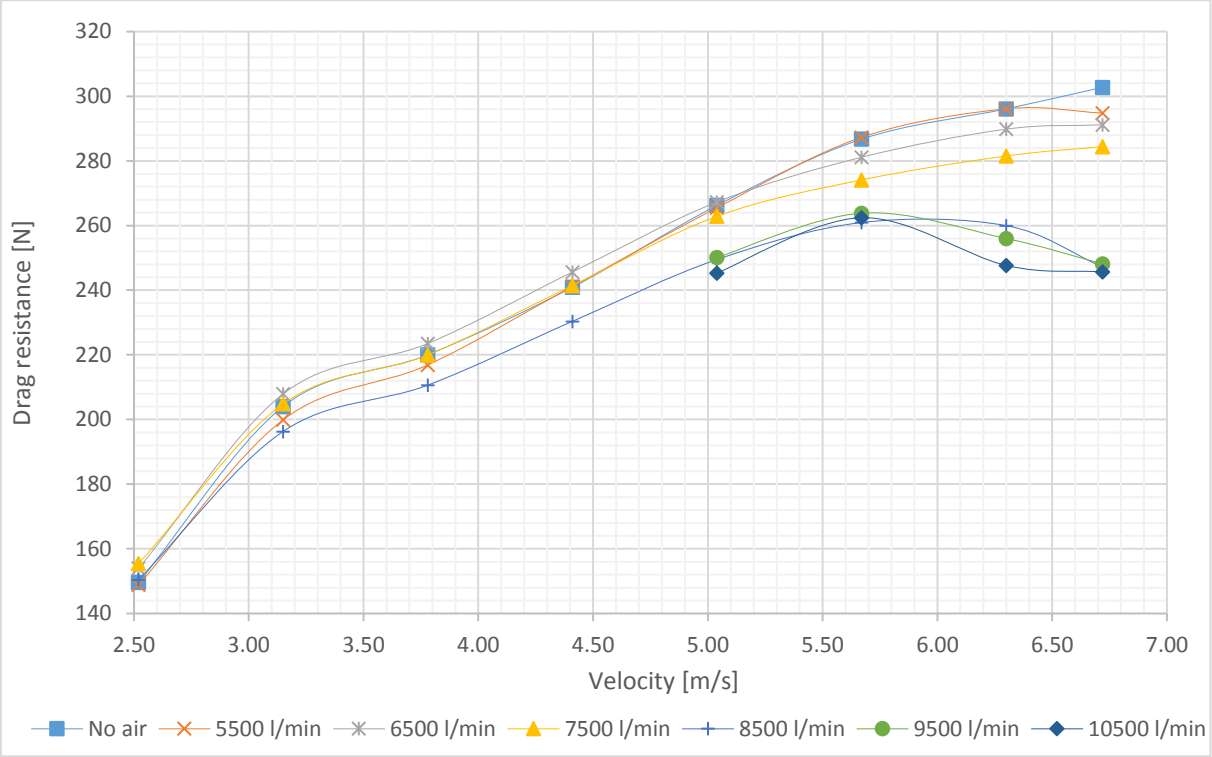

Figure 45 - Drag curves to vary flow rate- Model D

The curves of drag resistance vs flow rate highlights that between 12 knots and 24 knots, and between 6000 l/min and 8000 l/min, there is a negative effect of the air injection with respect to the hull without air. In order to have an evident decrease of resistance the value of flow rate must be high in each condition of velocity. The drop of the curves, in this models is not very evident and, for appreciating the effect of the air injection, the flow rate has to be greater than 7500 l/min and at a velocity of 5.04 m/s (Figure 46).

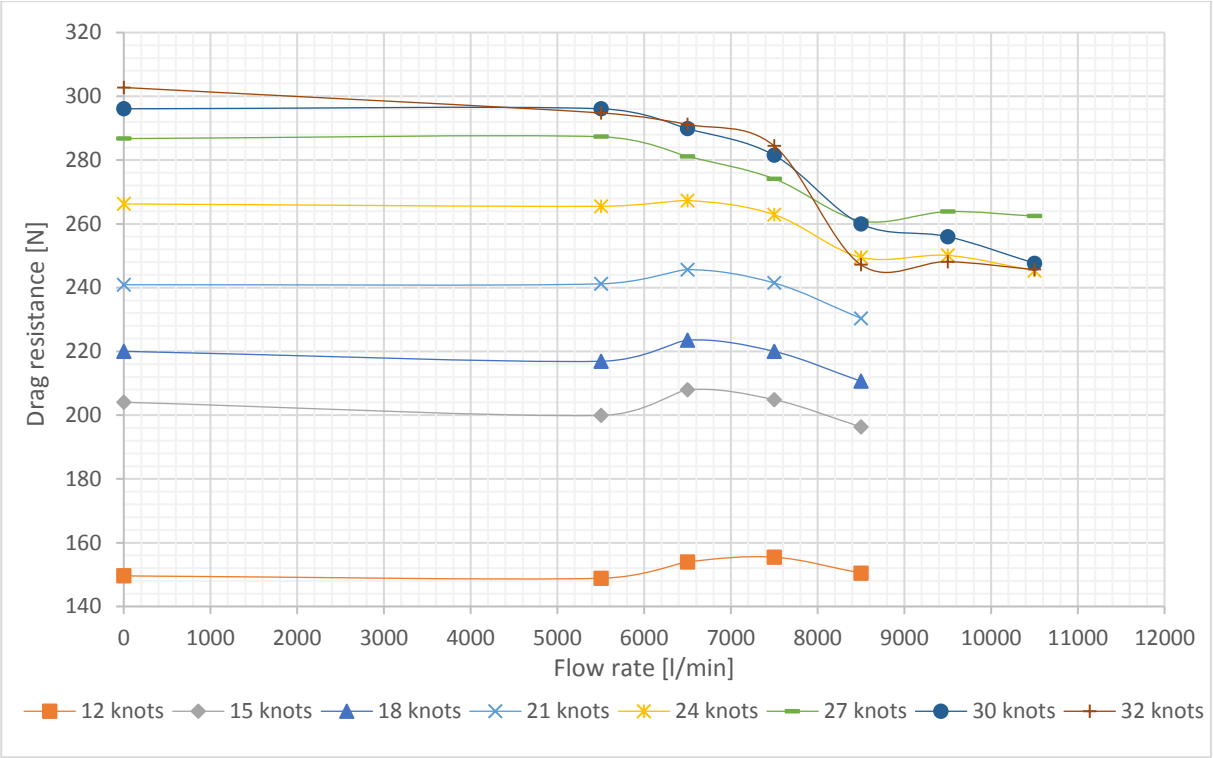

Figure 46 - Drag resistance VS flow rate to vary velocities - Model D

In Table 9 is reported the power saving with respect to the Model A. The values are the best one for that condition of velocity. In this case it is evident that the power saving is very low until to 4.41 m/s.

V_M	Minimum Drag	Flow rate to minimum drag	Power Saving respect to Model A
[m/s]	[N]	[l/min]	%
2.52	148.8	5500	-6.1%
3.15	196.3	8500	-4.1%
3.78	210.6	8500	-2.7%
4.41	230.4	8500	1.3%
5.04	245.3	10500	7.8%
5.67	260.9	8500	6.6%
6.30	247.7	10500	11.0%
6.72	245.7	10500	11.9%

Table 9 - Maximum power saving and correspondent flow rate - Model D

The power saving respect to original hull (Model A) are shown in the Table 7, Table 8 & Table 9, respectively for the Model B, C and D. Increasing the velocity, there is a great increase of power saving, and the Model B is the better performing in every condition of velocity and air flow rate.

The resistance data are presented, in Figure 47 to Figure 49, in terms of an air entrainment coefficient, defined as

$$CQ = \frac{Q}{S_{IN} V_M}$$

As reported by Pearce (Pearce et al., 2015), this parameter influences length and stability of the cavity. If the air cushion is stationary inside the cavity, this value is about 1. For this reason, in traditional displacement hulls, this value is rather small.

Instead, for this kind of planing ACS, rather than an air-cushion, it is produced an air-layer, taking advantage of the natural bottom low pressure. This approach allows obtaining a bottom cavity with a shallow step that does not alter very much the original hull geometries and that is less invasive, in particular for the seakeeping and the increment of the wetted surface. Therefore, the CQs are very high. The graphs report the curves of the resistance respect to CQ at each Fn.

In the graphs, for each model, is possible to distinguish two different zones: one for Fn<1 and one for Fn>1. For Fn<1, the Model B and Model C have almost the same trend with a first zone where there is a reduction of resistance increasing the flow rate (value of CQ<3) and a second zone where the resistance is almost independent from CQ. For Fn>1, the trend is similar but the start of the decrease of the resistance happens with a CQ smaller in the Model C than in the Model B.

In the Model D, for Fn<1, the behavior is quite different respect to the other two models. There is an interval of CQ where the resistance increase (this zone shifts toward smaller values of CQ, with the increase of the Froude number). Instead for Fn>1, the trend is almost the same of Model B.

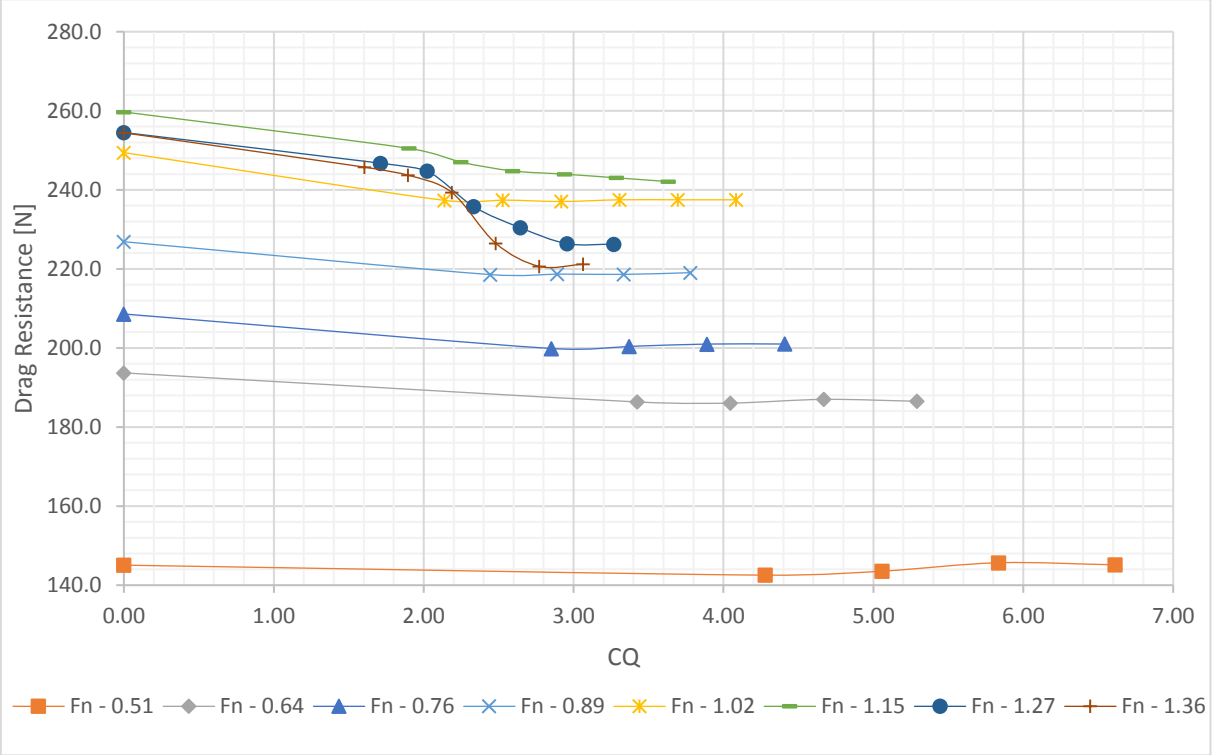

Figure 47 - Requested drag resistance vs CQ to vary Fn - Model B

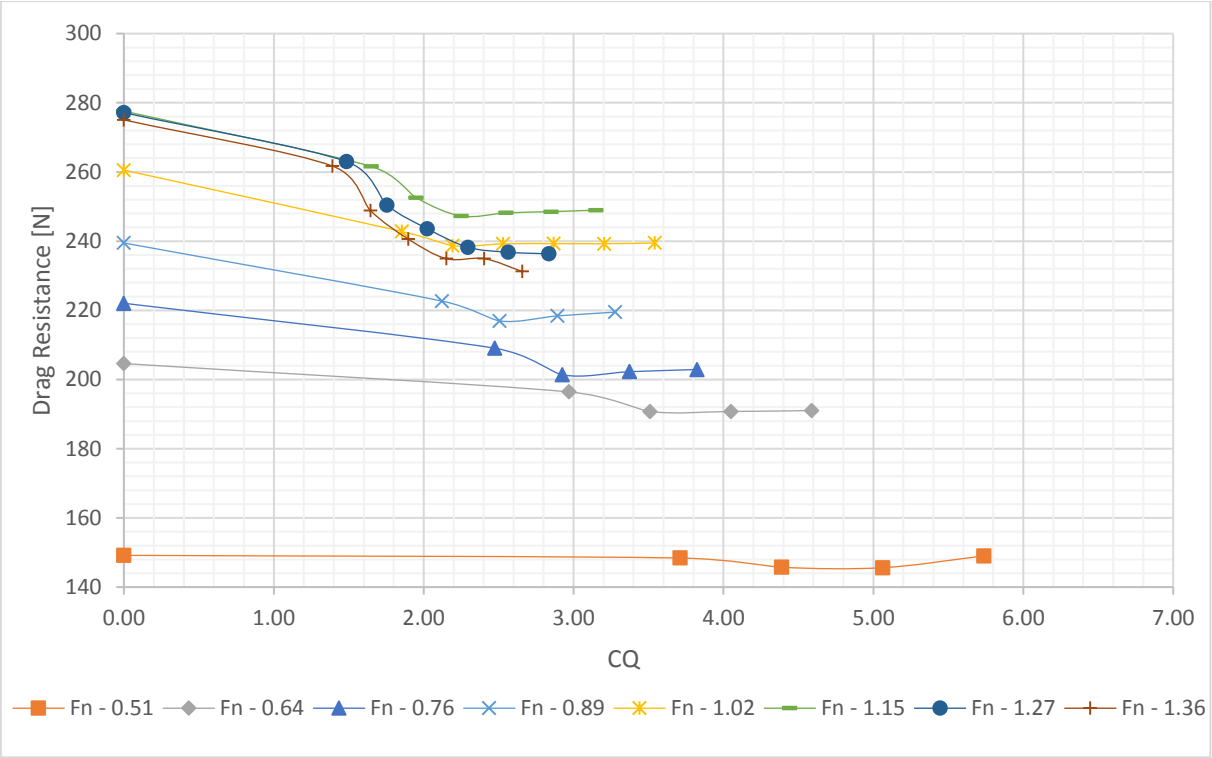

Figure 48 - Requested drag resistance vs CQ to vary Fn - Model C

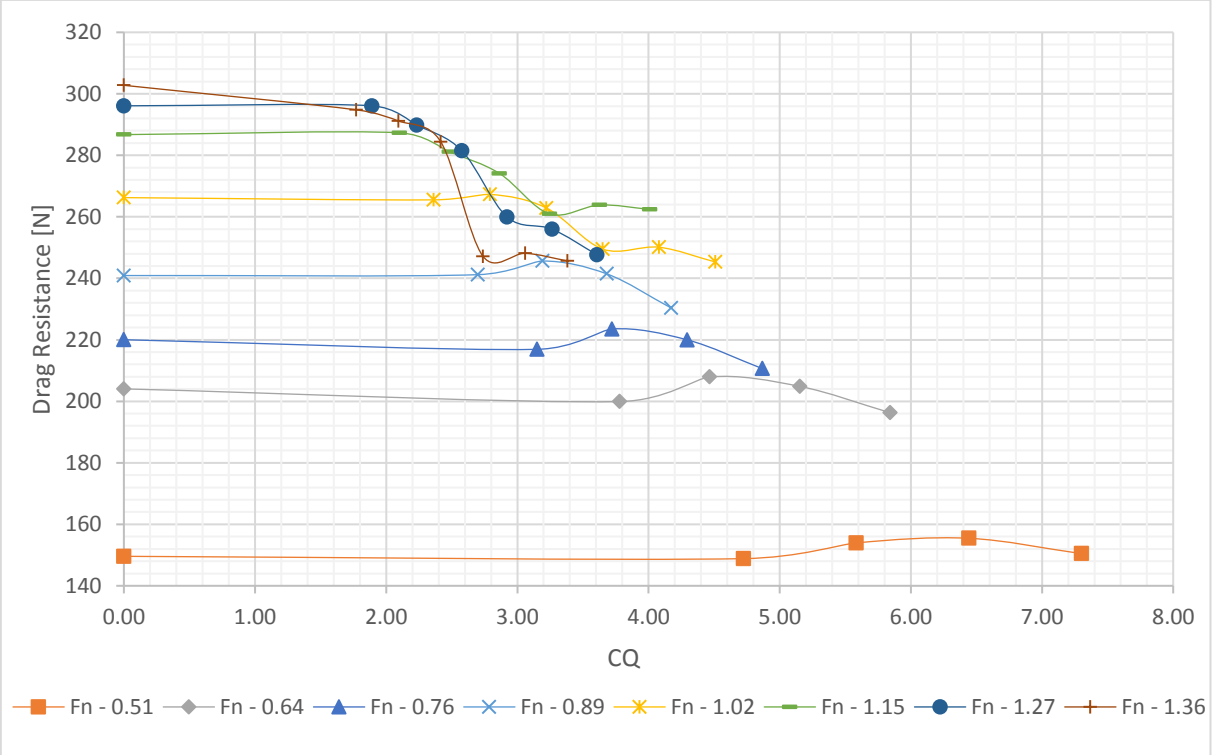

Figure 49 - Requested drag resistance vs CQ to vary Fn - Model D

The Table 9 shows that the Model D has the minor impact in terms of power saving compared to the Model B and C. The reason for these results is attributable to the presence of a greater wetted surface that damps the effect of air cavity.

This is even more evident if are drawn the curves obtained, for each model of hull, tracing at each speed the lowest drag resistance obtained by varying the air flow rate. In the Figure 50 these curves are called as Optimized Model.

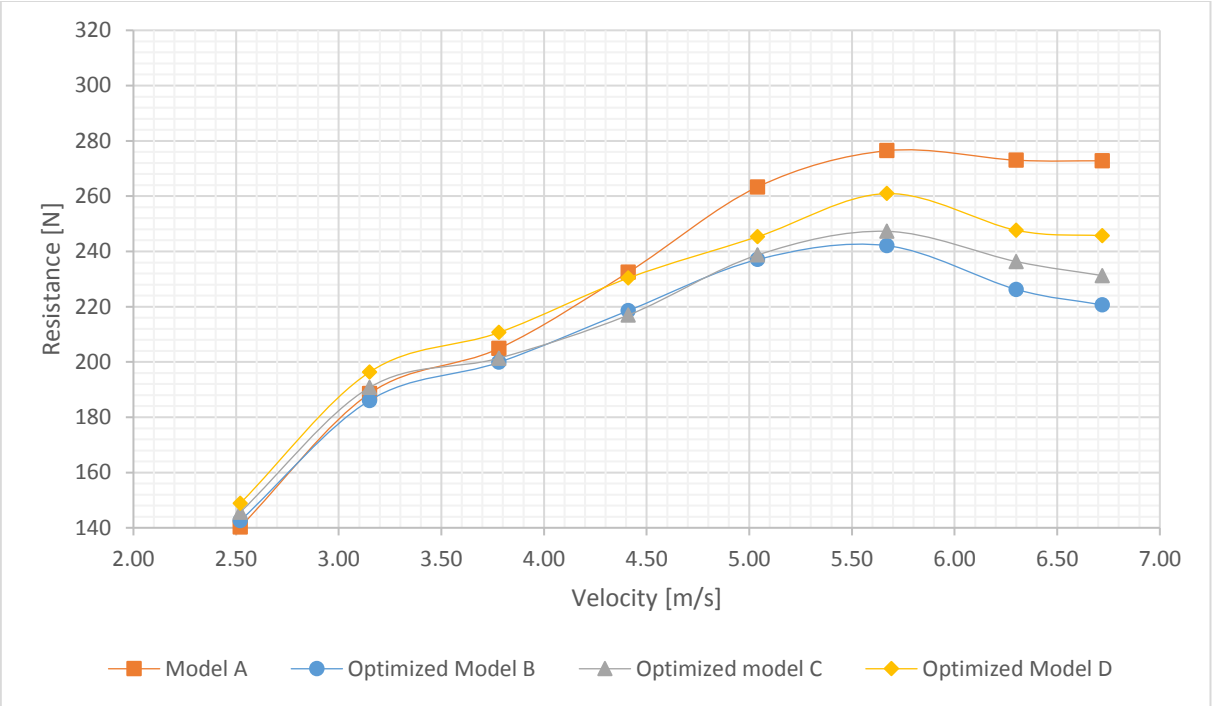

Figure 50 – Resistance curves of the optimized models (defined as the curves that, at each velocity, have the lowest drag resistance, varying the air flow rate)

In general it is possible to observe that a more complex geometry, designed to accommodate a more stable air layer, is really not a real plus. This is because, unlike the displacement hulls, planing hulls tend to develop a natural low pressure on the bottom that helps to keep the air layer, preventing its rupture or the air escape through the chain.

The Figure 51 and the Figure 52 show that there are no big differences in terms of trim and sinkage between the various models. This shows that, compared to the original hull, the presence of the air cavity leads to a reduction of the drag without changing appreciably the lift.

In order to make the measurement independent from the shapes of the bottom in the different models, trim and sinkage were evaluated by two lasers that measured continuously the distance between two fixed points, in correspondence of the aft and forward perpendiculars, and the deck of the model. The reported sinkage is at amidships (i.e. the average value between the sinkage on the forward and aft perpendiculars).

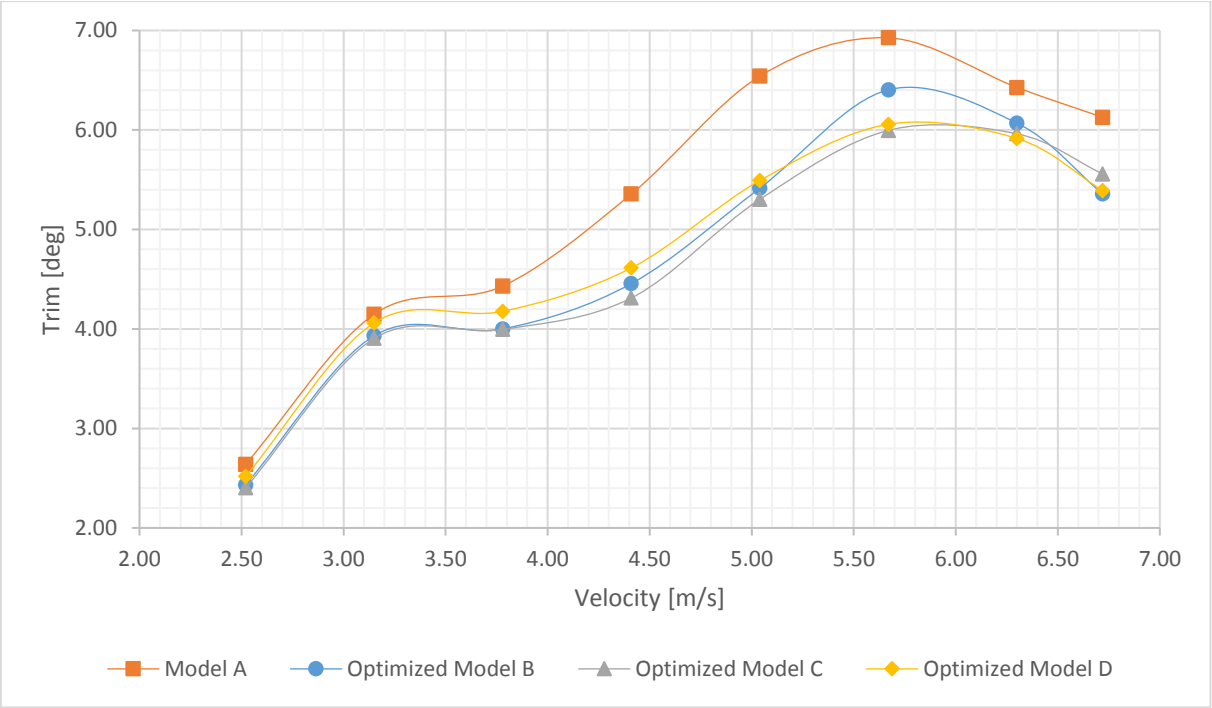

Figure 51 – Longitudinal trim of the optimized models

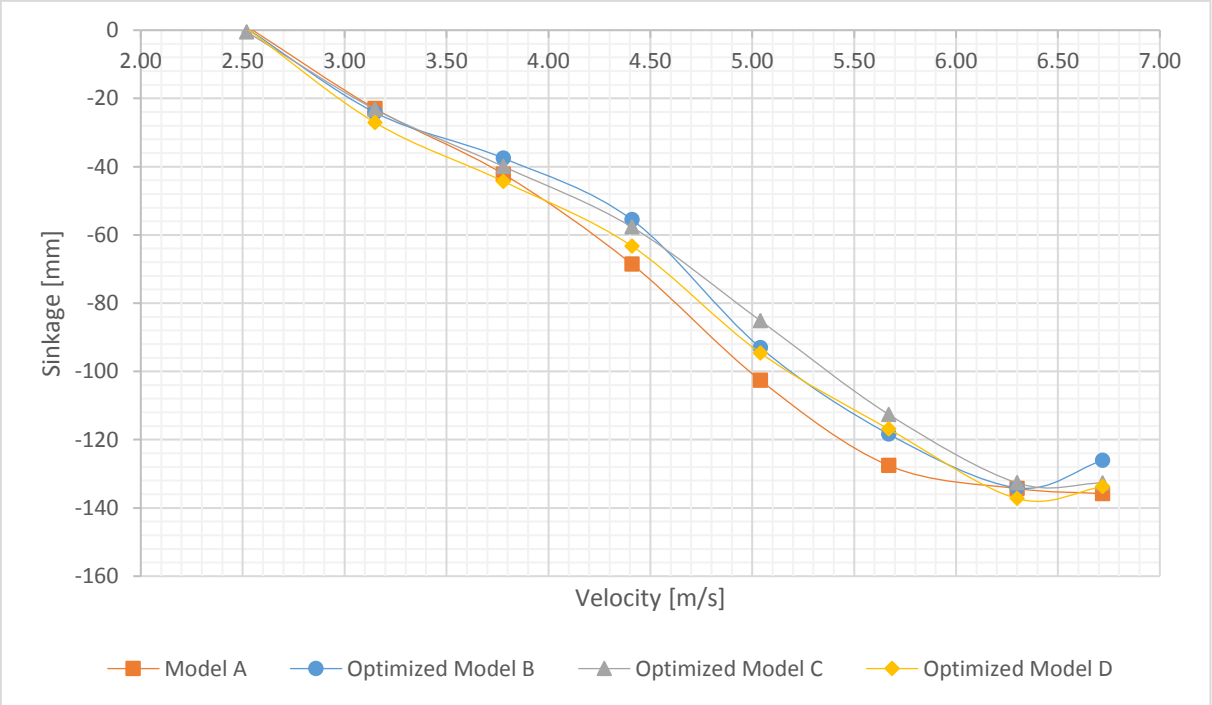

Figure 52 – Amidships sinkage of the optimized models

6. Computational Fluid Dynamics simulations

Abstract

The first part of chapter describes the theory to the base of all commercial numerical approaches and highlights step-by-step all settings in order to solve the problem of resistance prediction without and with air injection. A brief review of uncertainty analysis is proposed. Results and Discussion are presented for the hull without air injection, for the uncertainty analysis and the results relative to the hull with air injection.

6.1 Introduction

Part of the research has been developed in collaboration with the towing tank of Vienna. Thanks to the experience of the technical office and the capacity of the engineers inside the towing tank has been possible to define a methodology, described below, for the computational fluid dynamic simulation of this kind of problem.

Figure 53 - Towing tank of Vienna

6.2 CFD Method

The principal aim of the CFD methods is solving hydrodynamic phenomena in order to quantify the unknown variables like velocity, pressure, free-surface position and/or rigid body motion. The equations that govern the physic of this problem are the Navier Stokes ones. They are based on two main principia: mass conservation and momentum conservation. These equations are a system of partial differential equations with a non-linearity and with a 2^{nd} order. Only for simplified hydrodynamic cases is possible to find a hand-solution. For complex phenomena, these equations must be solved with a numerical approach. With the increase of the computing power, this set of equations is solved with various discretization methods (Ferziger and Peric, 2002). A Finite Volume Method implemented in a commercial software is used in order to understand if this tool is suitable for this kind of problem.

The URANSe equations are solved thanks to an implicit and time-marching solver, the results allow to have all the hydrodynamic unknown variables during each time step. The first choice was the method for solving the pressure and velocity field, in this case a segregated flow approach is used, the linkage between the momentum and continuity equations is achieved with a predictor-corrector method (Deng and Tang, 2002). The turbulence model used in all simulations is the k-omega SST Menter (Menter and Kuntz, 2004; Wilcox, 2008), it is suitable both for planing hull and for the successively injection of the air. The process of discretization leads to an algebraic system of equations that in this case is solved with an Algebraic Multigrid method (Stüben, 2001). The Hybrid method Gauss-Least Square (Gauss-LSQ) solves all the gradients during the process of discretization; it is a blending between the Gauss method and Least Square method. Each simulation is conducted with a time-marching approach in order to capturing the unsteady phenomena; the temporal discretization is a 2nd order one. The choice of the time step (Δ_t) is influenced by the general dimension and velocity of the ship, like suggested by the ITTC (ITTC, 2011) with the equations 6.1 and by the grid dimensions with the Courant Number. This last parameter must be kept low in order to have a good convergence condition.

$$\Delta_t = 0.01 \sim 0.005 \ \frac{l}{v} \qquad (6.1)$$

Another important choice is the interface tracking method for the free surface and successively for the air injection. In addition to the Navier Stokes equations, a one more transport equation must be solved for the volume fraction of the two immiscible fluids. The more suitable one is Volume of Fluid method (VoF). The convection scheme used for the VoF method is the HRIC (High-Resolution Interface Capturing), it allows to keep always a sharp interface between the two immiscible fluids. The planing hull during the simulations is free to pitch and heave. In order to capture the strong interaction between air and water, a multiphase interaction with a surface tension equal to 0.072 N/m between the two fluids is imposed. The Dynamic Body interaction solver is activated and it allows to evaluate the acting hydrodynamic forces inside each time step and solving the rigid body equations for calculating the sinkage and trim of the hull. A minimum of ten inner iterations are used in order to define the new position of the ship for each time step. The mesh motion in consequence of the ship movement is managed with the Overset technique that for high speed craft is better than morphing methodology, as reported by De Marco et al. (De Marco et al., 2017). Thanks to this technique, there isn't degradation of the cell elements, principally when the trim angles are high, and the accuracy near all the boundaries is kept always high. A linear interpolation scheme is used for link the results between the background region and overset one. A summary of the all setup for the numerical simulation is reported in Table 10.

Table 10 - Summary of numerical setup

Discretization method	Finite Volume Method
Solver	Implicit Unsteady
Approach	Segregated Flow
Continuity and Momentum Equation coupling	SIMPLE - Algorithm
Convection Term	2nd Order
Turbulence Model	k-Omega Menter
Temporal Discretization	2nd order
Iteration for Time Step	10
Time Step	Equation (6.1)
Gradient Discretization	Hybrid Gauss-LSQ
Algebraic system of Equations solver	AGM - Algebraic Multigrid Solver
Interface	VoF - Volume of Fluid
Convection Scheme for VoF	HRIC - High-Resolution Interface Capturing
Ship hull motion	DBI - Dynamic Fluid Body Interaction
Inner Iterations for Ship Motion	10
Mesh motion	Overset Mesh
Interpolation for Overset	Linear

Two different regions, the background one and the overset one divide the mesh. Figure 54 shows the principal dimensions of the background and overset regions like suggested with the recommendation of ITTC (ITTC, 2011). There are not specific conditions for the dimension of the overset block but it is better if there are sufficient grid elements between the boundary surface inside the overset region (hull) and the background region.

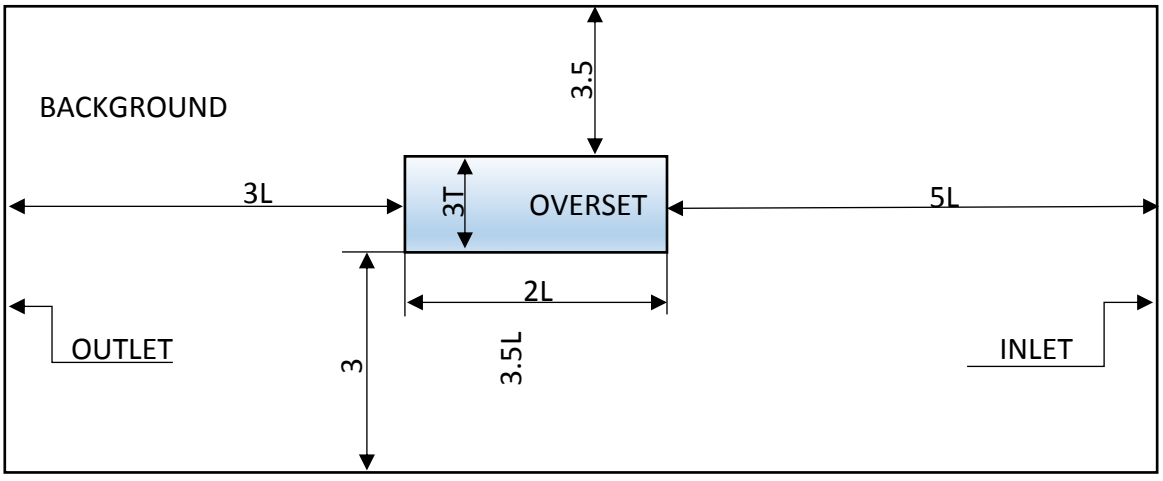

Figure 54 - General dimensions (L is the LWL). The width of background is 3.5LWL while the width of overset is 3BWL

A 3D representation of the background and overset block is reported in Figure 55 with the surfaces colored in function of the relative boundary condition. In this figure is possible to see the relative proportion of each dimension on left, a zoom of the overset zone with the relative hull geometry on right. In both images the boundary conditions applied are reported.

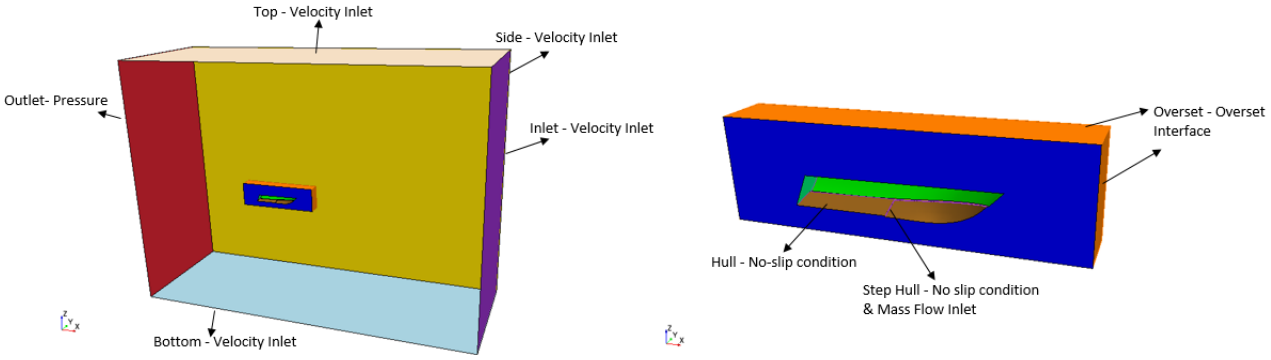

Figure 55 - Block geometry on left with boundary conditions, Overset Block with boundary conditions on right

The principal aspect for the mesh is to be able to capture the main characteristics of the flow. Different block refinements are applied in different regions of the domain. A general view of the mesh is reported in Figure 56. The mesh is a trimmed one for both the two regions. In Figure 56, it is also possible to see a refinement zone for the free-surface tracking and one in refinement zone in overset block. The expansion is low from the inside overset zone to the out background one.

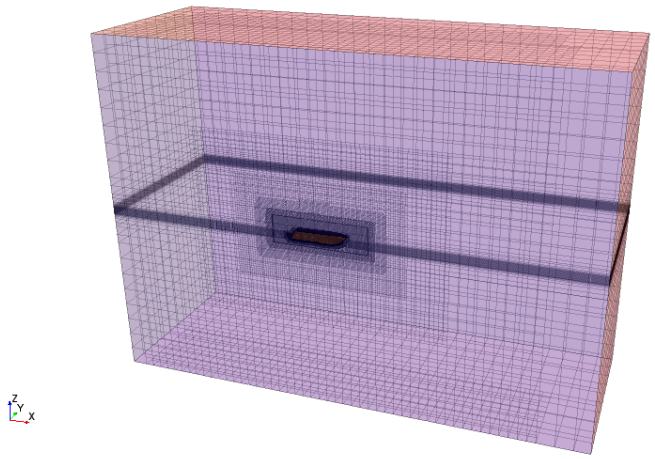

Figure 56 - Mesh in all the regions of the simulation

For a more detailed analysis, the grid has been refined for the Kelvin wake solution (Figure 57 - left), near the air-injection zone (Figure 57 - right) and in correspondence of the wetted surface (in order to avoid numerical ventilation).

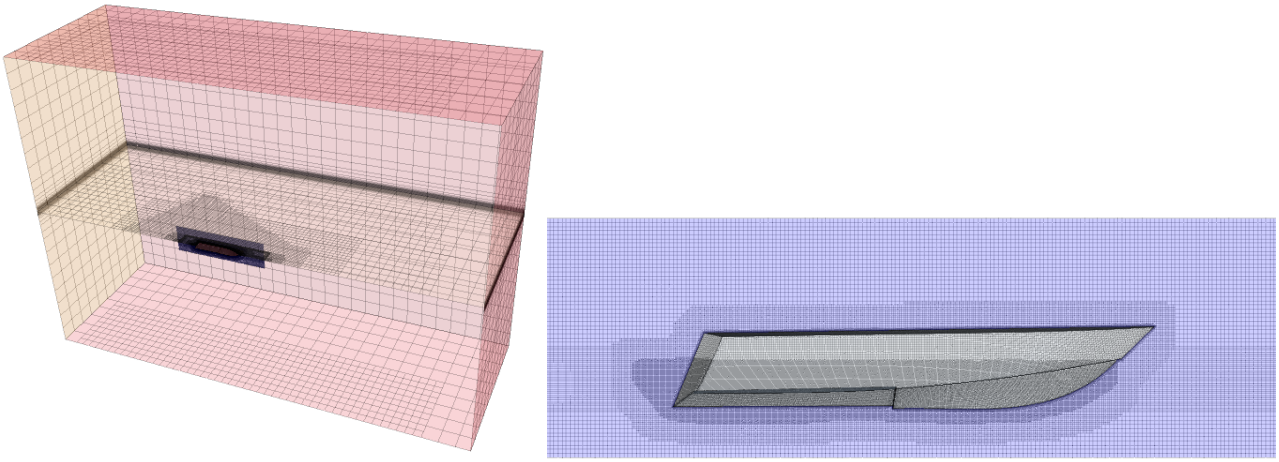

Figure 57 - Kelvin Wake refinement (left) and Hull refinement (right)

In the overlapping zone between the Overset Region and the Background one, the dimension of the elements must be very similar. In Figure 58, it is possible to see that there is not difference between the elements inside the overset region and the ones in background region directly in contact with the overset interface. This condition guarantees no-overflow errors during the simulation and a very good interpolation condition. In the Figure 58 it is also possible observing the particular refinement of the free surface called butterfly refinement.

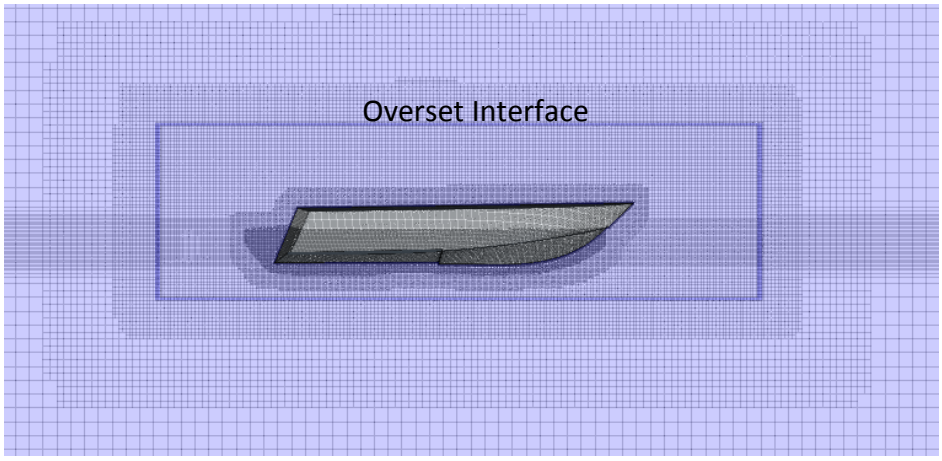

Figure 58 - Overlapping condition

The software allows to choice different methods for the treatment of the boundary layer. In order to keep the numbers of mesh low, a High Wall Y+ treatment is used. This particular approach allows to solve the boundary layer with the use of the wall functions. The mesh must be defined in order to keep the Wall Y+ with a value higher than 30. A good range is between 60 and 130. In all simulations, the average value of the Wall y+ is 60 as shown in Figure 59.

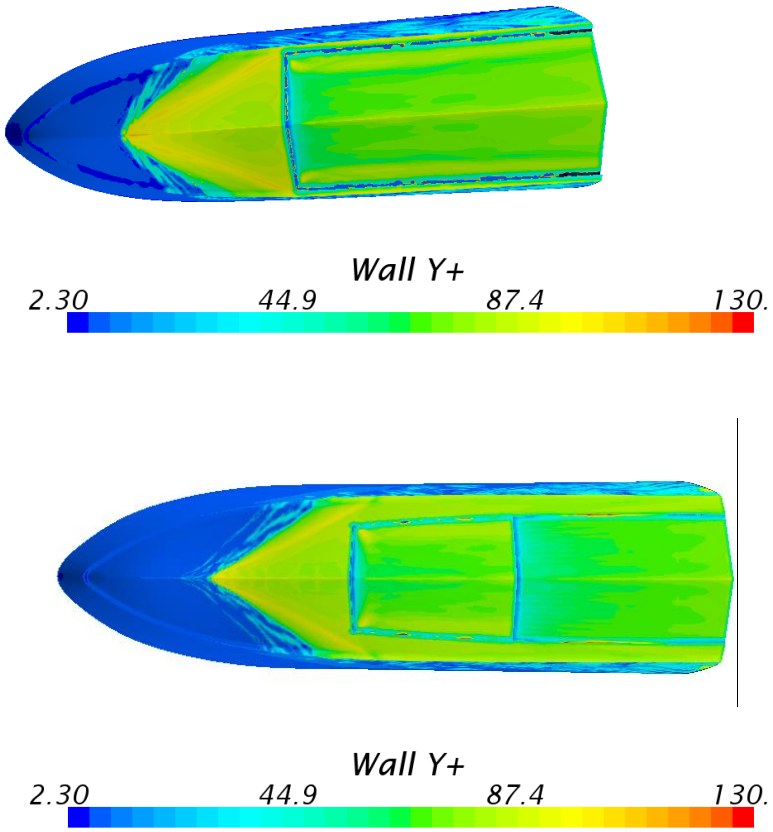

Figure 59 - Wall Y+ for the most critical condition - Water-Flow velocity of 6.72 m/s for Model A and B

The principal aspect for the boundary condition is imposing the initial free surface position (design draught) and the velocity of the flow. The use of VoF-Waves option allows simplifying this process. This particular option provides a series of field function for initializing the VoF calculation and defining the best profiles of the boundary conditions. In our case, the wave is flat and the inputs are the draught level and the velocities of the water (Table 12) inside the tank (Figure 60). All boundaries are directly linked to this particular option in order to take in account the presence of the two-phases. The Inlet, Side, Top and Bottom are imposed like Velocity inlet with a field function for the velocity and the volume fraction. The Outlet is a Pressure Outlet with a pressure defined by a field function dependent on the free surface position. In Overset region, the surfaces in contact with the Background one are Overset Surfaces. They are the surfaces where there is the interpolation of the results between the two regions. The surface of the step is treated separately from the rest of the hull. It is a Wall in the first campaign of simulations and a Flow-Rate inlet when there is the injection of the air.

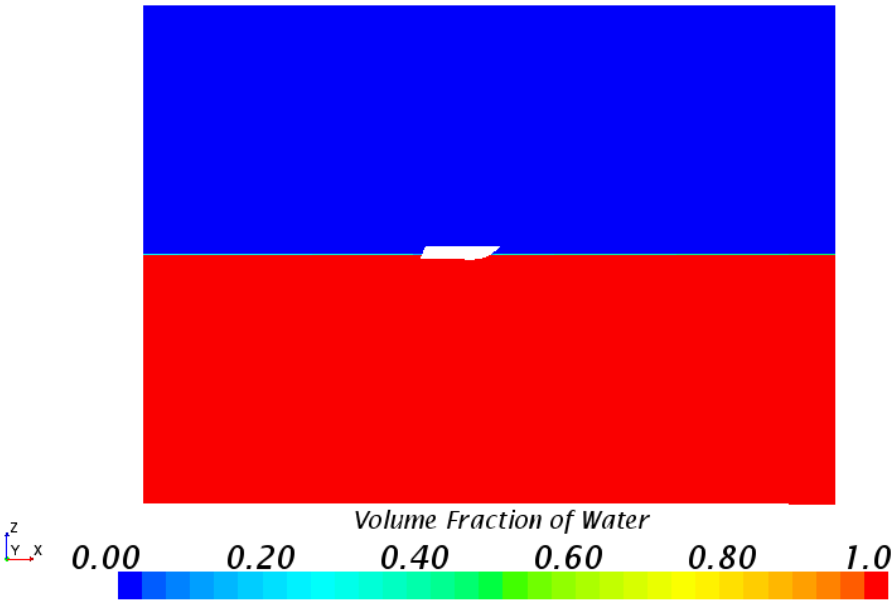

Figure 60 - Initial Condition for Flat-Wave

The simulations were carried out in two different campaigns: without air and with air injection. The first campaign of simulations involves essentially the evaluation of the resistance curve of the hull. The tested velocities are reported in Table 12. For each velocity, the simulation is conducted until to a stable condition of the all physical parameters like drag, trim and sinkage. An example of the monitoring of total drag force convergence is shown in Figure 61. These parameters are compared with experimental results.

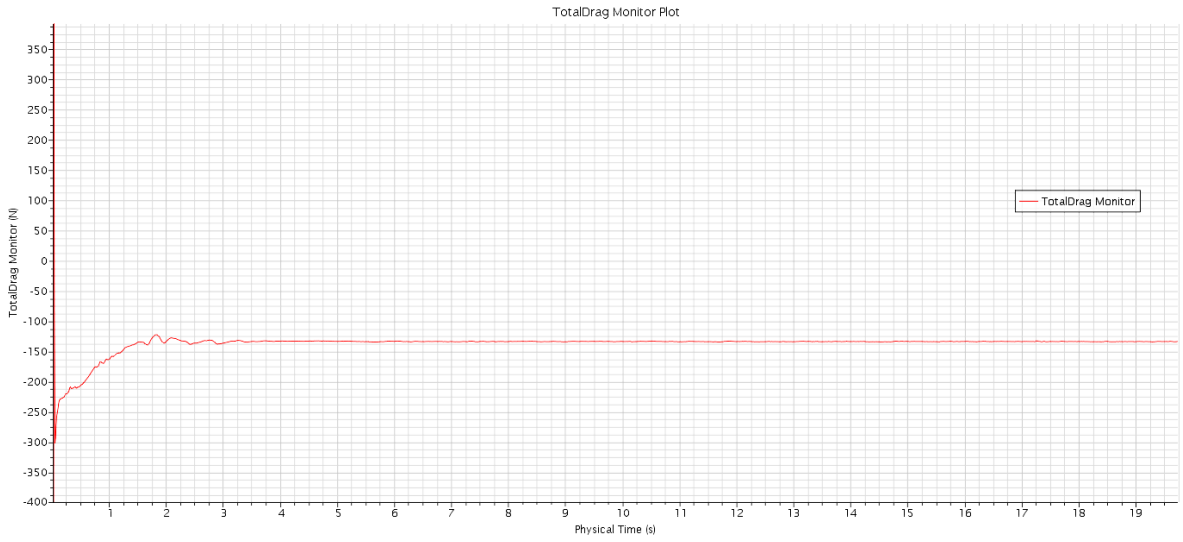

Figure 61 - Total Drag force convergence

During this campaign of simulations an uncertainty analysis is conducted following the guidelines proposed by ITTC (ITTC, 2011). In general, during a CFD simulation there are three main sources of uncertainty: iterative (U_I), grid (U_G) and time-step uncertainties (U_T). The most important term of

uncertainty is the grid, as shown by Stern (Stern et al., 2001). It has an order of magnitude greater than the other two and the evaluation of this quantity is recommended for each simulation. The used method has been the Richardson one (Richardson, 1911). The method consists in solving the same simulation problem with a minimum of three different meshes (fine subscript 1, medium 2 and coarse 3) with a ratio between the number of cells (r_k) constant. The solutions of the n-th parameter are respectively: S_{n1}, S_{n2} and S_{n3}. Thanks to these three different solutions is possible to calculate the rate change for the solutions between the coarse mesh and medium mesh (2) and between the medium mesh and the fine mesh (3).

$$\varepsilon_{n21} = S_{n2} - S_{n1} \qquad (Eq. 6.2)$$

$$\varepsilon_{n32} = S_{n2} - S_{n3} \qquad (Eq. 6.3)$$

With these two quantities, it is possible to evaluate the convergence ratio (4) and the order of accuracy (5) of the simulation. The behavior of the convergence ratio is important in order to understand the simulation tendency (Table 11).

$$R_G = \frac{\varepsilon_{n21}}{\varepsilon_{32}} \qquad (Eq. 6.4)$$

$$P_G = \frac{\ln\left(\frac{\varepsilon_{n32}}{\varepsilon_{21}}\right)}{\ln r_k} \qquad (Eq. 6.5)$$

Table 11 - Convergence ratio

Dimensions	Model
$\boldsymbol{0 < R_G < 1}$	Monotonic convergence
$\boldsymbol{R_G < 0}$ & $\boldsymbol{\lvert R_G \rvert < 1}$	Oscillatory convergence
$\boldsymbol{R_G > 1}$	Monotonic divergence
$\boldsymbol{R_G < 0}$ & $\boldsymbol{\lvert R_G \rvert > 1}$	Oscillatory divergence

The generalized form of the Richardson extrapolation method allows evaluating the uncertainty with the relation (6). The safety factor F_S can be a constant value as defined by Roache (Roache, 1998) or a dynamic value that change in function of the type of convergence of the simulation. As suggested by Stern et al. (Stern et al., 2001), in all cases where a monotonic convergence is obtained, the safety factor is equal to 1.

$$U_n = F_S \left| \frac{\varepsilon_{n21}}{{R_G}^{P_G} - 1} \right| \qquad (Eq. 6.6)$$

The results of the first campaign are the boundary condition for the second campaign of tests. In this case, the Step Hull boundary condition becomes an Air Flowrate Inlet. The simulation evolves until to reach a stable condition. The flowrate tested are included between 5500 l/min and 10500

l/min with a step of 1000 l/min. The time-step in this case is lower than the one used for the curve resistance simulations.

Table 12 - Velocities and Froude numbers tested

V_M (m/s)	Fn
2.52	0.510
3.15	0.638
3.78	0.765
4.41	0.893
5.04	1.020
5.67	1.148
6.30	1.275
6.72	1.360

6.3 CFD results and comparison with experimental tests – Model B

The first part of this chapter concerns the evaluation of the resistance curve and the parameters that have been extrapolated by the CFD simulations. The resistance curve and ship motion characteristics are compared with experimental data. The second part concerns the evaluation of the uncertainty of the results respect to the used mesh. Finally, the air injection problem was investigated. For this aim, the results of the first campaign are used as boundary condition.

Table 13 shows the values of the resistance in both cases, experimental and simulated. The percentage difference is always under the value of 5%, except for the first velocity condition where it reaches the 8%. A representation of the resistance curve, as shown Figure 62, allows seeing the characteristic humps and hollows of the planing hull.

Table 13 - Resistance comparison with error indications

Fn	R_{Texp} [N]	R_{Texp}/Δ	RT_{CFD} [N]	RT_{CFD}/Δ	Abs Difference	Percentage
0.510	145.1	0.096	157.9	0.105	0.088	8.8%
0.637	193.7	0.129	193.1	0.128	0.003	3%
0.764	208.6	0.139	210.3	0.140	0.008	0.8%
0.892	226.9	0.151	229.1	0.152	0.010	1%
1.019	249.4	0.166	257.0	0.171	0.030	3%
1.146	259.7	0.173	265.3	0.176	0.021	2.1%
1.274	254.5	0.169	266.4	0.177	0.047	4.7%
1.359	254.4	0.169	266.0	0.177	0.045	4.5%

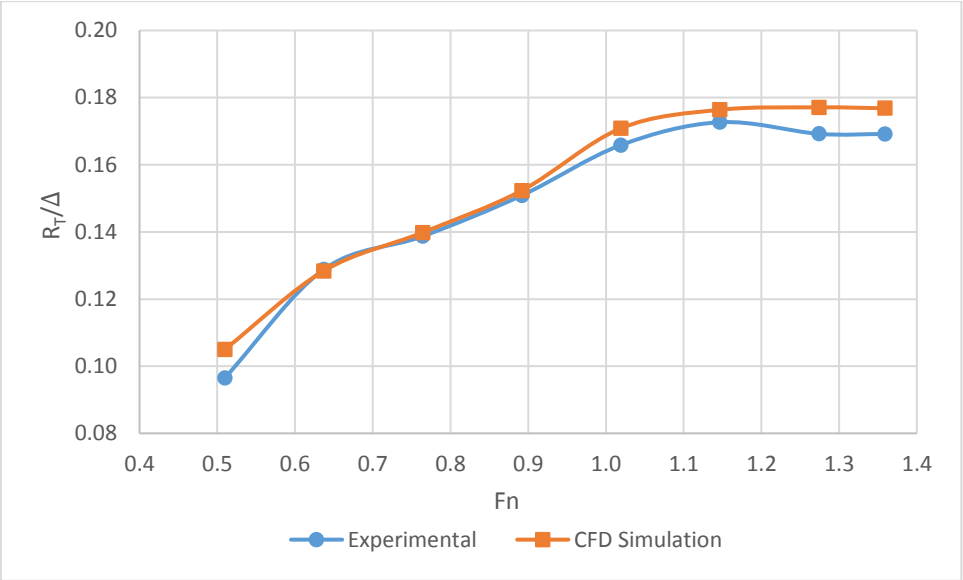

Figure 62 - Resistance comparison between experimental and simulation

The other parameters that have been compared between experimental and virtual tests are trim and sinkage of the boat. Also in this case, as shown Figure 63, the humps and hollows in the curves during the experimental tests are solved also with the CFD simulation.

Table 14 - Ship motion comparison

Fn	τ_{EXP} [deg]	τ_{CFD} [deg]	%Difference	$DTBow_{EXP}$ [mm]	$DTBow_{CFD}$ [mm]	% Abs Difference
0.510	2.31	2.50	8%	-47.6	-53.8	13%
0.637	3.83	3.52	8%	-103.0	-104.4	1%
0.764	3.99	3.67	8%	-125.2	-114.6	8%
0.892	4.38	3.87	12%	-152.0	-130.2	14%
1.019	5.33	5.30	1%	-200.0	-193.4	3%
1.146	6.06	5.80	4%	-244.8	-226.0	8%
1.274	5.70	5.20	9%	-245.7	-222.6	9%
1.359	5.42	5.00	8%	-242.3	-223.6	8%

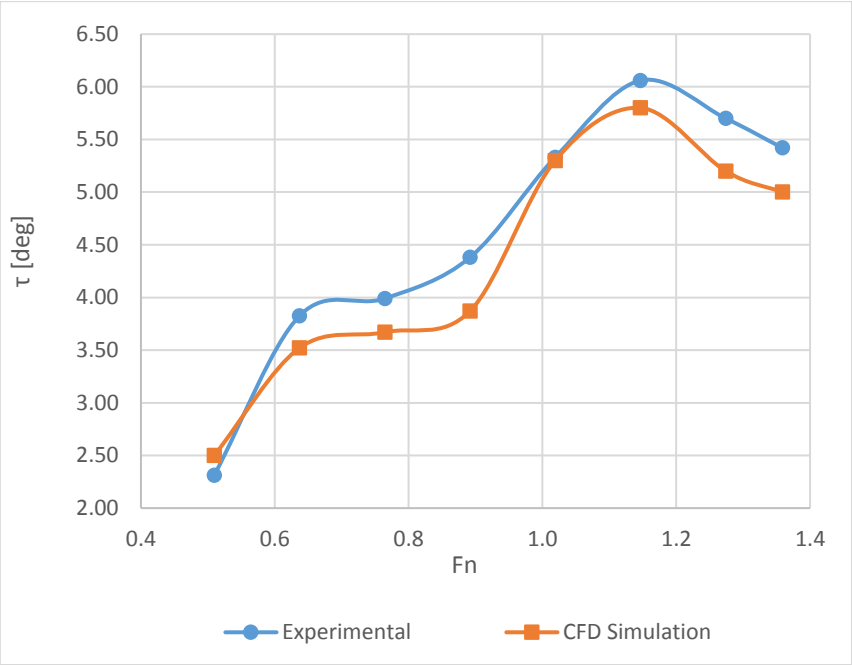

Figure 63 - Trim comparison

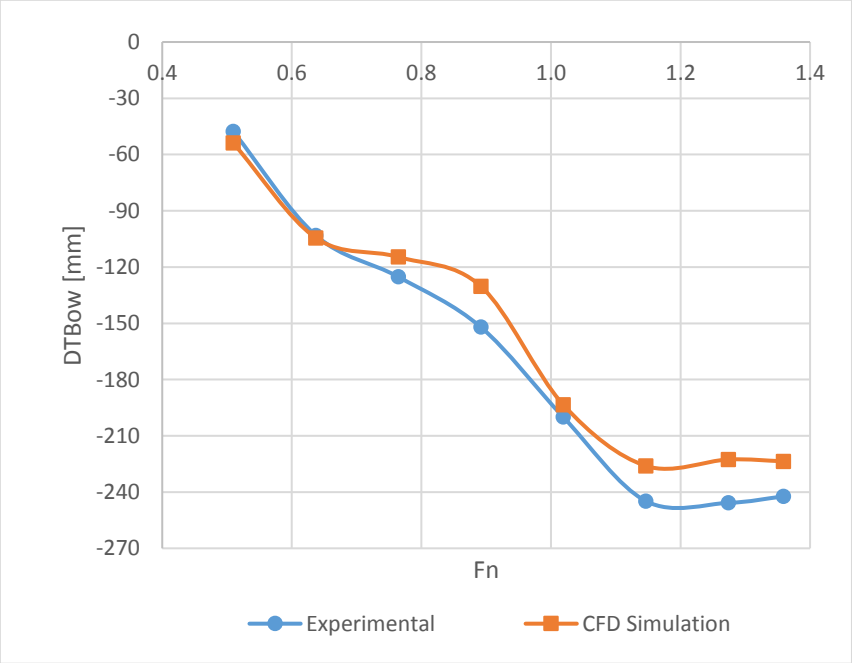

Figure 64 - Sinkage comparison

Thanks to CFD simulations, it is possible to split the total resistance in its principal components: frictional and pressure drag. The impact of each of them on the total resistance is shown in Table 15. The pressure component is the most important and it takes in account the effects of the waves and spray energy losses. However, increasing the velocity, the percentage of the frictional resistance increases in an important way.

Table 15 - Frictional and Pressure components of resistance

Fn	R_F [N]	R_F/Δ	R_P [N]	R_P/Δ	% R_F	% R_P
0.510	17.9	0.012	140.0	0.093	11.3	88.7
0.637	26.1	0.017	167.0	0.111	13.5	86.5
0.764	35.4	0.024	174.9	0.116	16.8	83.2
0.892	47.0	0.031	182.1	0.121	20.5	79.5
1.019	53.0	0.035	204.0	0.136	20.6	79.4
1.146	55.4	0.037	209.9	0.140	20.9	79.1
1.274	64.0	0.043	202.4	0.135	24.0	76.0
1.359	71.0	0.047	195.0	0.130	26.7	73.3

The wetted surface is another variable that can be evaluated during the CFD simulations. In the experimental tests, the wetted surface is conventionally considered the same of the static condition, regardless of the tested velocity and the consequent trim and sinkage, besides the wave and spray wetted surfaces. This approximation leads to an incorrect assessment of the drag components, mostly in the case of planing hulls. It is a great approximation because the wetted surface decreases rapidly increasing the velocity, principally when the hull reaches the planing condition. Table 16 shows this decrease. In particular, when the Fn is bigger than 0.9, the wetted surface goes rapidly down and it becomes about 70% of the static one (Figure 65). The assessment of this quantity is important also to evaluate the effect of the air injection successively.

Table 16 - Dynamic wetted surface and dynamic/static surfaces ratio

Fn	S_D [m^2]
0.510	1.90
0.638	1.92
0.765	1.88
0.893	1.84
1.020	1.68
1.148	1.44
1.275	1.38
1.360	1.30

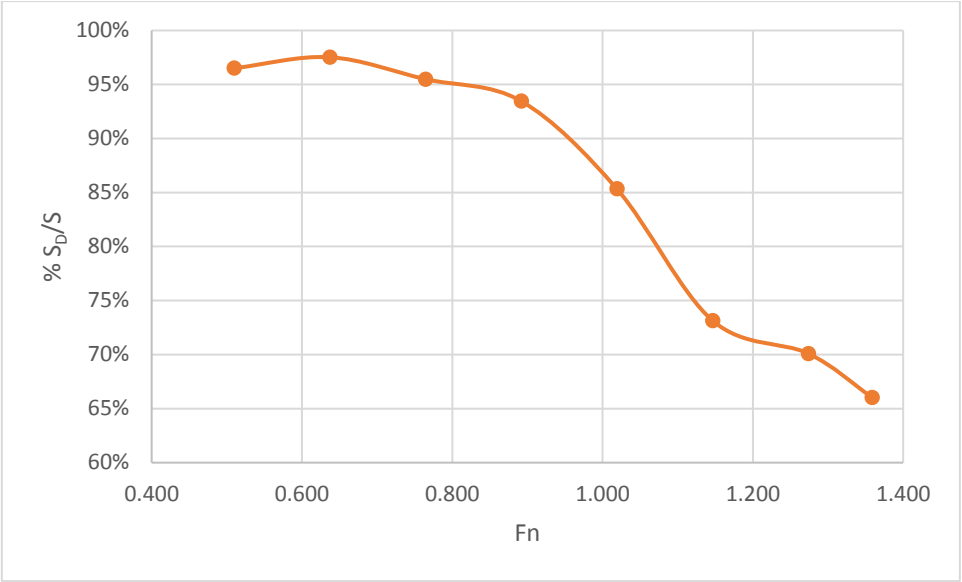

Figure 65- Percentage of dynamic wetted surface respect to the static one – Model B

Figure 66 shows the air Volume Fraction under the hull. It is important to note that the refinement of mesh near the keel allows keeping the artificial numerical ventilation under control and the impacts on the results are negligible. In the same Figure, it is also possible to see the difference between low and high Froude conditions; when the boat reaches 6.3 m/s, the sides are completely out of water.

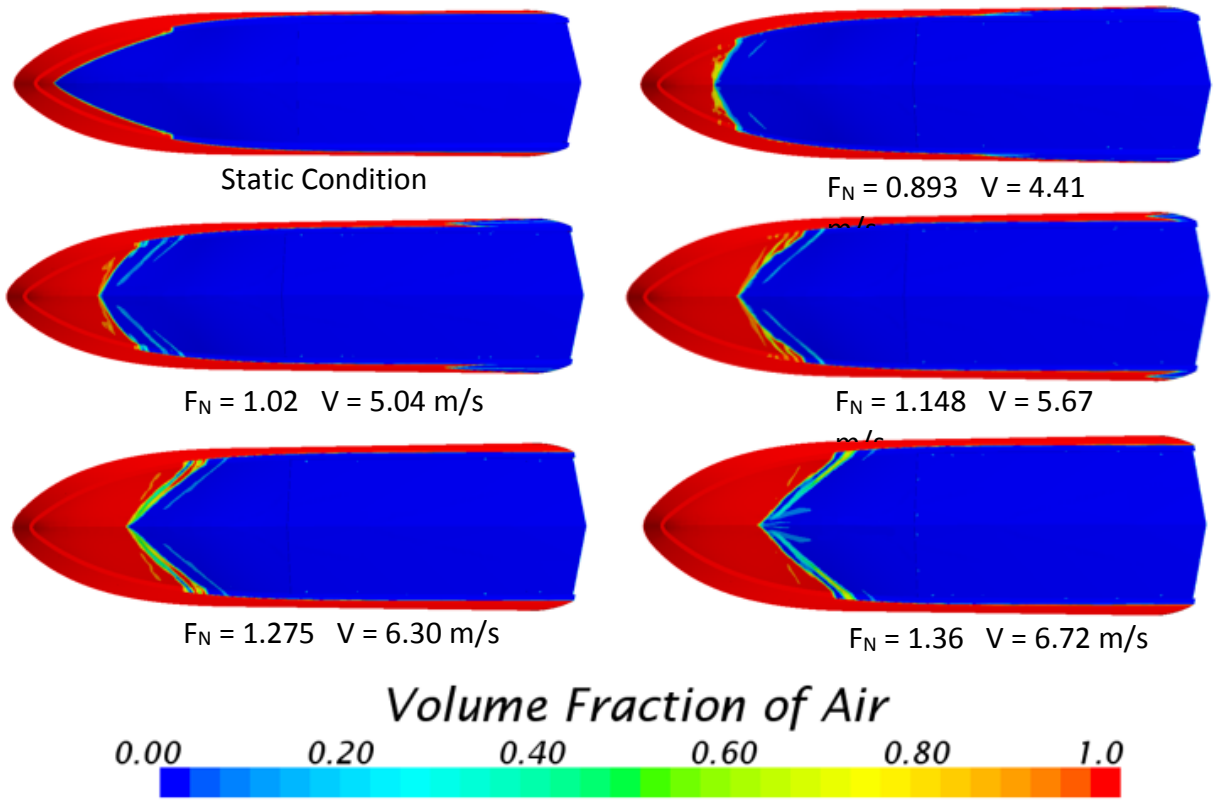

Figure 66 - Comparison between different velocity conditions of the wetted surfaces – Model B

Figure 67 helps to compare experimental and numerical wave pattern at a low Froude condition (Fn <1) and at the maximum velocity condition. It is also interesting to see that the detachment of the spray, in both cases along the chine, that, at high speed, can reduce dramatically the wetted surface.

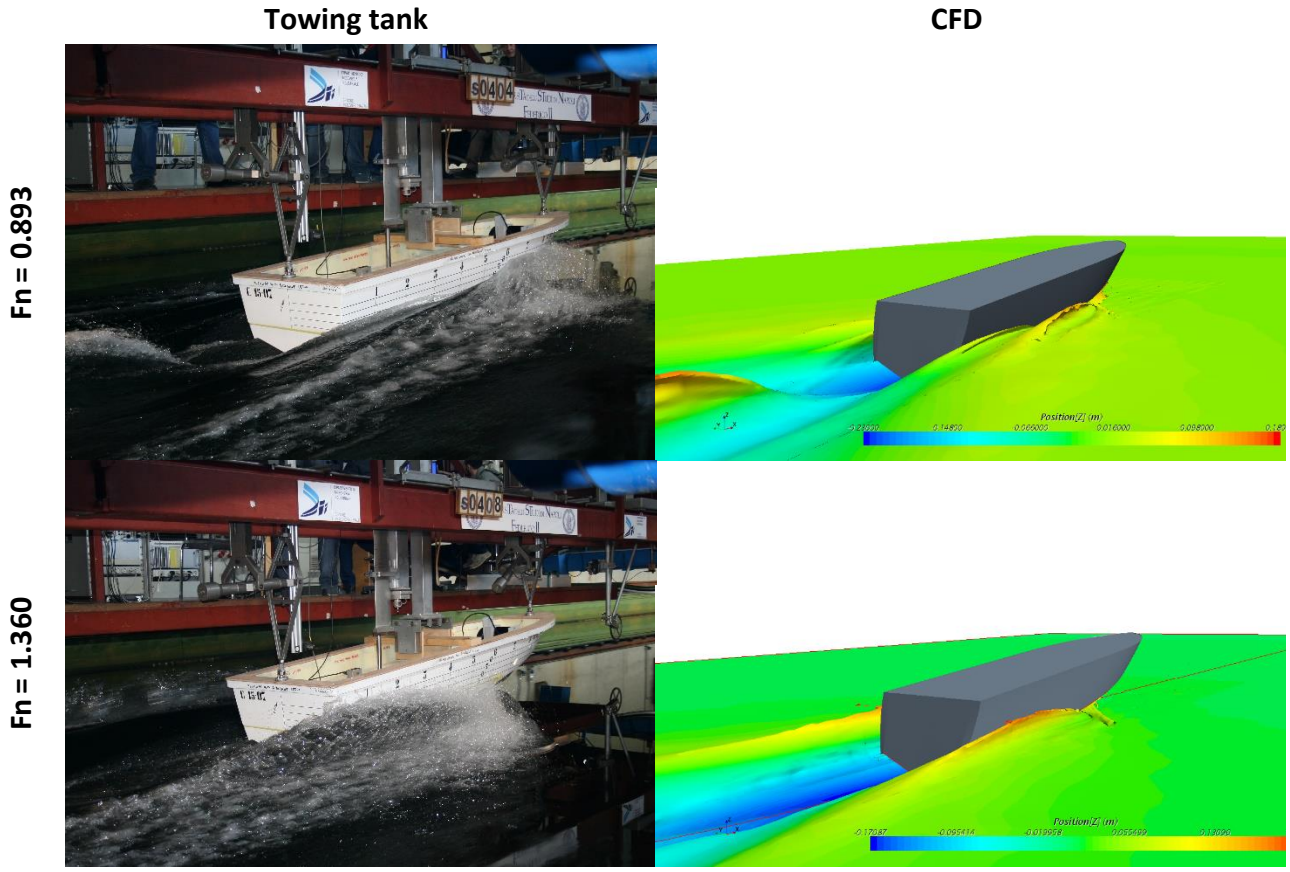

Figure 67 – Wave and spray in two different velocity conditions

The uncertainty analysis has been carried out with three different meshes. The condition analyzed is the one corresponding to the maximum value of Froude. The three different meshes have a ratio, like suggested by the ITTC procedures, about equal to 1.41. Table 17 and Table 18 show the parameters and results of the uncertainty analysis.

Table 17 – Parameters solution comparison

Parameter	Fine	Medium	Coarse
Elements	2,225,821	1,578,234	1,110,257
RT_{CFD}/Δ	0.177	0.181	0.187
τ_{CFD} [deg]	5.00	4.85	4.63
$DTBow_{CFD}$ [mm]	224	219	213
S_{DYN} [m^2]	1.30	1.26	1.20

Table 18 - Uncertainty analysis

	Medium/Fine	Coarse/Medium			
Parameter	ε_{n21}	ε_{n32}	R_G	P_G	**U [%]**
RT_{CFD}/Δ	-0.0033	-0.006	0.56	1.7	2.3
τ_{CFD}	0.15	0.22	0.68	1.11	6.4
$DTBow_{CFD}$	4.6	6	0.77	0.77	6.8
S_{DYN}	0.04	0.06	0.67	1.17	6.2

For each parameter, the grid convergence ratio is lower than 1 and therefore the solution is convergent. In the case of planing hull a coarse mesh leads to numerical diffusion. This phenomenon influences the total resistance that is the most affected parameter, as it is showed by the lowest value of R_G. The value U is expressed as a percentage of the respective result for the finest mesh.

The results of the first part of simulations are used as boundary conditions for these simulations. As reported above, in this campaign the step surface become a Flow Rate inlet. For each condition of flow rate, a comparison between the experimental resistance curves and CFD results are reported.

Figure 68 shows the resistance curve with the injection flow rate equal to 5500 l/min. In this case there is a good compromise between the CFD simulation and experimental tests. Only for the high velocity condition there is a little difference near the 10%.

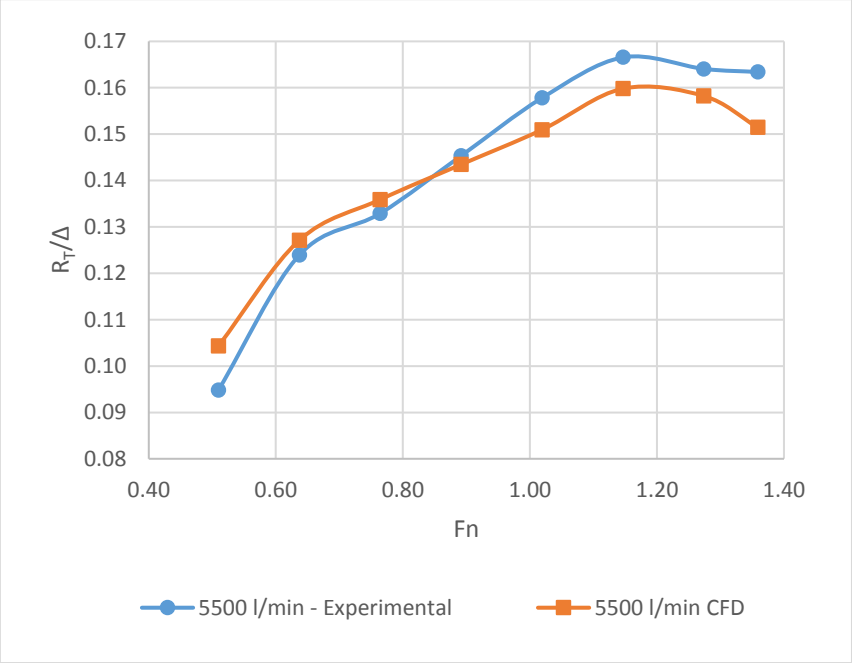

Figure 68 - Comparison with flow rate 5500 l/min

Figure 69 shows the same picture but with flow rate equal to 6500 l/min. Also in this case the error percentage is always below the 10 %. This value is reached for high values of velocity.

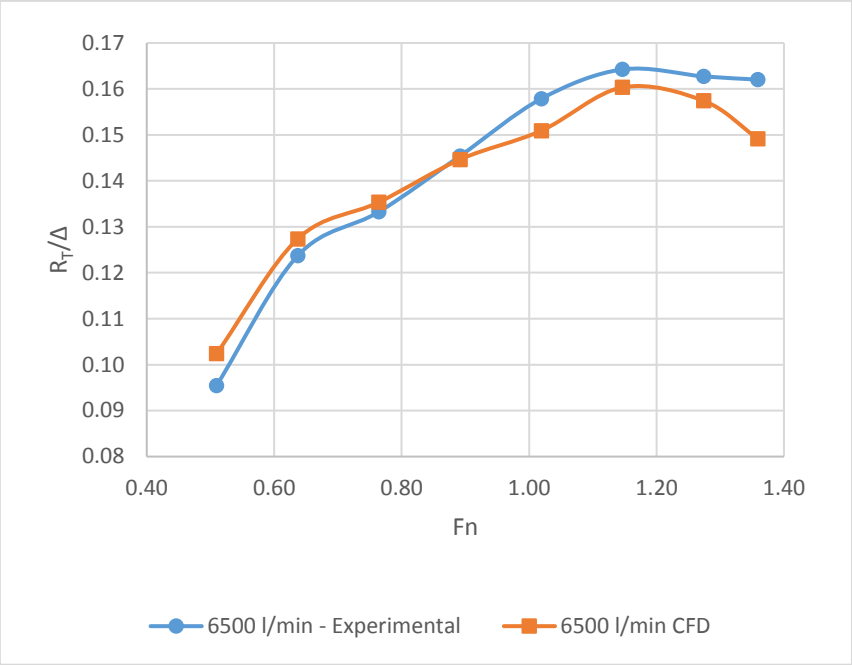

Figure 69 - Comparison with flow rate 6500 l/min

Also in Figure 70 and Figure 71 the curves agree well with the experimental tests. In general the difference between experimental and CFD simulations is below 6%.

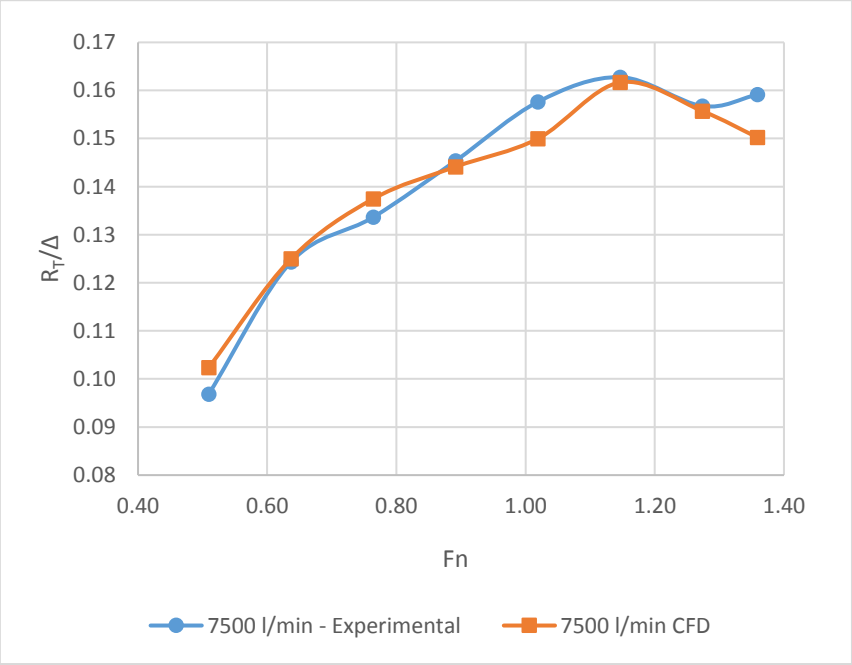

Figure 70 - Comparison with flow rate 7500 l/min

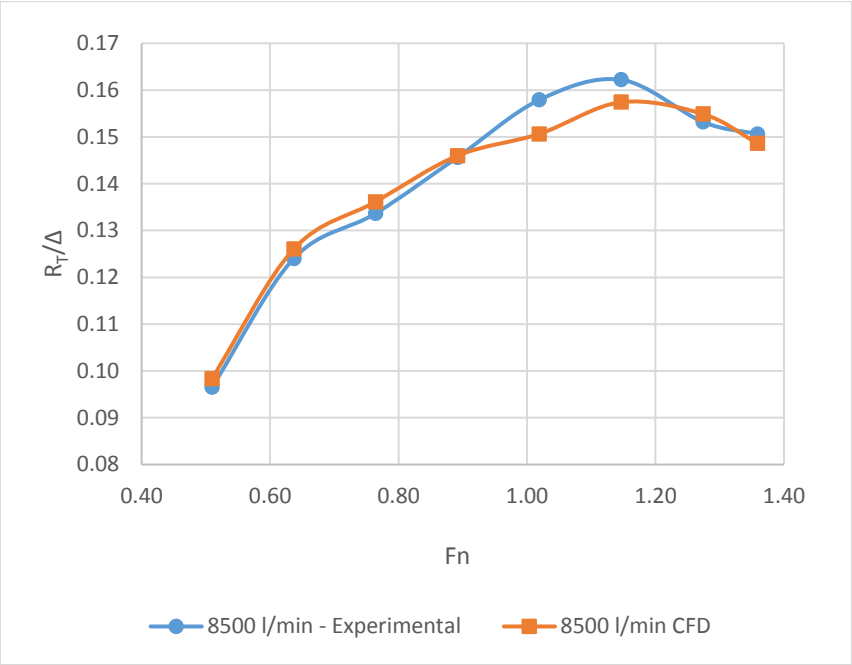

Figure 71 - Comparison with flow rate 8500 l/min

In this two cases have been simulated only the velocity between the Fn = 1 and maximum value of Fn (Figure 72 & Figure 73). In the case of flow rate of 10500 l/min (Figure 73) with a Froude number equal to 1.148 this difference reaches values of 8%. In all cases, the differences are largely acceptable.

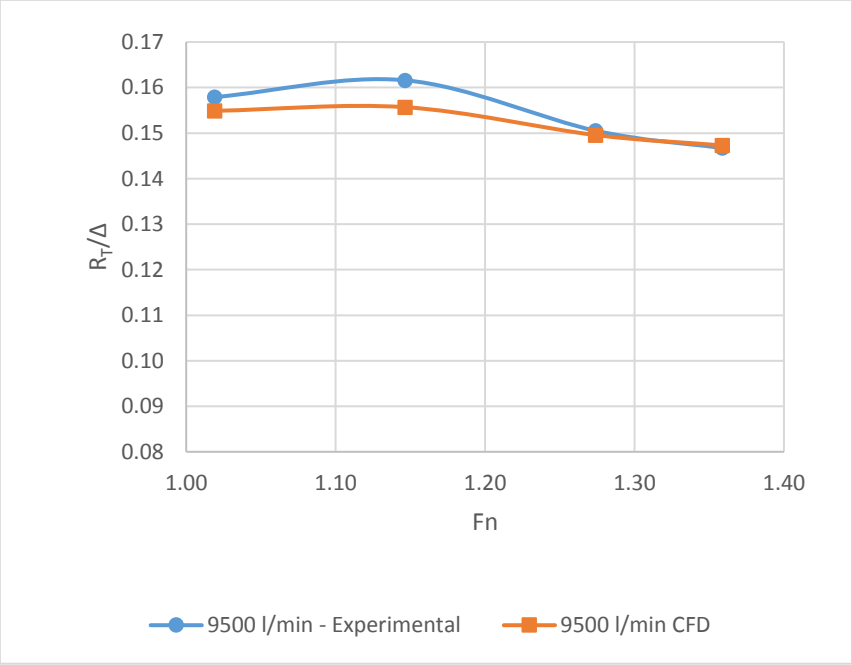

Figure 72 - Comparison with flow rate 9500 l/min

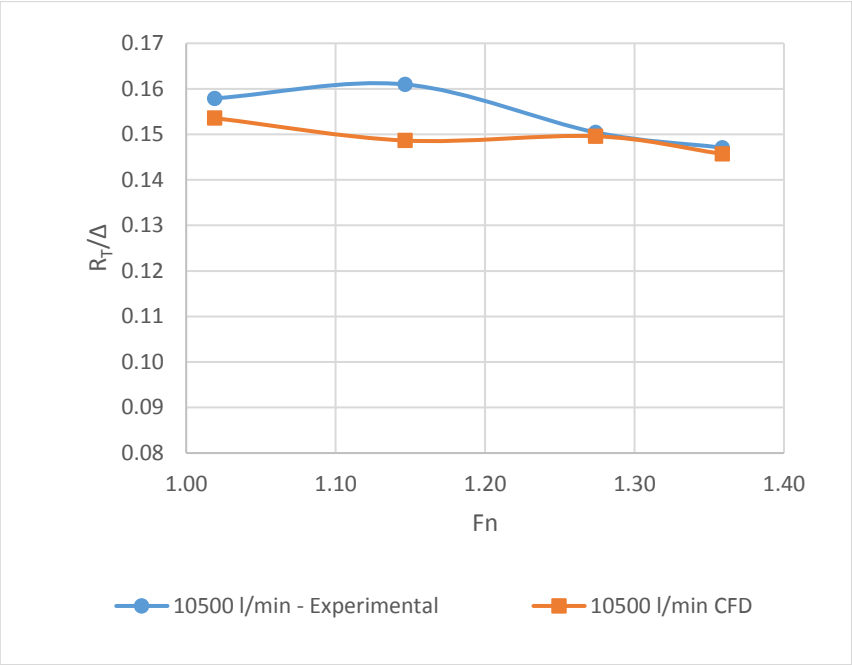

Figure 73 - Comparison with flow rate 10500 l/min

In Figure 74, all the CFD curves are plotted in the same graph. They are always below the one without air, therefore the injection of the air is a benefit in all conditions. In the same Figure, the trend is the same of experimental tests (Figure 41). There are two different zones. A first one, for a Froude number less than 1 where the flow rate does not influence the decrease of the resistance and the curves are very similar to each other. A second zone, with the Froude higher than 1, where the flow rate is important and there is a separation of the curves. In this condition of velocity, a higher value of flow rate leads to a greater decrease of resistance.

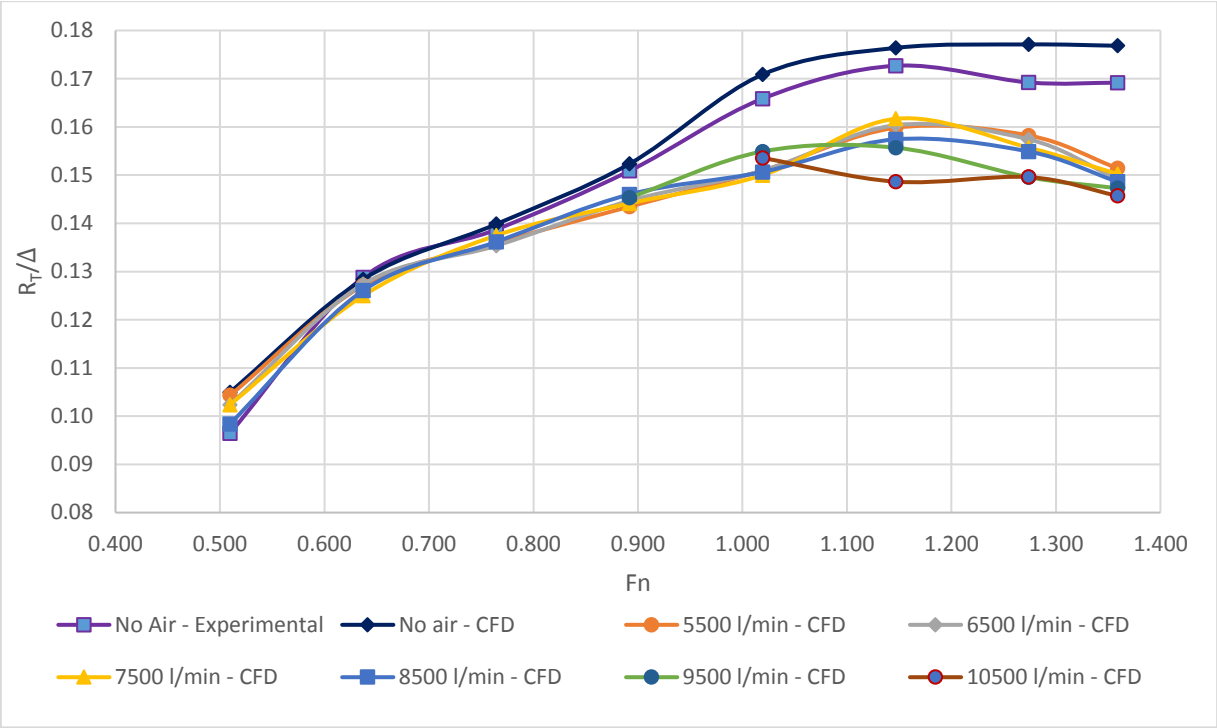

Figure 74 - All resistance curves to different flow rates

Another important aspect, in which CFD plays a crucial role, is the assessment of distribution of the air under the hull. Thanks to CFD, it is possible to evaluate the wetted area that decreases increasing the air injection. In the curves showed in Figure 75, it is reported the ratio between the dynamic wetted area with air injection and the dynamic wetted area without air injection, varying the flow rate and the Fn. There is a general similar trend with a shift downward when the flow rate increases.

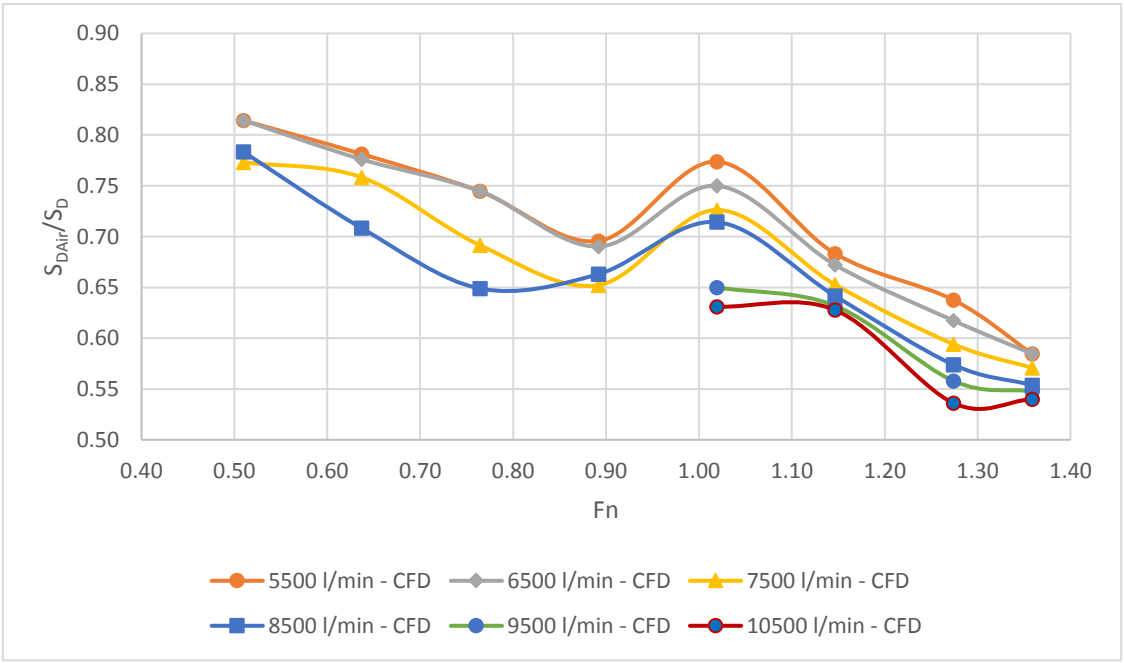

Figure 75 - Ratio between Wetted Surface with air injection and Wetted Surface without air injection

A particular aspect is the peak for all curves near the value of 1 of the Fn. This peak is a consequence of the starting of the boat planing. The Figure 76 shows the distribution of the air under the hull to an equal flow rate but at different Froude numbers. The high velocity condition (Fn >>1) helps to keep the air under the hull with a good drag reduction. For lower velocities (Fn<1), the air starts to escape by the sides and less air is distributed under the hull. Moreover, the air that escapes along the sides has a good effect in the displacement condition, thanks to the reduction of the wetted surface in that zones. Instead, when the planing is starting (Fn ≈1), the air lost along the sides is useless, because the sides are already naturally dried and the bottom is widely wetted. This leads to the peak on the curves on Figure 75.

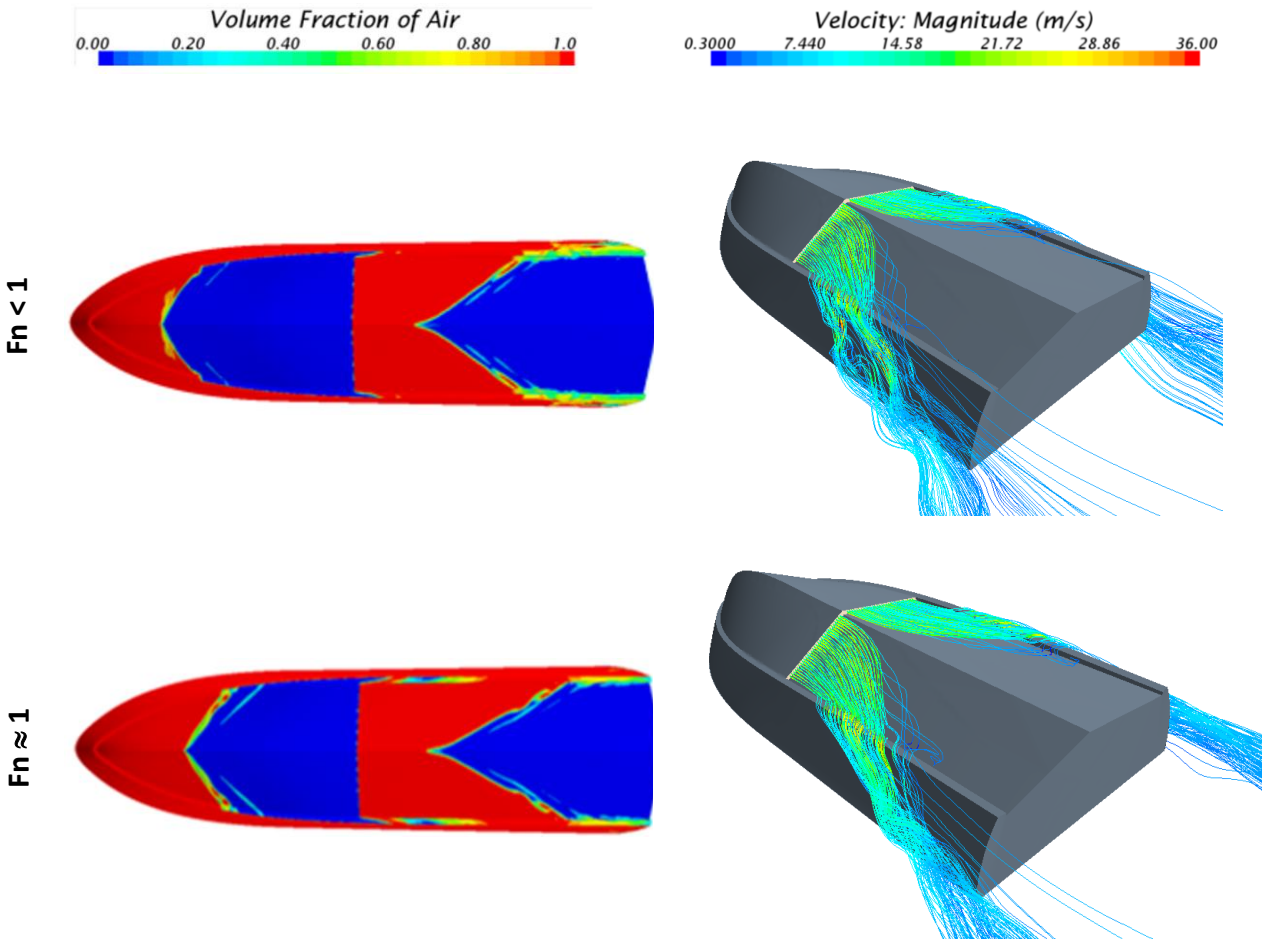

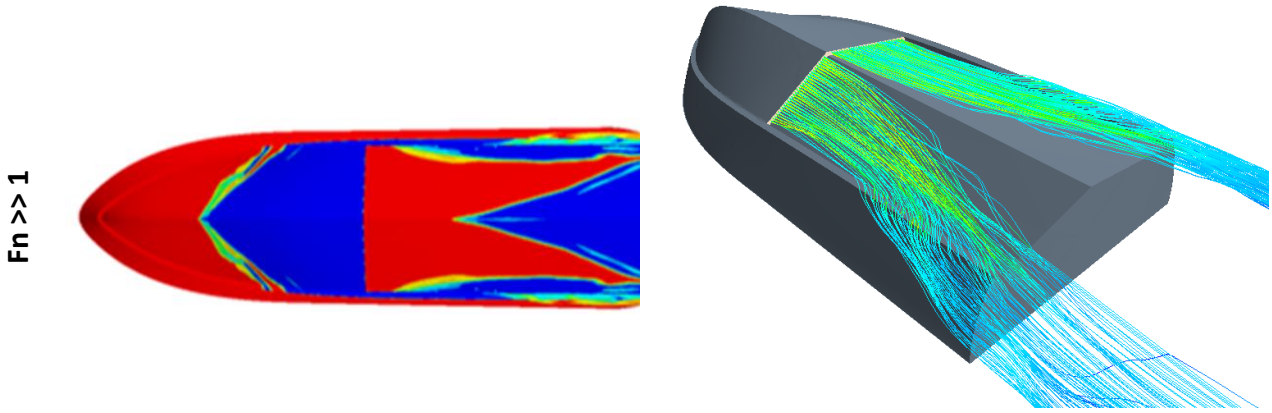

Figure 76 – Volume fraction and streamlines on the cavity, at three Fn conditions

The Figure 77 shows the volume fraction in the sections. It is possible to observe that, in planing condition, the sides are well ventilated also without the air injection. Moreover, thanks to the air injection the model has a wide ventilation also along the hull bottom. The Figure 77 shows also the thickness distribution. Near the nozzles, in correspondence of the step, the layer is developed along the entire breadth and the thickness of this air-layer is equal to the height of the step.

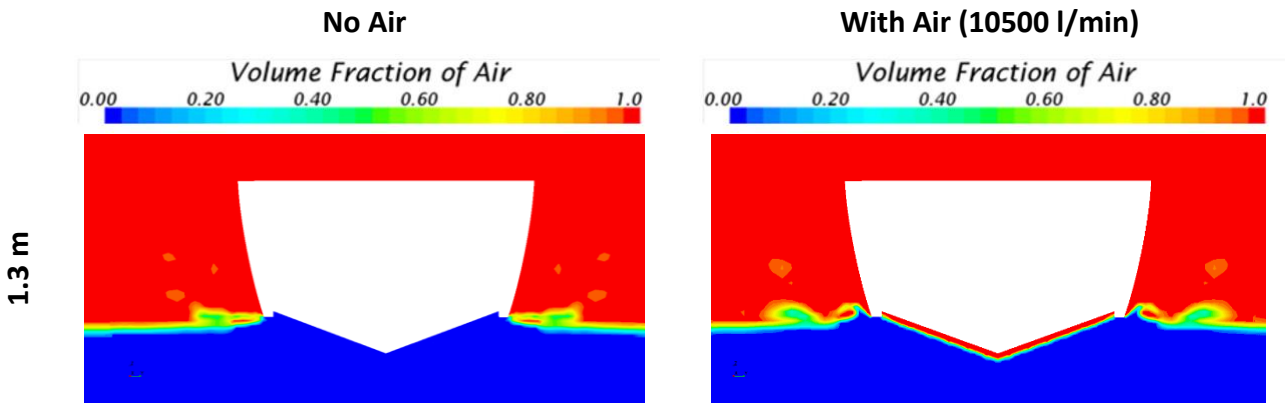

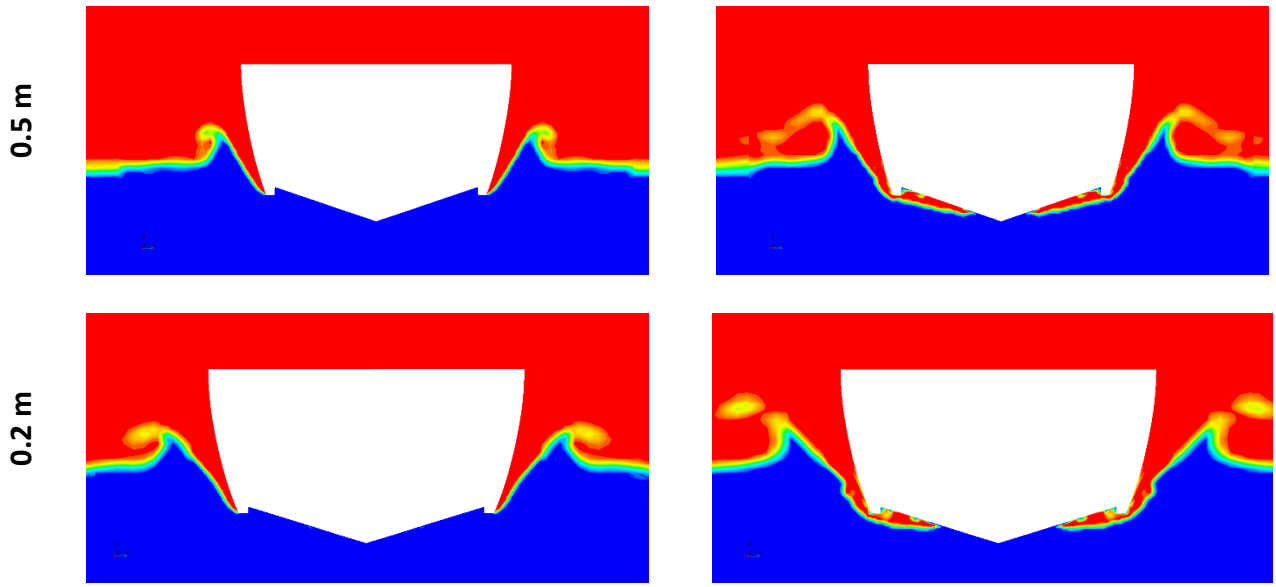

Figure 77 – Sections at different distances from the transom for Fn = 1.36 (v = 6.72 m/s)

The effect of the cushion around the hull is even more visible in displacement condition (Fn < 1) in which the sides are wetted during the navigation without air injection (Figure 78 - Left). Instead, in Figure 78 – on the right, the air injection is shown that produces a clear separation between the water and the sides of the hull.

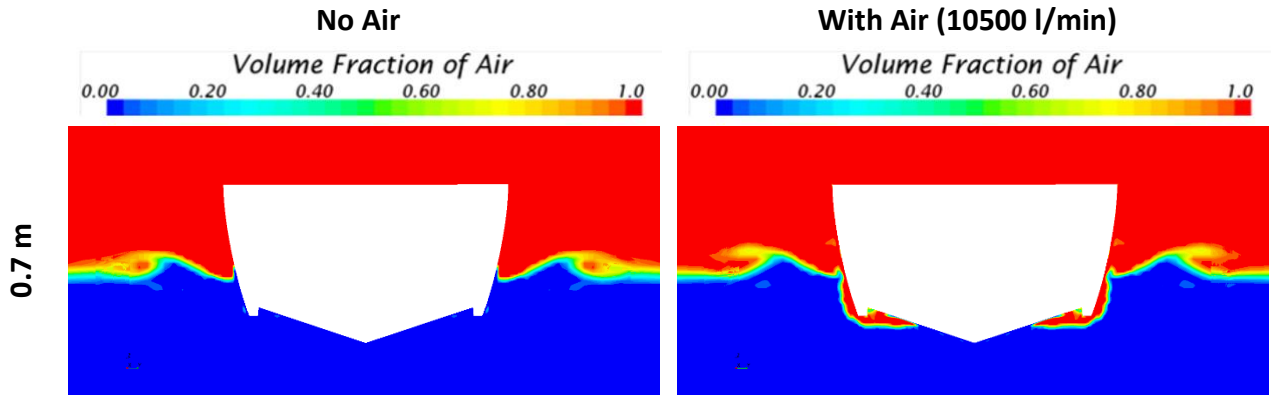

Figure 78 - Section at a distance from the transom of 0.7 m for Fn = 0.894 (v = 4.41 m/s)

6.4 CFD results and comparison with experimental tests – Model C

The method used for the Model C is the same of the Model B above described. The uncertainty analysis has not been developed because the mesh conditions and the boundary conditions are the same of the Model B. Table 19 shows the values of the resistance in both cases, experimental and simulated. The percentage difference is always under the value of 5%. A representation of the resistance curve, as shown Figure 79, allows seeing the characteristic humps and hollows of the planing hull. Also in this case, the humps and hallows present during the experimental tests, have been simulated also with simulation.

Table 19 - Resistance comparison with error indications

Fn	R_{Texp} [N]	R_{Texp}/Δ	RT_{CFD} [N]	RT_{CFD}/Δ	Abs Difference	Percentage
0.510	149	0.099	153	0.102	0.025	2.5%
0.637	204.6	0.136	200	0.133	0.023	2.3%
0.764	222.1	0.148	214	0.143	0.036	3.6%
0.892	239.5	0.160	234	0.156	0.023	2.3%
1.019	260.6	0.174	256	0.171	0.018	1.8%
1.146	277.6	0.185	266	0.177	0.042	4.2%
1.274	277.2	0.185	267	0.178	0.037	3.7%
1.359	275.1	0.183	267	0.178	0.03	3%

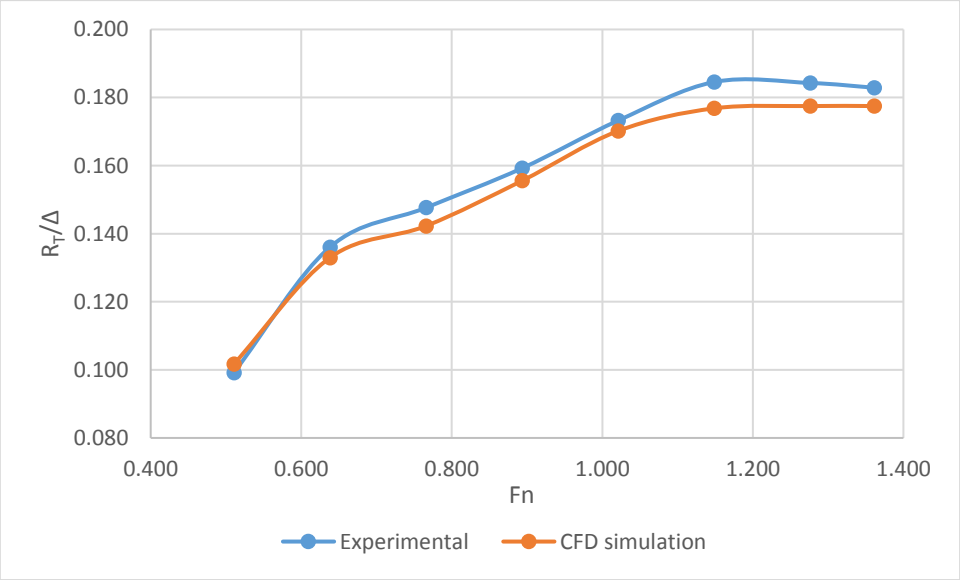

Figure 79 - Resistance comparison between experimental and simulation

The other parameters that have been compared between experimental and virtual tests are trim and sinkage of the boat.

Table 20 shows this comparison and the percentage of error between the experimental tests and numerical simulations.

Table 20 - Ship motion comparison

Fn	τ_{EXP} [deg]	τ_{CFD} [deg]	%Difference	$DTBow_{EXP}$ [mm]	$DTBow_{CFD}$ [mm]	% Abs Difference
0.510	2.29	2.45	6.5%	-47.8	-50.0	5%
0.637	3.86	4.1	5.8%	-104.2	-113.5	9%
0.764	3.97	4.2	5.5%	-123	-127.5	4%
0.892	4.1	4.6	12.2%	-141	-154.7	10%
1.019	4.88	5.36	8.9%	-178	-193.1	8%
1.146	6.28	5.8	8.2%	-244.8	-228.5	7%
1.274	5.49	5.32	3.1%	-244	-228.0	7%
1.359	5.23	4.94	5.9%	-238	-221.3	7%

Also in this case, as shown in Figure 80 and in Figure 81 , the humps and hollows in the curves during the experimental tests have been solved also with the CFD simulation.

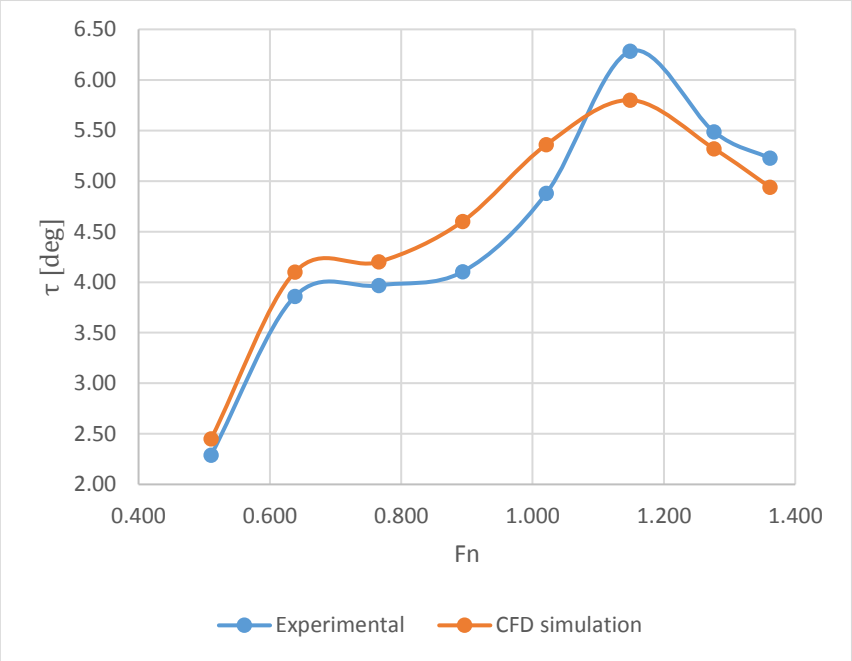

Figure 80 - Trim comparison

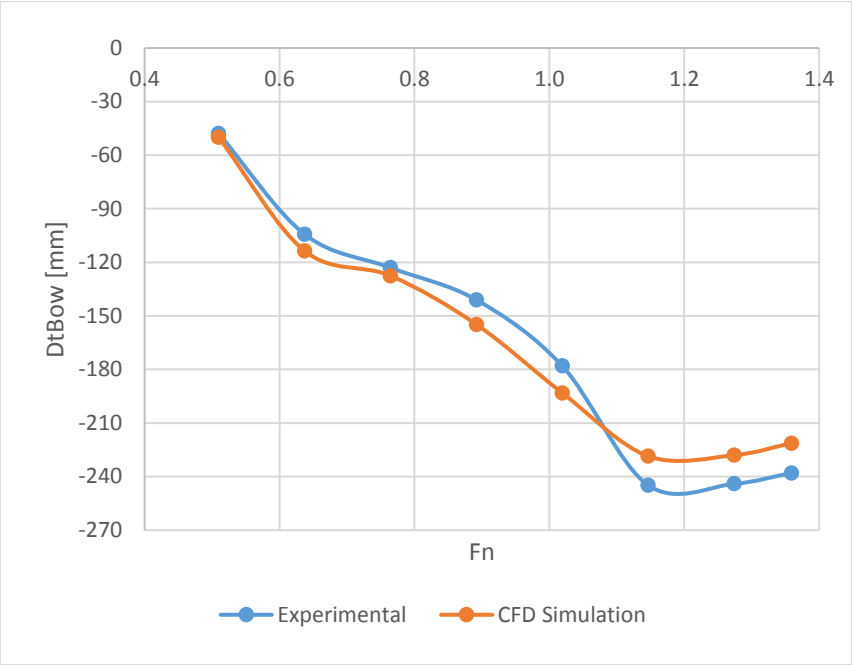

Figure 81 - Sinkage comparison

Also in this case the resistance component has been divided in the two principal components, the pressure one and the frictional one. The impact of each of them on the total resistance is shown in Table 21. Also in this case the pressure component is the most important and it takes in account the effects of the waves and spray energy losses. Increasing the velocity, the percentage of the frictional resistance increases in an important way.

Table 21 - Frictional and Pressure components of resistance

Fn	R_F [N]	R_F/Δ	R_P [N]	R_P/Δ	% R_F	% R_P
0.510	15	0.01	138.0	0.093	11.3	88.7
0.637	26.2	0.017	174.0	0.111	13.5	86.5
0.764	36.4	0.024	178	0.116	16.8	83.2
0.892	45.2	0.031	189	0.121	20.5	79.5
1.019	50	0.035	206	0.136	20.6	79.4
1.146	55	0.037	212	0.140	20.9	79.1
1.274	59	0.043	208	0.135	24.0	76.0
1.359	67	0.047	200.0	0.1	26.7	73.3

Table 22 shows the trend of the Dynamic wetted surface. The effect of planning also in this case produces a rapidly decrease of wetted surface. The value of Froude of this condition is bigger than 0.8. Figure 82 shows the ratio between the dynamic wetted surface and the static one. The decrease to maximum velocity reaches value of 35 %. The assessment of this quantity is important also to evaluate the effect of the air injection successively.

Table 22 - Dynamic wetted surface and dynamic

Fn	S_D [m^2]
0.510	1.90
0.638	1.91
0.765	1.88
0.893	1.71
1.020	1.52
1.148	1.33
1.275	1.28
1.360	1.26

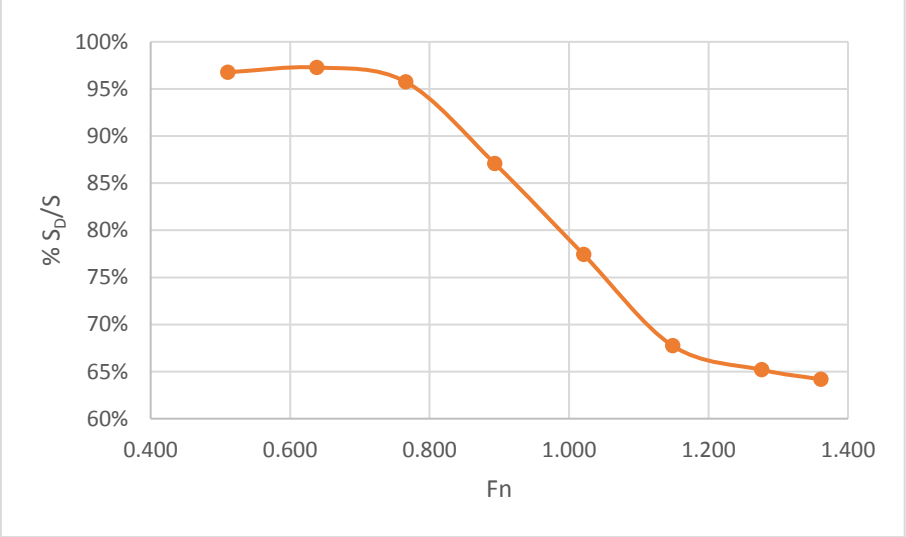

Figure 82- Percentage of dynamic wetted surface respect to the static one – Model C

Figure 83 shows the air Volume Fraction under the hull. It is important to note that the refinement of mesh near the keel allows keeping the artificial numerical ventilation under control and the impacts on the results are negligible. In the same Figure, it is also possible to see the difference between low and high Froude conditions; when the boat reaches 6.3 m/s, the sides are completely out of water.

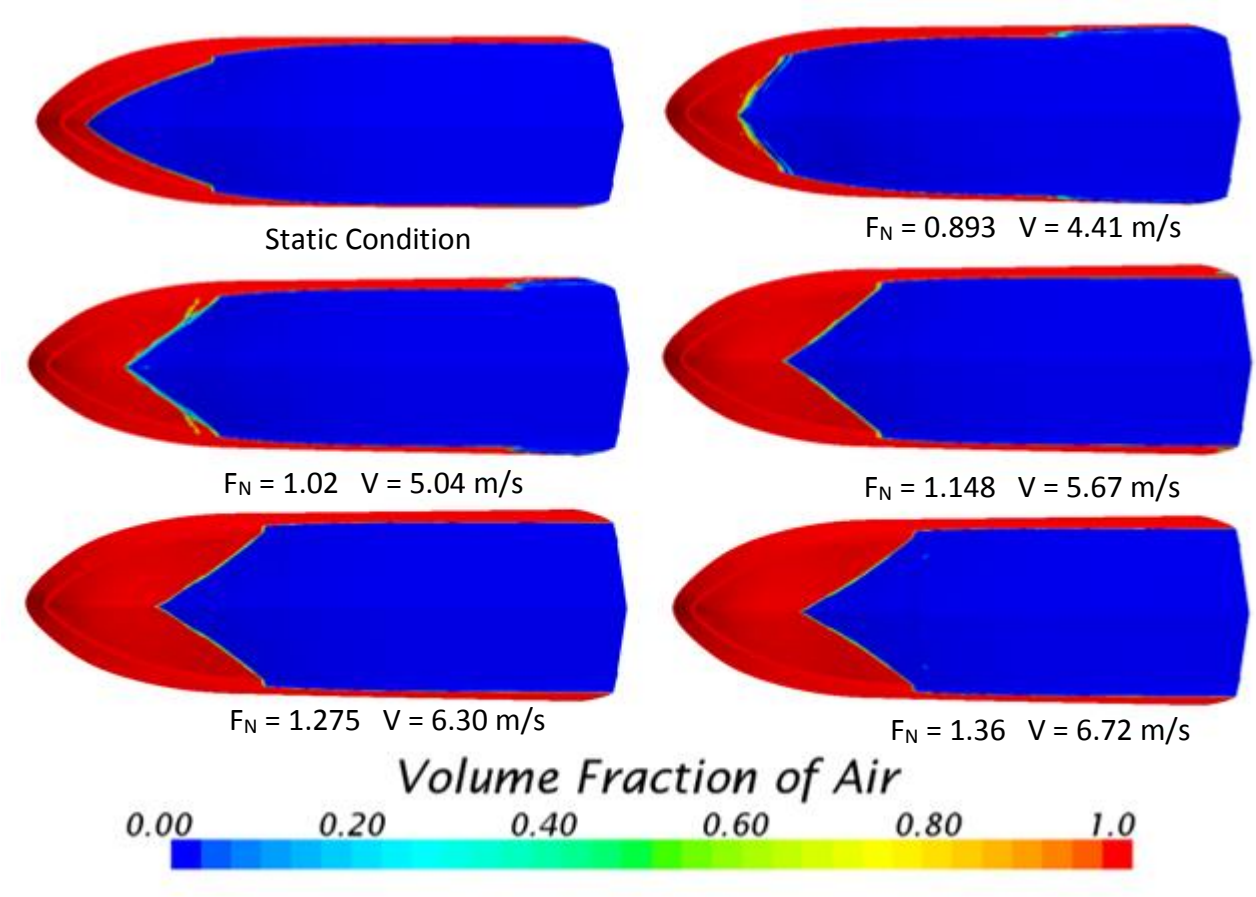

Figure 83 - Comparison between different velocity conditions of the wetted surfaces – Model C

Figure 84 shows a comparison between the model during the experimental tests and during the numerical simulation. For the Fn condition equal to 0.893 there is an evident quantity of spray in both cases, also the stern wave is solved correctly by the numerical simulation.

Towing tank **CFD**

Fn = 0.893

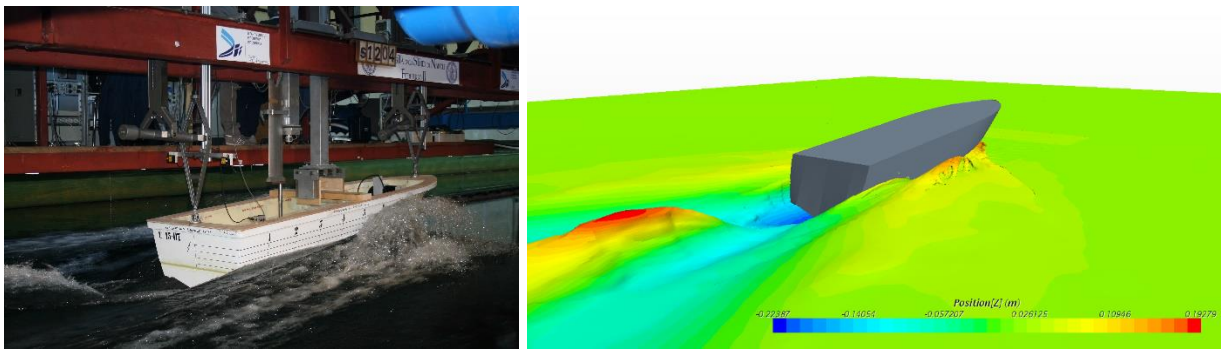

Fn = 1.360

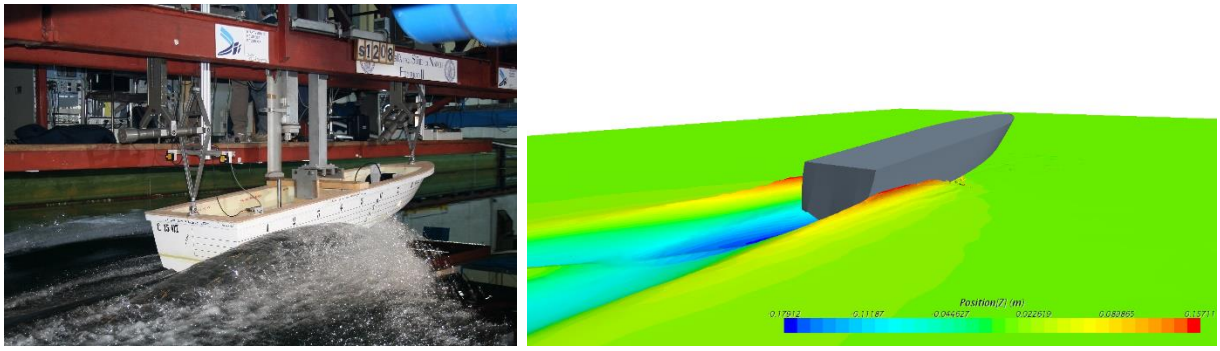

Figure 84 – Wave and spray in two different velocity conditions

The results of the first part of simulations have been used as boundary conditions for the air-injections simulations. The flow rate has been divided equally in the two steps. This type of division is an approximation because the air flow is not equally distributed between the two steps, it depends by the external pressure condition and by the piping system inside the boat. For each condition of flow rate, a comparison between the experimental resistance curves and CFD results is reported. All the velocities have been simulated with all flow rate testes during the experimental tests. Figure 85 and Figure 86 show the comparison to flow rate respectively equal to 5500 l/min and 6500 l/min. The results show a good agreement between the simulations and the experimental tests. Also in this case the biggest difference is to high values of velocity.

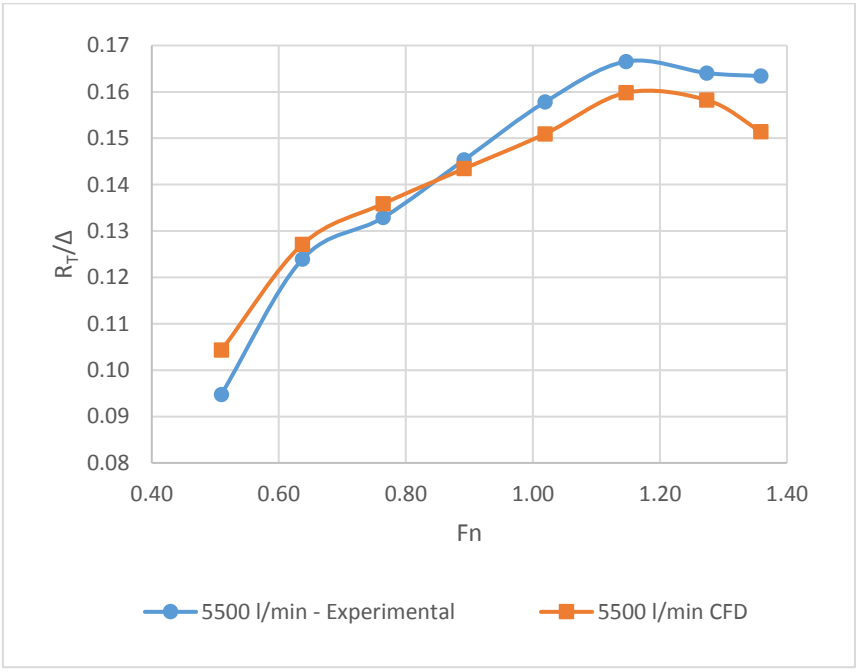

Figure 85 - Comparison with flow rate 5500 l/min

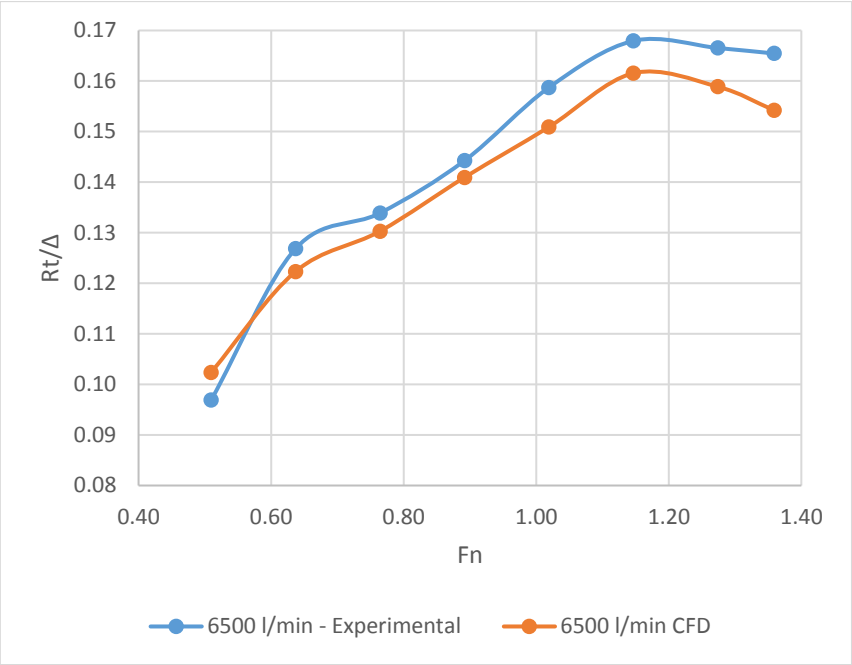

Figure 86 - Comparison with flow rate 6500 l/min

The worst case in term of percentage of error is the 7500 l/min injection. In this case this percentage reaches values of 10 %.

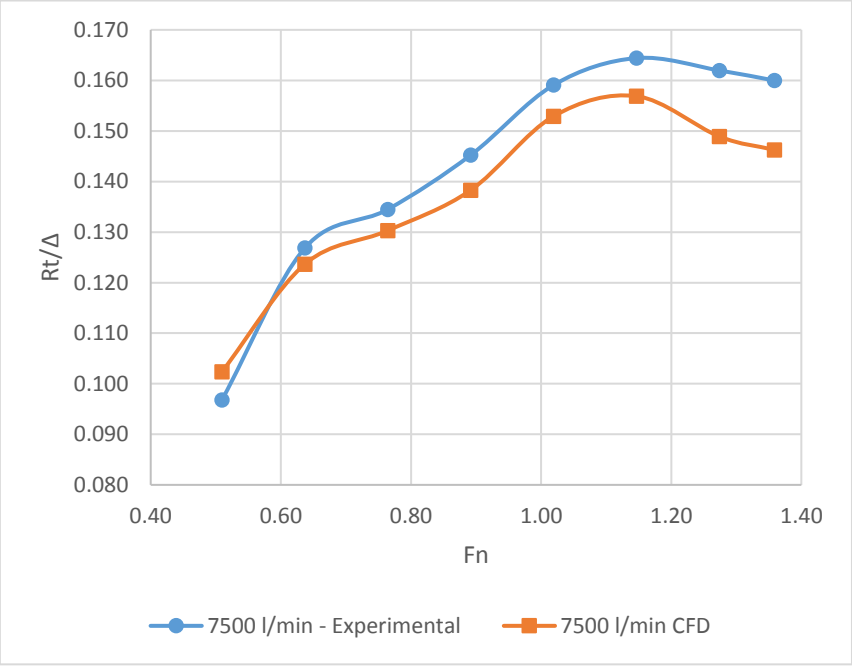

Figure 87 - Comparison with flow rate 7500 l/min

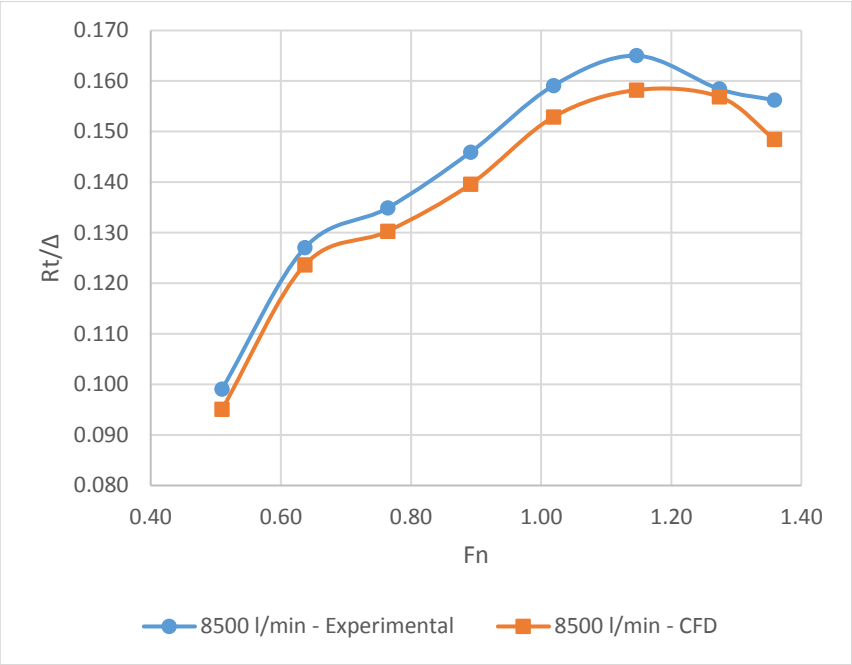

Figure 88 - Comparison with flow rate 8500 l/min

In this two cases have been simulated only the velocity between the Fn = 1 and maximum value of Fn (Figure 89 and Figure 90). The curves have the same trend of the experimental ones and the difference in this two cases is below the 10 %.

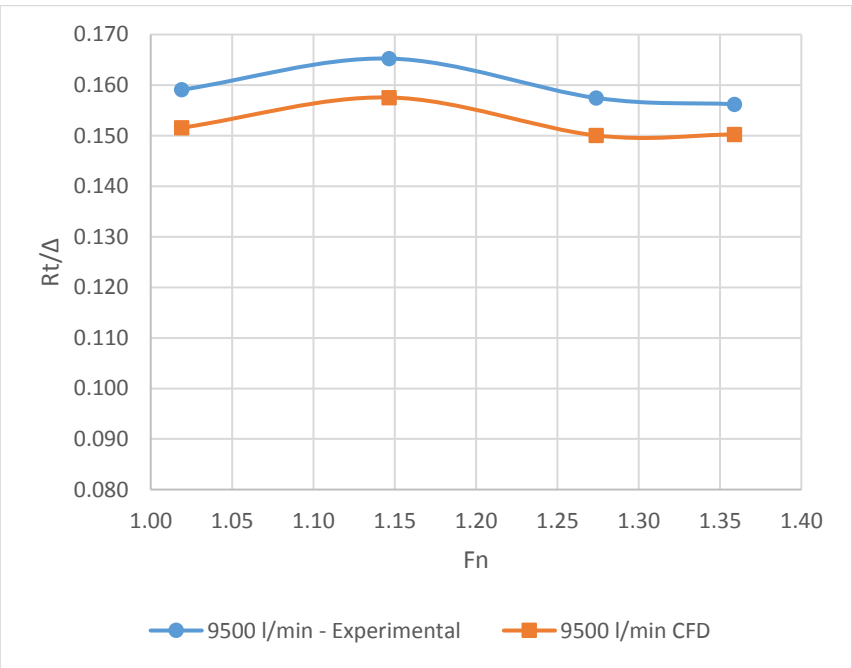

Figure 89 - Comparison with flow rate 9500 l/min

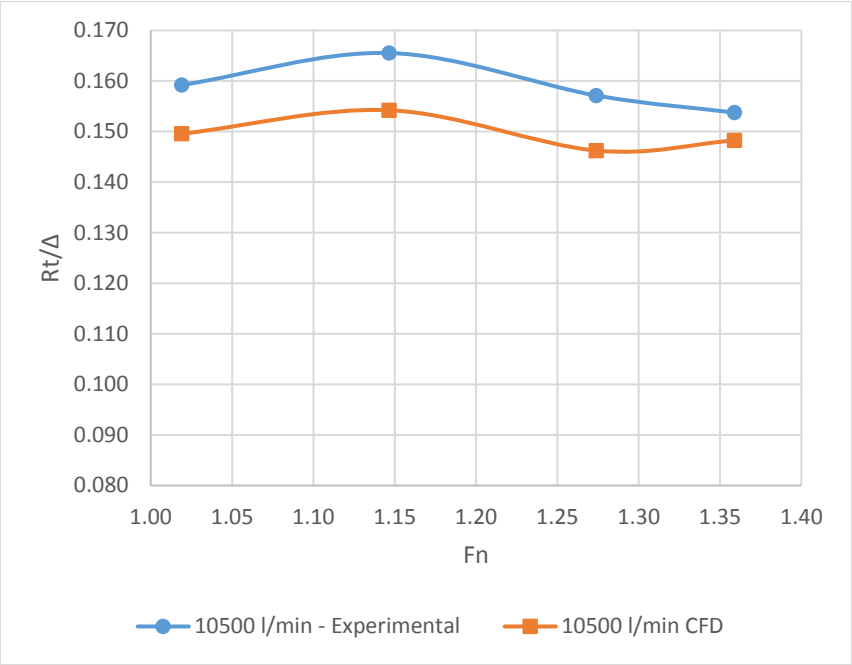

Figure 90 - Comparison with flow rate 10500 l/min

In Figure 91, all the CFD curves are plotted in the same graph. They are always below the curve without air so the injection of air is always a benefit. In the same Figure, the trend is the same of experimental tests (Figure 43). There are two different zones, a first one, for a Froude number less than 1 where the flow rate does not influence the decrease of the resistance and the curves are very similar to each other. A second zone, with the Froude higher than 1, where the flow rate is important and there is a separation of the curves. In this condition of velocity, a higher value of flow rate leads to a greater decrease of resistance.

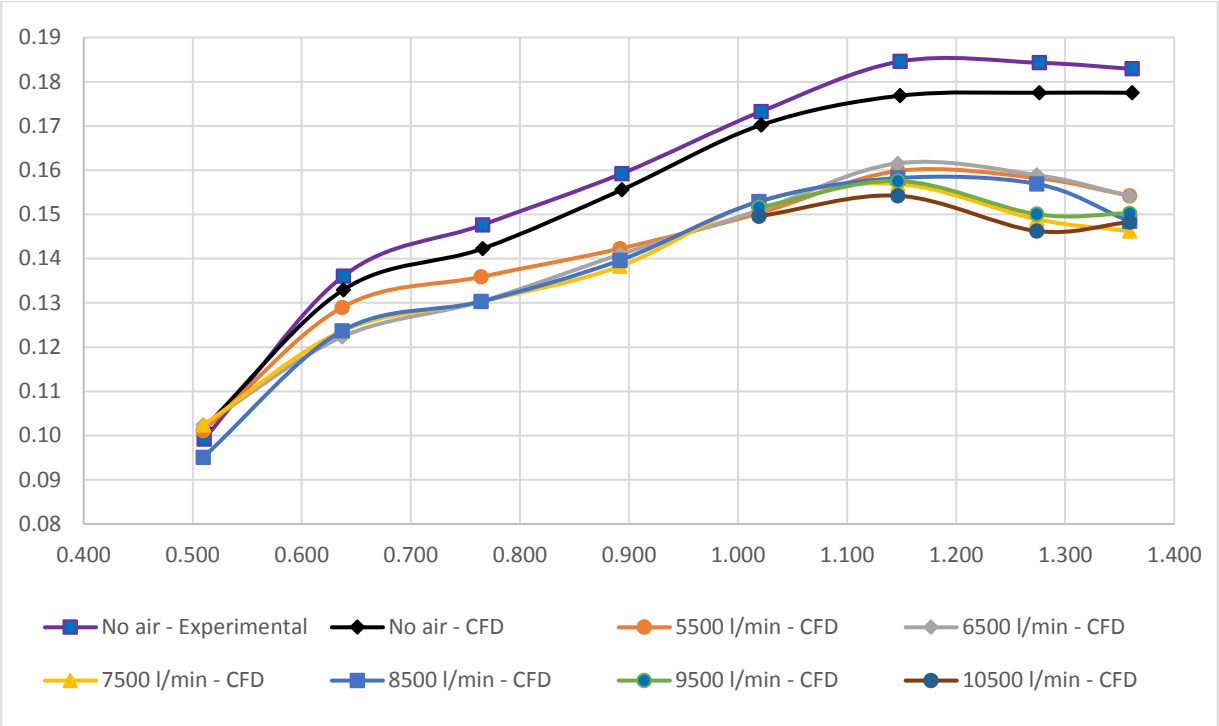

Figure 91 - All resistance curves to different flow rates

Also in this case the assessment of distribution of the air under the hull is very important, in order to understand the effects of different flow rate. Thanks to CFD, it is possible to evaluate the wetted area that decreases increasing the air injection. In the curves shown in Figure 92 is reported the ratio between the dynamic wetted area with air injection and the dynamic wetted area without air injection, varying the flow rate and the Fn. In the case of Model C there is less difference between the curves because the two steps guarantee a homogenous distribution of air under the hull. The curves show in a minimum to value between 1.1 and 1.2 of Fn. A particular condition is the one to 10.500 l/min where the percentage of wetted surface by the air is higher than other ones. The explanation of this phenomena is described with the air flow distribution

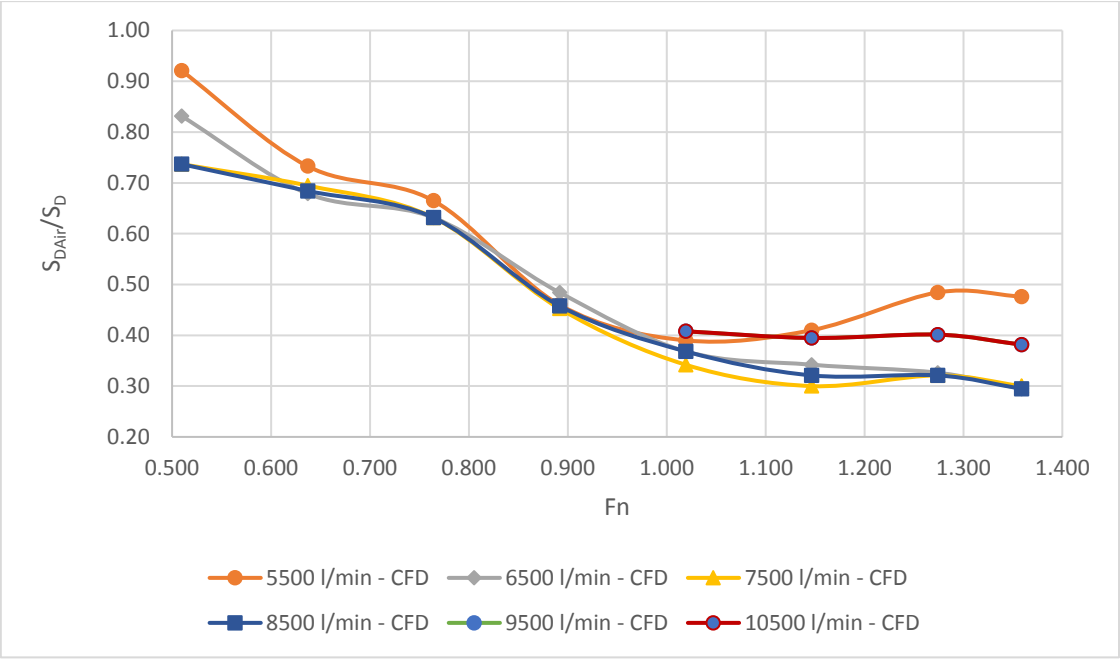

Figure 92 - Ratio between Wetted Surface with air injection and Wetted Surface without air injection

The Figure 93 shows the distribution of the air under the hull to an equal flow rate but at different Froude numbers. For lower velocities (Fn<1), the air starts to escape by the sides and less air is distributed under the hull but in this case, this effect is reduced because the width of the step is reduced with respect to the one of the Model B. This condition allows to keep the air trapped under the hull but it has not a good effect for reducing the wetted surface of the sides in displacement condition. The sides of the hull in this case are always wetted by the water. The streamlines on right of the same picture show the direction of the flow. The second step is useful in order to keep the air under the hull but the air escape by the sides because the step is width almost as the width of the chine.

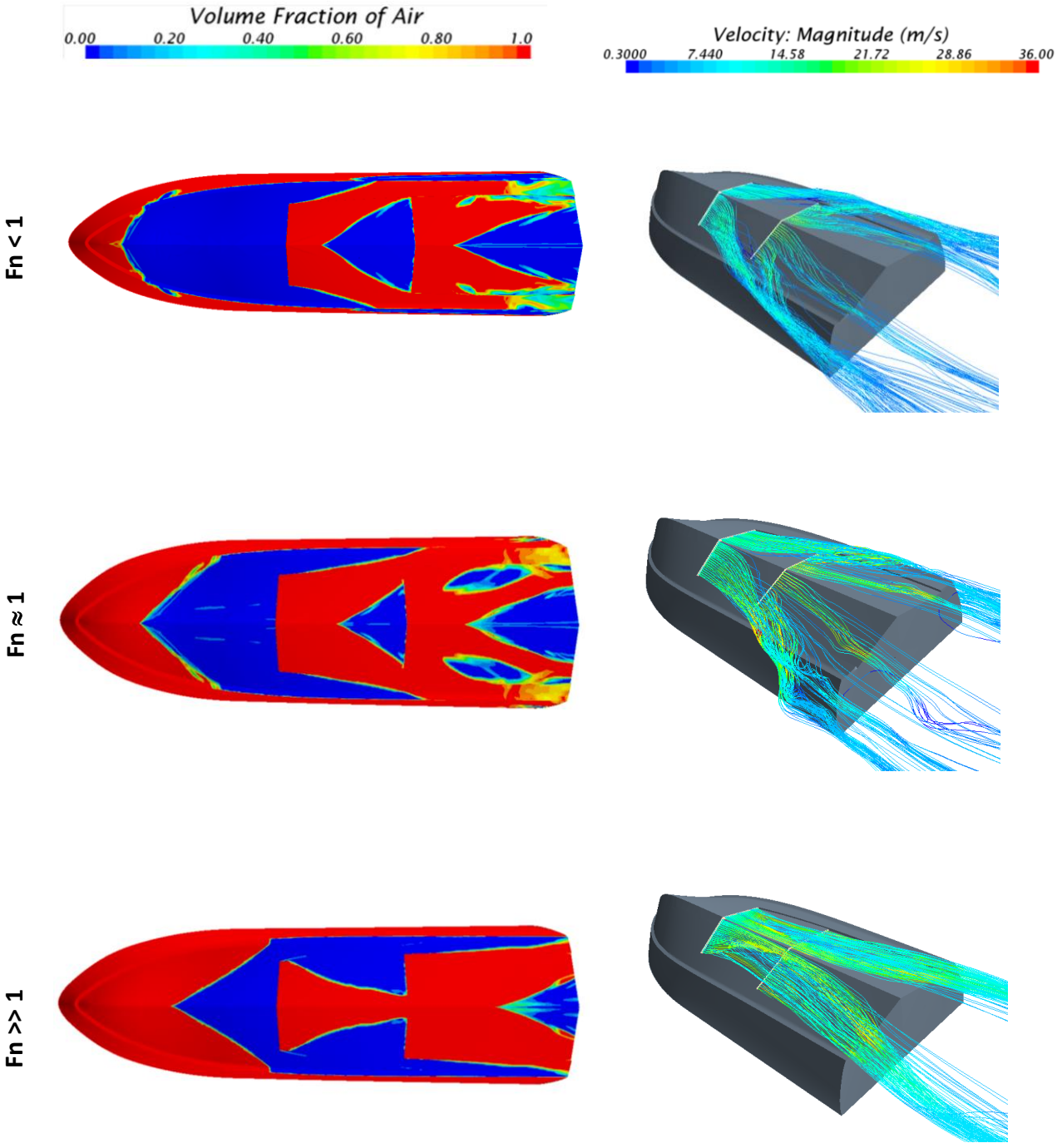

Figure 93 – Volume fraction and streamlines on the cavity, at three Fn conditions

The Figure 94 shows the volume fraction in the sections. It is possible to observe that, in planing condition, the sides, also in this case, are well ventilated also without the air injection. Moreover, thanks to the air injection the model has a wide ventilation also along the hull bottom. Thanks to these pictures is possible to observe that for the sections near the step (1.3 m and 0.5 m) there is a zone under the hull completely wetted by the water and the air is trapped under the hull. In the same condition of velocity, to the section 0.5 m in the Model B there is a complete cushion of air. In this case there is a zone wetted by the water because the first step is less width. The same picture shows also the thickness distribution. Near the nozzles, in correspondence of the step, the layer is developed along the entire breadth and the thickness of this air-layer is equal to the height of the step.

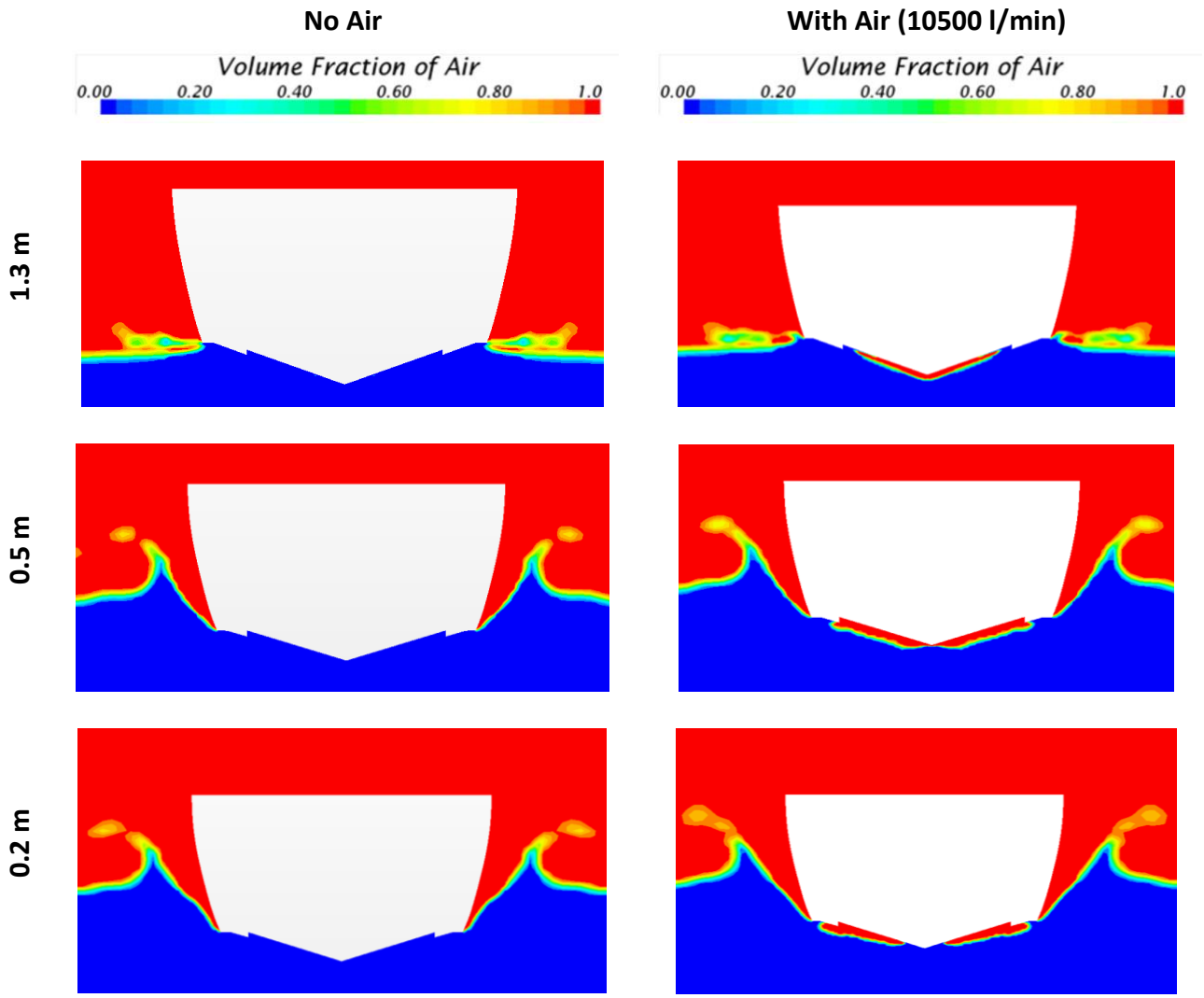

Figure 94 – Sections at different distances from the transom for Fn = 1.36 (v = 6.72 m/s)

The Figure 95 shows a particular condition where is visible that the sides of the hull during the condition first of planing are not completly wetted by the air like the sides of the first model (Figure 78).

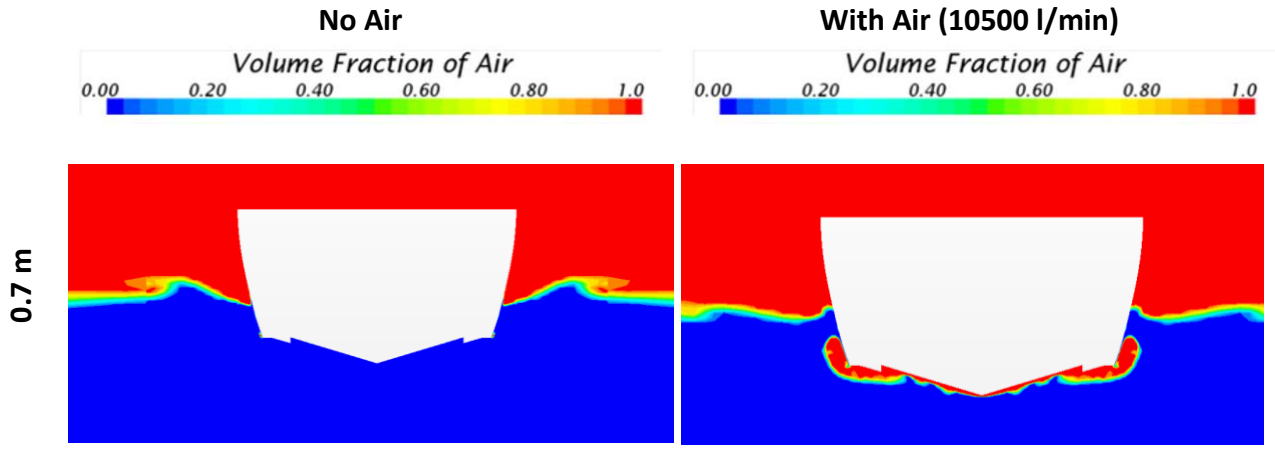

Figure 95 - Section at a distance from the transom of 0.7 m for Fn = 0.894 (v = 4.41 m/s)

Another interesting observation is the air flow to maximum velocity condition. In this case like in the case of Model B the air flow is deviated towards the center line of the hull. This effect is evident in the case of this model. Figure 96 and Figure 97 show the difference of air distribution under the hull. In the first case (Figure 96) there is not a complete cushion of air because it is deviated towards the centre line (principally in the zone of the first step injection). In the second case, to a lower velocity, the cushion is completely developed.

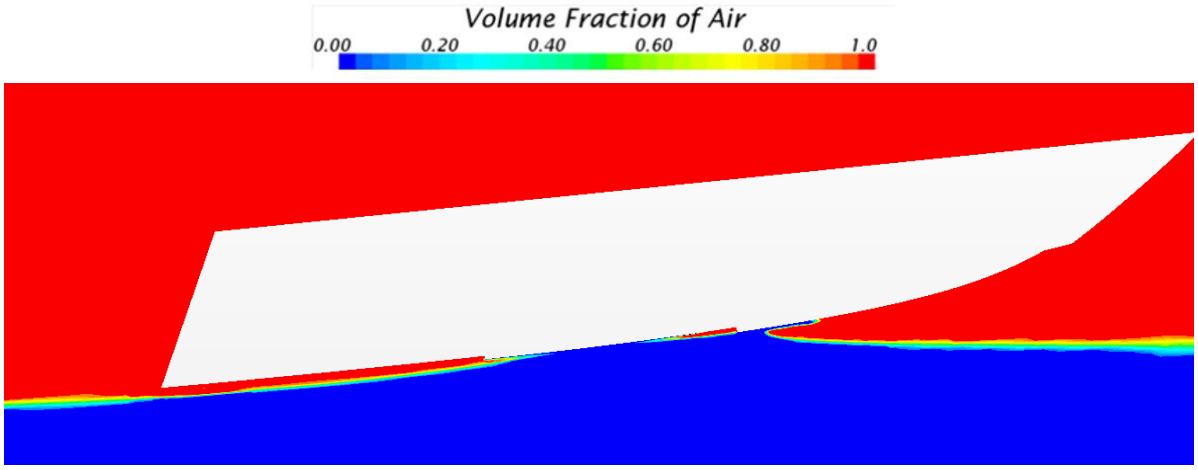

Figure 96 - Longitdunal section to 0.2 m away from the centre line - Velocity Fn= 1.36 (6.72 m/s) - Flow rate 10500 l/min

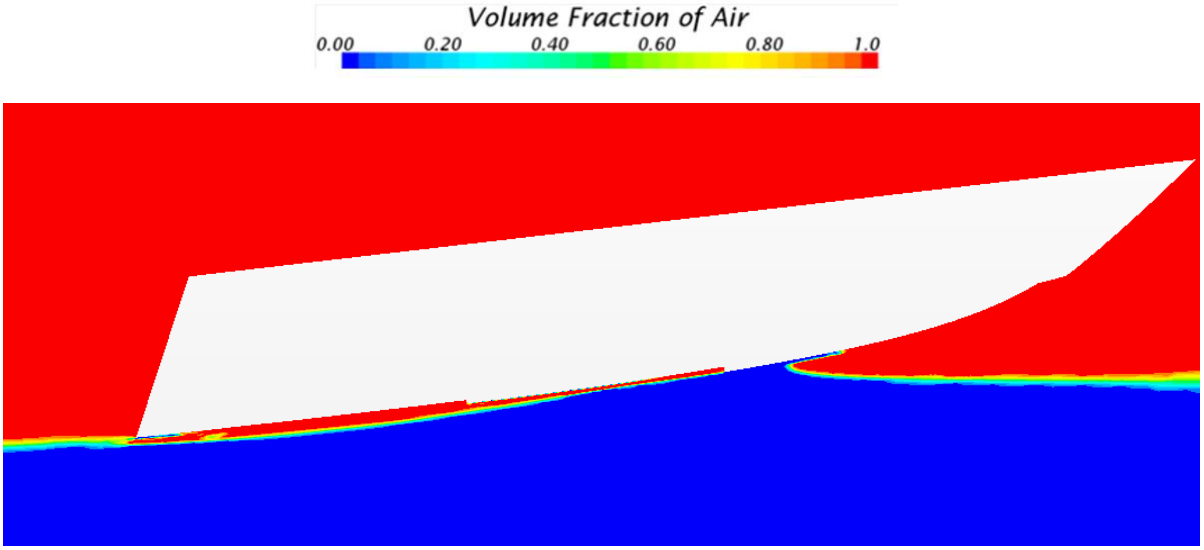

Figure 97 - Longitdunal section to 0.2 m away from the centre line - Velocity Fn=1.148 (5.67 m/s) - Flow rate 10500 l/min

7. Conclusions

In this research, an ACS planing hull has been investigated by the experimental comparison of three different air cavity shapes with respect to the original mother hull. The design philosophy has been to propose an air-layer configuration, instead of the traditional air-cushion, taking advantage of the natural low pressure under planing hulls. All the steps for injection of air have been positioned near the natural depression zone of the planing hull.

The tests have been carried out in the towing tank of the University of Naples, using the ITTC '57 methodology. More than 200 different tests have been conducted by varying bottom cavity shape, velocity and air flow rate. Results show that also planing hull can reach important resistance reduction, compared to conventional hull. More complex cavity shapes, designed to prevent the air escape from the chain, did not lead to satisfying results. This phenomenon is due to the sufficient low pressure under the bottom of the high speed craft and to the increment of the wetted surfaces.

The presence of air layer, although involves a good drag reduction, does not influence the lift of this kind of boats. In addition, the differences between mother hull and ACS models, in terms of trim and sinkage, are negligible.

The air injection leads to a decrease of resistance between the 6% and 20 %. The power requested for the air injection is about the 3% of the entire propulsion power.

The first part of CFD research involved the use URanse methods. The principal aim is to understand the potentiality of the CFD simulations for this kind of problem. A first part concerns the evaluation of the resistance curve without air injection and the prediction of the trim and sinkage. By post-processing of the CFD results, the wetted area has been evaluated. All setup for the mesh and the solver are described and the technique of overset mesh is used in order to take in account the

motion of the hull. A comparison between the experimental tests and simulations results is proposed in order to validate the virtual tests and verify the differences. The difference between the two methods is always lower than 5%. During this phase, an assessment of the uncertainty is conducted in order to quantify the percentage of uncertainty respect to the mesh used during all simulations (the finest one).

The second part deals with the injection of the air with different flow rates. The flow rates investigated are between 5500 l/min and 10500 l/min with steps of 1000 l/min. With the injection of the air, for each condition of flow rate, the resistance curve is lower than one without air injection. The dependence on flow rate starts to increase with the increase of velocity. All the CFD resistance curves are compared with the experimental ones. In this case, the differences are always lower than 5%, except for one case. An important aspect of the CFD is the post-processing, in particular the visualization of the streamlines and of the air distribution under the hull. At the same flow rate condition, the increase of velocity allows to keep the air completely in the cavity. When the velocity decreases, part of this air escapes along the sides. This effect is positive when the sides are wetted by water (displacement condition). The peaks in the curves highlight the passage between a positive effect and negative effect. The phenomenon occurs around the Froude number of one. The distribution of the thickness of the air under the hull is showed for different transversal sections.

The methodology developed for the first model has been used for the second model in order to verify the validity in another case. The behavior of the Model C is different, principally in the distribution of the air under the hull.

An interesting phenomenon in both of models has been observed during the maximum velocity. The air converge towards the symmetry of the ship. In the case of the first model this effect is less evident than Model C.

The CFD method, principally in preliminary phase, is a very useful tool for these kind of problems. It helps better understanding the distribution of the air injected under the hull. With the use of CFD is possible to verify different shapes of bottom hull and the influence of each parameter. The CFD analysis allows to speed up the optimization process and to improve the knowledge of new and no standard applications. It clears that the CFD is an important tool in order to improve the knowledge of particular phenomena but for new type of hull is always important to test the

In conclusion, experimental tests and numerical analysis can be used in order to understand complex phenomena. The experimental tests are necessary when for two main reasons: for obtaining results of new technology and in order to validate numerical simulations. CFD methods, after an important validation, can be useful in preliminary design for simulating different shapes and solution in a rapid way.

8. Bibliography

Ahmadzadehtalatapeh, M., Mousavi, M., 2016. A Review on the Drag Reduction Methods of the Ship Hulls for Improving the Hydrodynamic Performance. Int. J. Marit. Technol. 4, 51–64.

Amromin, E.L., 2016. Analysis of interaction between ship bottom air cavity and boundary layer. Appl. Ocean Res. 59, 451–458. doi:10.1016/j.apor.2016.03.009

Baker, G., 1937. Development of hull form of merchant vessels. NECI Trans. 54.

Balaras, E., Schroeder, S., Posa, A., 2015. Large-Eddy Simulations of Submarine Propellers. J. Sh. Res. 59, 227–237. doi:10.5957/JOSR.59.4.150047

Brusca, S., Cucinotta, F., Galvagno, A., Lanzafame, R., Mauro, S., 2015. Oscillating water column wave energy converter by means of straight-bladed Darrieus turbine. Energy Procedia 1–10.

Butterworth, J., Atlar, M., Shi, W., 2015. Experimental analysis of an air cavity concept applied on a ship hull to improve the hull resistance. Ocean Eng. 110, 2–10. doi:10.1016/j.oceaneng.2015.10.022

Butuzov, A.A., 1968. Limiting parameters of an artificial cavity formed on the lower surface of a horizontal wall. Fluid Dyn. 1, 116–118. doi:10.1007/BF01013836

Butuzov, A.A., Vasin, A.I., Drozdov, A.L., Ivanov, A.N., Kalyuzhny, V.G. Matveev, I.I., Ruzanov, V.E., 1988. Full-scale trials of a boat with an air cavity. Shipbuild. Probl. 28, 45–51.

Carl-Erik Janson, 1997. Potential Flow Panel Methods for the Calculation of Free-surface Flows with Lift. Chalmers University of Technology.

Ceccio, S.L., 2010. Friction Drag Reduction of External Flows with Bubble and Gas Injection. Annu. Rev. Fluid Mech. 42, 183–203. doi:10.1146/annurev-fluid-121108-145504

Cella, U., Cucinotta, F., Sfravara, F., 2017. Sail Plan Parametric CAD Model for an A-Class Catamaran Numerical Optimization Procedure Using Open Source Tools. pp. 547–554. doi:10.1007/978-3-319-45781-9_55

Cucinotta, F., Nigrelli, V., Sfravara, F., 2017a. A preliminary method for the numerical prediction of the behavior of air bubbles in the design of Air Cavity Ships. pp. 509–516. doi:10.1007/978-3-319-45781-9_51

Cucinotta, F., Nigrelli, V., Sfravara, F., 2017b. Numerical prediction of ventilated planing flat plates for the design of Air Cavity Ships. Int. J. Interact. Des. Manuf. doi:10.1007/s12008-017-0396-x

Dawson, C.W., 1977. A practical computer method for solving ship-wave problems, in: In Proceedings of the 2nd International Conference on Numerical Ship Hydrodynamics. Berkeley, Calif, USA.

De Marco, A., Mancini, S., Miranda, S., Scognamiglio, R., Vitiello, L., 2017. Experimental and numerical hydrodynamic analysis of a stepped planing hull. Appl. Ocean Res. 64, 135–154. doi:10.1016/j.apor.2017.02.004

Deng, Q.-H., Tang, G.-F., 2002. SPECIAL TREATMENT OF PRESSURE CORRECTION BASED ON

CONTINUITY CONSERVATION IN A PRESSURE-BASED ALGORITHM. Numer. Heat Transf. Part B Fundam. 42, 73–92. doi:10.1080/10407790190053842

Elbing, B.R., Mäkiharju, S., Wiggins, A., Perlin, M., Dowling, D.R., Ceccio, S.L., 2013. On the scaling of air layer drag reduction. J. Fluid Mech. 717, 484–513. doi:10.1017/jfm.2012.588

Ferrante, A., Elghobashi, S., 2004. On the physical mechanisms of drag reduction in a spatially developing turbulent boundary layer laden with microbubbles. J. Fluid Mech. 503, 345–355. doi:10.1017/S0022112004007943

Ferziger, J.H., Peric, M., 2002. Computational methods for Fluid Dynamics, 3rd Editio. ed. Berlin, Heidelberg.

Formaggia, L., Miglio, E., Mola, A., Parolini, N., 2008. Fluid–structure interaction problems in free surface flows: Application to boat dynamics. Int. J. Numer. Methods Fluids 56, 965–978. doi:10.1002/fld.1583

Froude, W., 1955. Observations and suggestions on the subject of determining by experiment the resistance of ships, in: Architects, R.I. of N. (Ed.), The Papers of William Froude. London.

Fureby, C., 2016. Challenges for Large Eddy Simulation of Engineering Flows, in: Whither Turbulence and Big Data in the 21st Century? pp. 375–400.

Gokcay, S., Insel, M., Odabasi, A.Y., 2004. Revisiting artificial air cavity concept for high speed craft. Ocean Eng. 31, 253–267. doi:10.1016/j.oceaneng.2003.05.002

Havelock, T.H., 1951. Wave resistance theory and its application to ship problems. Trans. Soc. Nav. Archit. Mar. Eng. 59, 13–24.

He, W., Diez, M., Zou, Z., Campana, E.F., Stern, F., 2013. URANS study of Delft catamaran total/added resistance, motions and slamming loads in head sea including irregular wave and uncertainty quantification for variable regular wave and geometry. Ocean Eng. 74, 189–217. doi:10.1016/j.oceaneng.2013.06.020

Hess, J.L., 1990. Panel Methods in Computational Fluid Dynamics. Annu. Rev. Fluid Mech. 22, 255–274. doi:10.1146/annurev.fl.22.010190.001351

Hino, T., 1995. Viscous Flow Computations around a Ship Using One-Equation Turbulence Models. J. Soc. Nav. Archit. Japan 178, 9–22. doi:http://doi.org/10.2534/jjasnaoe1968.1995.178_9

Hino, T., 1994. A Study of Grid Dependence in Navier-Stokes Solutions for Free Surface Flows around a Ship Hull. J. Soc. Nav. Archit. Japan 176, 11–18. doi:http://doi.org/10.2534/jjasnaoe1968.1994.176_11

International Towing Tank Conference, I., 1978. Performance, Propulsion 1978 ITTC Performance Prediction Method.

Inui, T., 1980. From bulbous bow to free surface shock wave-Trend of twenty years research on ship waves at the Tokyo University Tank. J. Sh. Res. 25, 147–180.

Inui, T., Kajitani, H., 1977. A study on local nonlinear free-surface effects in ship waves and wave resistance, in: Schiffstechnik,. p. 24.

ITTC, 2011. Uncertainty Analysis in CFD Verification and Validation Methodology and Procedures.

ITTC, 1957. Proceedings of the 8th ITTC, in: 8th International Towing Tank Conference. Madrid.

Jang, J., Choi, S.H., Ahn, S.M., Kim, B., Seo, J.S., 2014. Experimental investigation of frictional resistance reduction with air layer on the hull bottom of a ship. Int. J. Nav. Archit. Ocean Eng. 6, 363–379. doi:10.2478/IJNAOE-2013-0185

Ji, B., Luo, X.W., Arndt, R.E.A., Peng, X., Wu, Y., 2015. Large Eddy Simulation and theoretical investigations of the transient cavitating vortical flow structure around a NACA66 hydrofoil. Int. J. Multiph. Flow 68, 121–134. doi:10.1016/j.ijmultiphaseflow.2014.10.008

Kidanemariam, A., Uhlmann, M., 2014. Direct numerical simulation of pattern formation in subaqueous sediment. J. Fluid Mech. 750. doi:10.1017/jfm.2014.284

Kline, S.J., Coles, D.E., Hirst, E.A., 1968. Computation of turbulent boundary layers., in: Proceedings of the 1968 AFOSR-IFP-Stanford Conference.

Kodama, Y., Kakugawa, A., Takahashi, T., Sugiyama, T., 2002. Drag Reduction of Ships by Microbubbles, in: Proceedings of the 24th Symposium on Naval Hydrodynamics. Fukuoka, Japan.

Kodama, Y., Takheshi, H., Hinatsu, M., Hino, T., Uto S., 1994. Computational study of turbulent flows around two double-body ship model, in: Ship Research Institute. (Ed.), Proceedings CFD Workshop Tokyo 1994. Tokyo, Japan.

Kumagai, I., Takahashi, Y., Murai, Y., 2015. Power-saving device for air bubble generation using a hydrofoil to reduce ship drag: Theory, experiments, and application to ships. Ocean Eng. 95, 183–194. doi:10.1016/j.oceaneng.2014.11.019

Larsson, L., Eliasson, R., 2000. Principles of Yacht Design, Second Edi. ed. London.

Larsson, L., Patel, V.C., Dyne, G., 1990. Ship viscous flow, in: Shipbuilding, S.S., Experiment Tank, S. (Eds.), 990 SSPA-CTH-IIHR Workshop. Gothenburg.

Larsson, L., Raven, H., 2010. The Principles of Naval Architecture Series: Ship Resistance and Flow, Society of Naval Architects and Marine Engineers (…. The Society of Naval Architects and Marine Engineers, New Jersey.

Larsson, L., Stern, F., Bertram, V., 2003. Benchmarking of Computational Fluid Dynamics for Ship Flows: The Gothenburg 2000 Workshop. J. Sh. Res. 47, 63–81.

Lazauskas, L.V., 2005. Hydrodynamics of Advanced High-Speed Sealift Vessels. University of Adelaide, Australia.

Lee, C., Choi, C.-H., Kim, C.-J., 2016. Superhydrophobic drag reduction in laminar flows: a critical review. Exp. Fluids 57, 176. doi:10.1007/s00348-016-2264-z

Maimun, A., Nakisa, M., Ahmed, Y.M., Behrouzi, F., Koh, K.K., Priyanto, A., 2016. Hydrodynamic Resistance Reduction of Multi-Purpose Amphibious Vehicle due to Air Bubble Effect. Appl. Mech. Mater. 819, 335–340. doi:10.4028/www.scientific.net/AMM.819.335

Mäkiharju, S.A., Perlin, M., Ceccio, S.L., 2012. On the energy economics of air lubrication drag

reduction. Int. J. Nav. Archit. Ocean Eng. 4, 412–422. doi:10.1017/jfm.2012.588

Matveev, K.I., 2015. Hydrodynamic modeling of semi-planing hulls with air cavities. Int. J. Nav. Archit. Ocean Eng. 7, 500–508. doi:10.1515/ijnaoe-2015-0036

Matveev, K.I., 2012. Two-dimensional modeling of stepped planing hulls with open and pressurized air cavities. Int. J. Nav. Archit. Ocean Eng. 4, 162–171. doi:10.3744/JNAOE.2012.4.2.162

Matveev, K.I., 2007. Three-dimensional wave patterns in long air cavities on a horizontal plane. Ocean Eng. 34, 1882–1891. doi:10.1016/j.oceaneng.2006.08.015

Matveev, K.I., 2003. On the limiting parameters of artificial cavitation. Ocean Eng. 30, 1179–1190. doi:10.1016/S0029-8018(02)00103-8

Matveev, K.I., Perry, N.I., Mattson, A.W., Chaney, C.S., 2015. Development of a remotely controlled testing platform with low-drag air-ventilated hull. J. Mar. Sci. Appl. 14, 25–29. doi:10.1007/s11804-015-1287-9

McCormick, M.E., Bhattacharyya, R., 1973. DRAG REDUCTION OF A SUBMERSIBLE HULL BY ELECTROLYSIS. Nav. Eng. J. 85, 11–16. doi:10.1111/j.1559-3584.1973.tb04788.x

Menter, F.R., Kuntz, M., 2004. Adaptation of Eddy-Viscosity Turbulence Models to Unsteady Separated Flow Behind Vehicles. pp. 339–352. doi:10.1007/978-3-540-44419-0_30

Merkle, C.L., Deutsch, S., 1989. Microbubble Drag Reduction, in: Lecture Notes in Engineering. Springer Berlin Heidelberg, pp. 291–335. doi:10.1007/978-3-642-83831-6_6

Michell, J.H., 1898. The Wave-Resistance of a Ship. Philos. Mag. 45, 106–123. doi:10.1080/14786449808621111

Mizokami, S., Kawakado, M., Kawano, M., Hasegawa, T., Hirakawa, I., 2013. Implementation of ship energy-saving operations with mitsubishi air lubrication system. Mitsubishi Heavy Ind. Tech. Rev. 50, 44–49.

Moin, P., Mahesh, K., 1998. DIRECT NUMERICAL SIMULATION: A Tool in Turbulence Research. Annu. Rev. Fluid Mech. 30, 539–578. doi:10.1146/annurev.fluid.30.1.539

Morabito, M.G., 2014. Empirical equations for planing hull bottom pressures. J. Sh. Res. 58, 185–200.

Myoungkyu, L., Moser, R., 2015. Direct numerical simulation of turbulent channel flow up to. J. Fluid Mech. 774, 395–415.

Pearce, B.W., Brandner, P.A., Foster, S.J., 2015. Ventilated cavity flow over a backward-facing step. J. Phys. Conf. Ser. 656, 12164. doi:10.1088/1742-6596/656/1/012164

Quallen, S., Xing, T., 2016. CFD simulation of a floating offshore wind turbine system using a variable-speed generator-torque controller. Renew. Energy 97, 230–242. doi:10.1016/j.renene.2016.05.061

Richardson, L.F., 1911. The Approximate Arithmetical Solution by Finite Differences of Physical Problems Involving Differential Equations, with an Application to the Stresses in a Masonry

Dam. Philos. Trans. R. Soc. A Math. Phys. Eng. Sci. 210, 307–357. doi:10.1098/rsta.1911.0009

Roache, P.J., 1998. Verification and Validation in Computational Science and Engineering. Hermosa Publishers, New Mexico.

Slyozkin, A., Atlar, M., Sampson, R., Seo, K.C., 2014. An experimental investigation into the hydrodynamic drag reduction of a flat plate using air-fed cavities. Ocean Eng. 76, 105–120. doi:10.1016/j.oceaneng.2013.10.013

Stern, F., Wilson, R. V., Coleman, H.W., Paterson, E.G., 2001. Comprehensive Approach to Verification and Validation of CFD Simulations—Part 1: Methodology and Procedures. J. Fluids Eng. 123, 793. doi:10.1115/1.1412235

Stüben, K., 2001. A review of algebraic multigrid. J. Comput. Appl. Math. 128, 281–309. doi:10.1016/S0377-0427(00)00516-1

Takizawa, K., Tezduyar, T.E., Boswell, C., Tsutsui, Y., Montel, K., 2015. Special methods for aerodynamic-moment calculations from parachute FSI modeling. Comput. Mech. 55, 1059–1069. doi:10.1007/s00466-014-1074-5

Todd, F.H., 1951. The fundamentals of ship model testing. Soc. Nav. Archit. Mar. Eng. Trans. 59.

Tursini, L., 1953. Leonardo da Vinci and the problems of navigation and naval design. Q. Trans. Inst. Nav. Archit. 95, 97–102.

White, F.M., 2014. Fluid mechanics. doi:10.1146/annurev.fluid.36.050802.122132

Wilcox, D.C., 2008. Formulation of the k-w Turbulence Model Revisited. AIAA J. 46, 2823–2838. doi:10.2514/1.36541

Wilcox, D.C., 2006. Turbulnce Modeling for CFD.

Wilson, W., Hendrix, D., Gorski, J., 2010. Hull Form Optimization for Early Stage Ship Design. Nav. Eng. J. 122, 53–65. doi:10.1111/j.1559-3584.2010.00268.x